九州大学学術情報リポジトリ
Kyushu University Institutional Repository

Creep Properties of SUS304 in Hydrogen and Consideration of the Creep Deformation Mechanism in the Presence of Hydrogen

髙﨑, 大裕

https://hdl.handle.net/2324/4475119

出版情報：Kyushu University, 2020, 博士（工学）, 課程博士
バージョン：
権利関係：

Creep Properties of SUS304 in Hydrogen and Consideration of the Creep Deformation Mechanism in the Presence of Hydrogen

Daisuke Takazaki

Creep Properties of SUS304 in Hydrogen and Consideration of the Creep Deformation Mechanism in the Presence of Hydrogen

2020

Daisuke Takazaki

Contents

1 Introduction

1.1 Societal relevance of a study on the degradation of materials in high-temperature hydrogen in the recent world energy situation

After the "Paris Agreement" adopted at the 21st Conference of the Parties (COP21) of the United Nations Framework Convention on Climate Change (UNFCCC), efforts to reduce greenhouse gas emissions are actively being progressed around the world. One of the key energy technology requirements to meet this agreement is the drastic transition from carbon-source energy to renewable energy. Since renewable energy doesn't emit greenhouse gas during its use, deployment of renewable energy has been accelerated around the world. Figure 1.1 shows the outlook for the global CO_2 reduction from the present to 2050 announced by the International Energy Agency (IEA) [1.1]. It is expected that 30% of the CO_2 will be reduced by using renewable energy until 2050.

On the other hand, the use of solar power and wind power has a problem in instability of production. Variation of wind and solar power generation always occurs on momentarily, daily and seasonal scales. Difficulties with electricity in terms of storage in the long term and large amount and transport for long distances are other problems. According to the IEA, it is predicted that large-scale output control will be required in some countries due to the oversupply of renewable energy in the future [1.2]. Actually, in Japan, Kyushu Electric Power Company implemented "output control", which means temporarily stopping solar power generation, in Kyushu island over 70 times during this recent year [1.3]. The reason is to ensure the stability of the power grid. This example clearly shows that the increase in renewable energy faces major technical challenges, while the importance of renewable energy is recognized.

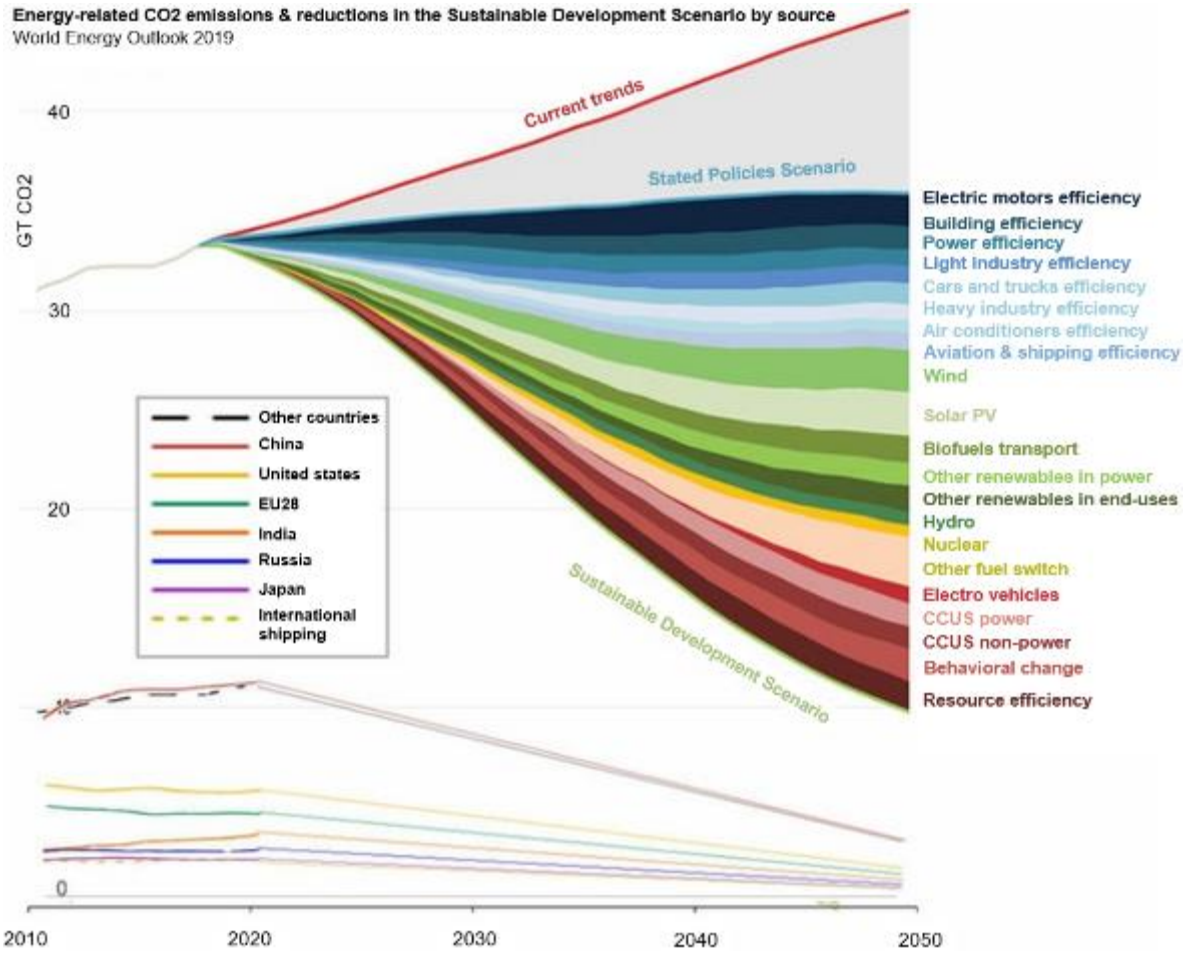

Fig. 1.1 Global carbon dioxide emissions in the IEA Sustainable Development Scenario [1.1].

Use of hydrogen has a great potential to solve this problem if the increase of renewable energy is suppressed. Hydrogen can be produced by water electrolysis using the excessive electricity of renewable energy power generation. In this way, the excessive electricity produced by solar can be temporarily stored as chemical energy. After that, the stored hydrogen is used for power generation on demand in terms of time and place. This idea is called "Power to gas (P2G)". Based on this background, in Japan, for a large full-scale Power-to-Gas demonstration, construction of the "Fukushima Hydrogen Energy Research Field (FH2R)" is underway in Fukushima Prefecture [1.4]. The planned output of FH2R is 10 MW.

In December 2017, the Japanese government determined the "Basic Hydrogen Strategy" [1.5]. The strategy shows action plans and future visions to realize a hydrogen energy society. The strategy sets a goal that Japan should reduce hydrogen costs to the same level as conventional energy sources. For example, the production cost of hydrogen is currently several hundred yen/Nm^3 (several dollar/ Nm^3), which is much higher than 16 yen/Nm^3 (0.15 dollar/ Nm^3) for the import cost of LNG [1.6].

This strategy for the realization of a hydrogen energy society have been updated in Japan. For example, the "Fifth Basic Energy Plan" was updated in July 2018, [1.7], and the "Strategic Roadmap for Hydrogen and Fuel Cells" was updated in March 2019 [1.8]. "Strategy for Developing Hydrogen and Fuel-Cell Technologies" was formulated in September [1.6]. Following Japan's first national strategy (Basic Hydrogen Strategy [1.5]) in 2017, the EU, France (2018) [1.9] and South Korea (2019) [1.10], etc. have also set national strategies for hydrogen.

In order to reduce the hydrogen price, advanced hydrogen-energy conversion systems such as solid oxide fuel cell (SOFC), solid oxide electrolysis cell (SOEC), regenerative fuel

cell (RFC) and hydrogen gas turbines become the mainstays in the hydrogen society. These systems and elements are actively being developed in the world, because these systems can create huge hydrogen demand which is directly link to the reduction of the hydrogen price. For instance, SOFCs and hydrogen gas turbines can be applied to hydrogen power generation. In addition, a large demand of hydrogen creates a new industry of hydrogen production. The SOEC is suitable to meet such demand because hydrogen is efficiently produced by steam electrolysis. If the electricity is generated by a renewable source, carbon-free hydrogen production is possible. By expanding the hydrogen supply chain in this way, independent growth of the hydrogen economy can be achieved.

There is an important keyword for advanced hydrogen systems such as the SOFC, SOEC, RFC and hydrogen gas turbines. It is "high-temperature hydrogen". An example of the SOFC system is shown in Fig. 1.2 [1.11]. The working temperature of the cell at which electricity is produced from oxidizing hydrogen reaches 800 ℃ [1.12, 1.13]. Also, the hydrogen supplied to the SOFC as fuel is preheated to around 600 ℃ in order to maintain the cell's working efficiency [1.11]. Therefore, the structural materials for the SOFC systems are exposed to high-temperature hydrogen not only inside the cell but also other components, such as the hydrogen preheater and hydrogen piping connecting the hydrogen preheater and cell.

This "high-temperature + hydrogen" environment is very aggressive for the structural materials and is well known as high temperature hydrogen attack (HTHA) (Described later). Hereafter, I will describe the present knowledge on the failures of structural materials that occur at elevated temperature under the effect of hydrogen. Then, I will make clear the necessity of the study on the degradation of material strength in high-temperature hydrogen.

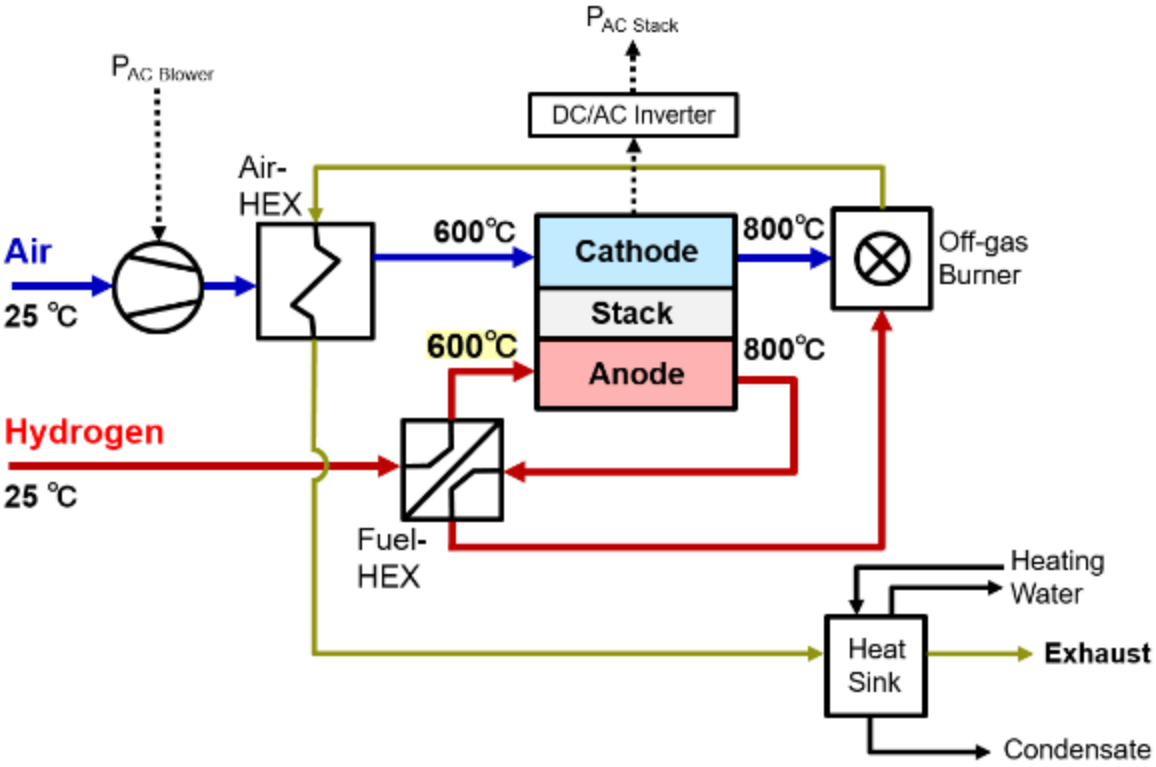

Figure 1.2 Basic system layout and hydrogen gas temperature of SOFC.
Adapted from [1.11].

1.2 Creep

Creep is the tendency of the time-dependent deformation of a solid material under constant loading and one of the most important phenomena for materials used at elevated temperature. When a constant loading is applied to the material at low temperature (roughly 0.4 T_m or less, T_m: melting point), deformation of the material stops at a certain extent due to work hardening. For more deformation, increase of the stress is necessary to overcome the hardening of the material. On the other hand, at high temperature (roughly 0.4 T_m and higher), the deformation of the material proceeds with the loading time without increase of load. This "time-dependent deformation" under a constant loading is called "creep". Usually it occurs at higher temperature than 0.4 times the melting point and it takes a long time to cause fracture [1.14, 1.15].

Figures 1.3 shows turbine blades in a helicopter engine that suffered from creep fracture [1.16]. The material of this turbine blade was HP2 steel. These blades are subjected to very high tensile force due to the centrifugal force produced by high speed rotor rotation during flight. The total operating time of the helicopter engine was 13,084 hours. The blades were exposed to 1000 ℃ or higher temperature. As the result, creep failure of the blades occurred.

Figure 1.4 shows a pipe with creep fracture [1.17]. The material of this pipe was grade SA-213 T-22 steel. The failure of the pipe was caused by creep due to a hoop stress of 40 MPa. (The temperature was not mentioned in Ref. 1.17.) These failures clearly indicate that creep is one of the most important factors in the design of the components subjected to high temperatures.

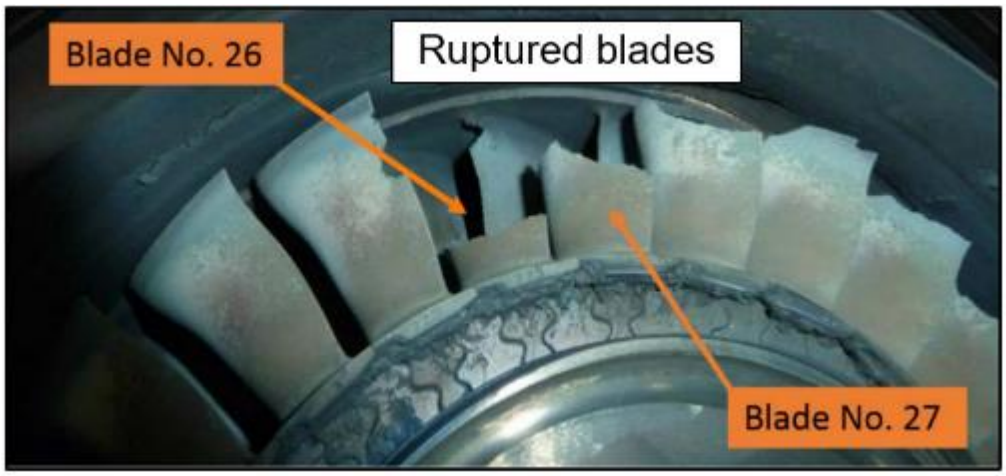

Figure 1.3 Creep ruptured turbine blades due to high centrifugal force [1.16].

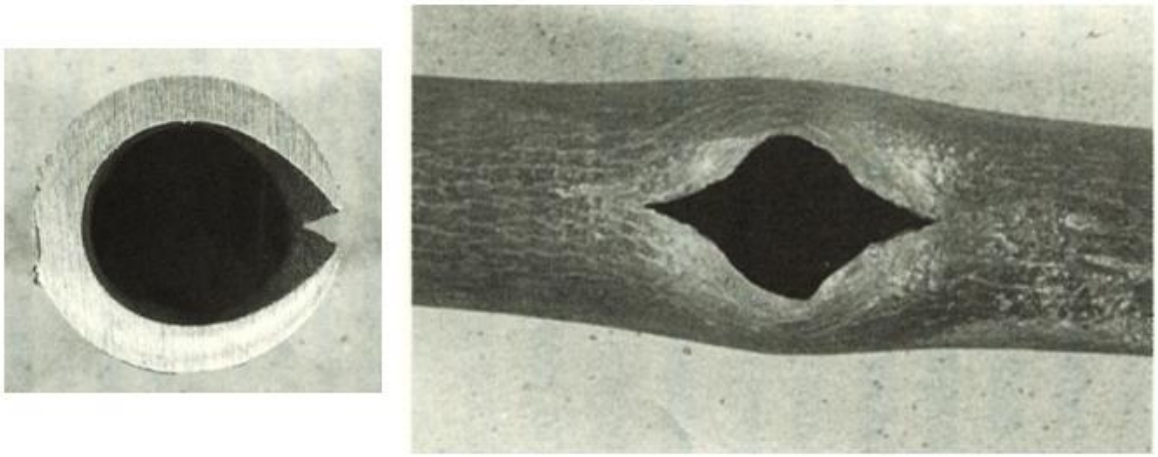

Figure 1.4 Creep ruptured heat exchanger tube due to high internal pressure [1.17].

Figure 1.5 shows the changes in strain with loading time under uniaxial constant stress [1.18]. This curve is called creep curve. The slope of the curve is called creep rate. When a constant load is applied, elastic or elastic-plastic initial strain is generated, and creep dominates the deformation thereafter. As shown in Fig. 1.5, the creep curve is separated into three regions, which are "transient creep (primary creep)", "steady state creep (secondary creep)" and "tertiary creep (accelerating creep)". In the transient creep region, the creep rate decreases with an increase in the loading time because dislocation density increases as creep deformation occurs and it results in strain hardening [1.19]. In the steady creep region, the creep rate is constant due to the balance between the strain hardening and recovery [1.19, 1.20]. In the tertiary creep region, the creep rate increases rapidly toward rupture due to growth of voids, cavities and cracks resulting from creep deformation [1.19].

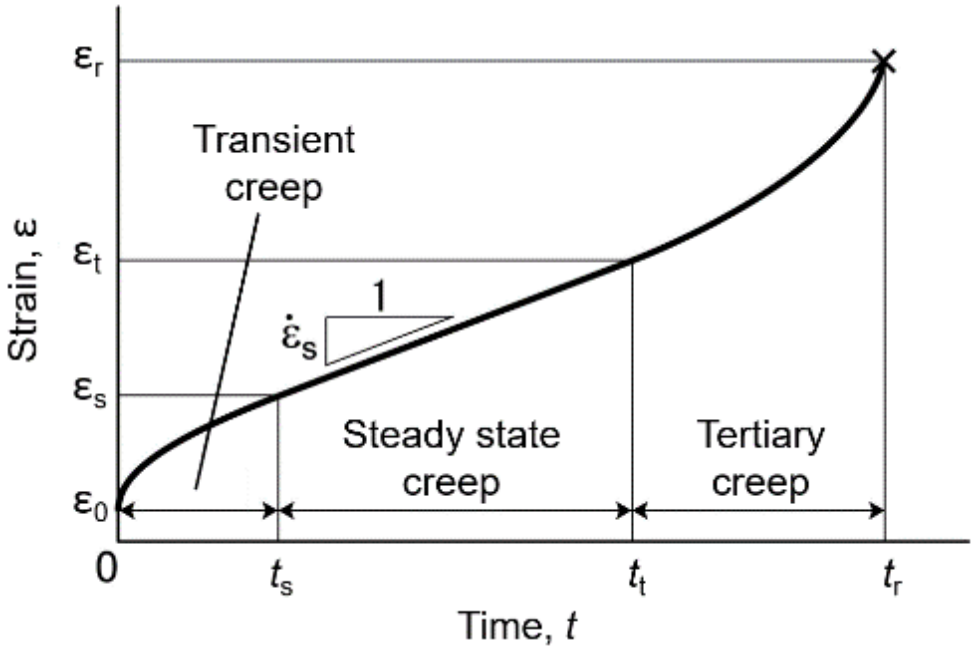

Figure 1.5 Typical creep curve under a constant load [1.18]. Redrawn by author.

The mechanism of creep deformation is classified into several types depending on the temperature and stress level. Figure 1.6 shows the creep deformation mechanism map produced by Frost and Ashby. In this map, the creep deformation mechanisms are classified according to temperature and stress [1.21]. The shear stress was calculated using

$$\sigma_s = \sqrt{\frac{1}{6}\{(\sigma_1 - \sigma_2)^2 + (\sigma_2 - \sigma_3)^2 + (\sigma_3 - \sigma_1)^2\}} \qquad (1.1)$$

where σ_1, σ_2 and σ_3 are the principal stresses. For the uniaxial creep test, the shear stress was calculated by $\sigma_s = \sigma/\sqrt{3}$.

In the relatively high stress and high temperature region, there is a region where the creep deformation is dominated by the "power-law creep". The mechanism of power-law creep is graphically shown in Fig. 1.7 [1.19]. When an obstacle of dislocation movement such as a precipitate exists on a slip plane, the dislocation on that slip plain is stopped by the obstacle. This means that the deformation is stopped. However, at high temperatures, the diffusion of an atom and vacancy can easily occur. As shown in Fig. 1.8 [1.22], when the vacancy migrates to immediately above the dislocation, the dislocation can move to the position that the vacancy occupies and change the slip plane. This phenomenon is called "dislocation climb". Consequently, the dislocation continues to glide again. This is the mechanism of power-law creep. In this context, the creep in this region is also called "dislocation creep".

On the other hand, in the relatively lower stress and high temperature region, another mechanism "diffusion creep (diffusional flaw)" dominates the creep deformation. The mechanism of diffusion creep is shown in Fig. 1.9 [1.23]. In this region, atomic diffusion causes creep deformation. When a stress is applied to the material, atomic diffusion occurs

from A to B through either grain boundary diffusion or lattice diffusion. As the result, the grains are elongated without dislocation movement.

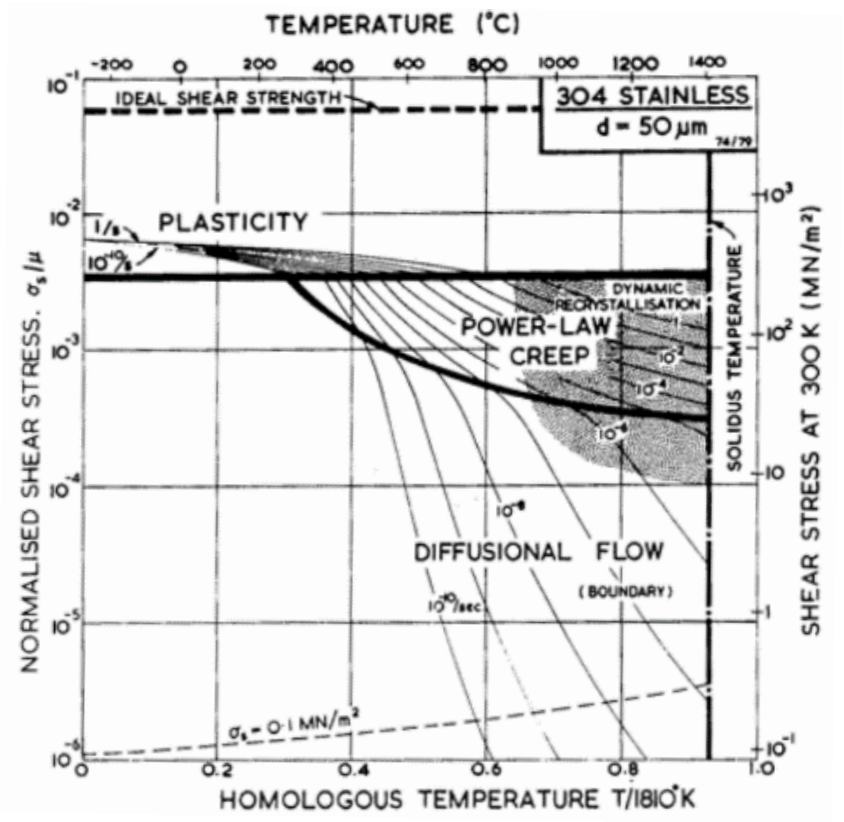

Figure 1.6 Creep deformation mechanism map of 304 stainless steel [1.21].

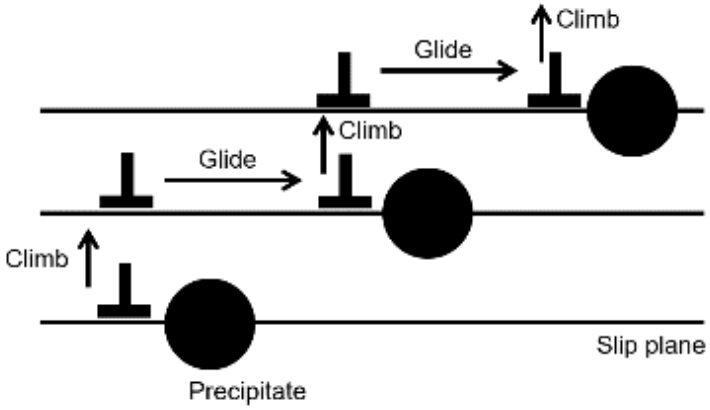

Figure 1.7 Mechanism of "power-law creep" [1.19]. Redrawn by author.

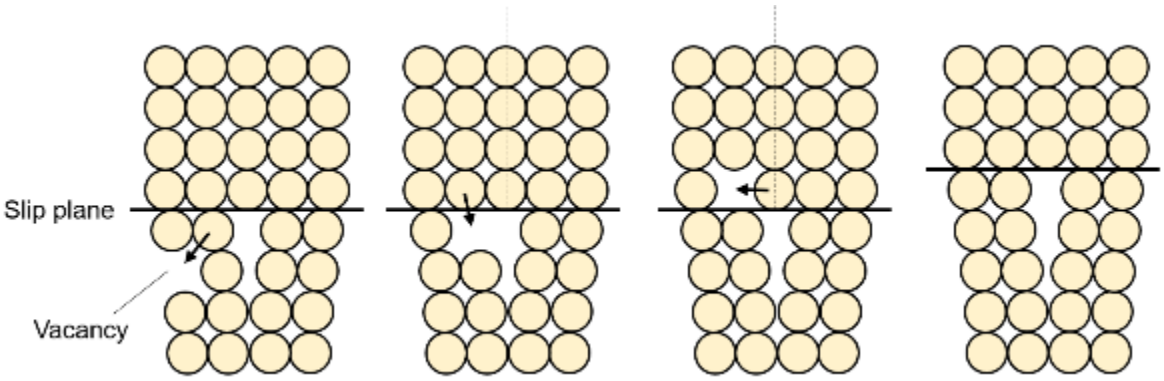

Figure 1.8 Dislocation climb due to vacancy diffusion [1.22]. Redrawn by author.

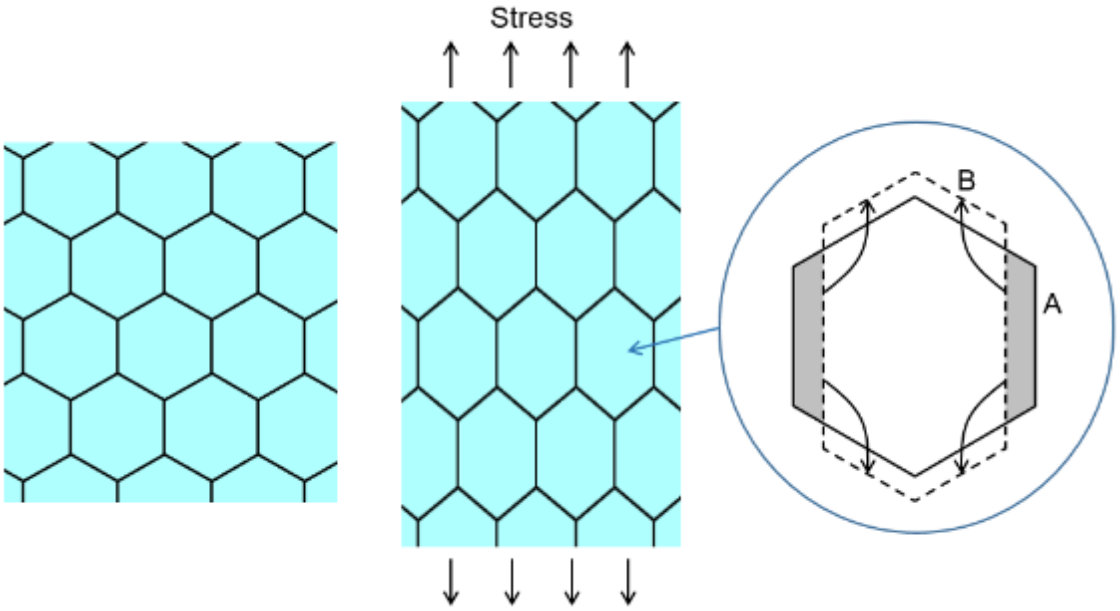

Figure 1.9 Mechanism of “diffusion creep” [1.23]. Redrawn by author.

Figure 1.10 shows the relationship between the activation energy of self-diffusion, Q_{SD}, and the activation energy of creep, Qc, in the power-law creep and lattice-diffusion creep region [1.24]. According to Fig. 1.10, these activation energies agree very well. This means that the creep deformation in the power-law creep and lattice-diffusion creep region is dominated by the diffusion of atoms [1.24, 1.25].

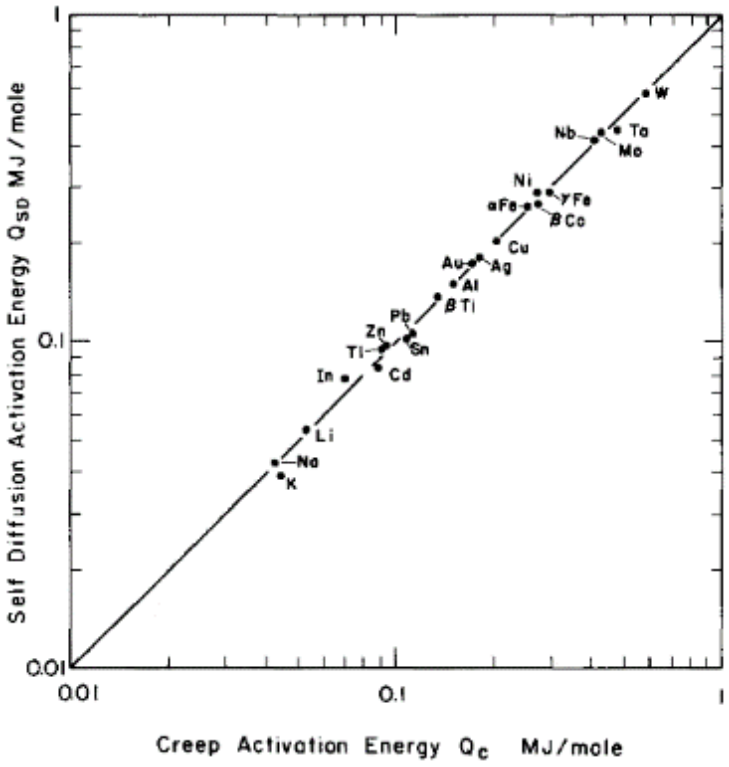

Figure 1.10 Relationship between activation energy of self-diffusion vs activation energy of creep for several materials [1.24].

There is another classification of creep mechanism based on the morphology of the fracture mode. The creep fracture mechanism map is shown in Figure 1.11 [1.26]. Transgranular fracture occurs in the short life region. Intergranular fracture occurs in the long life region. There are several mechanisms that grain boundary fracture causes. In a relatively short life region, wedge cracks occur at the grain boundary or inclusion at the grain boundary and grow along the grain boundary due to the grain boundary sliding. In the long life region, intergranular slip is suppressed, instead cavities are generated at the grain boundary and grow by vacancy aggregation at grain boundary carbides and σ phase interface.

The important point is that the slope of the graph changes when the mechanism of the creep fracture changes. This is one of the reasons that very long creep data is required for the design of the mechanical component subjected to creep [1.27-1.29]. Since the mechanism is changed, it is difficult to predict the long-life from short-life data.

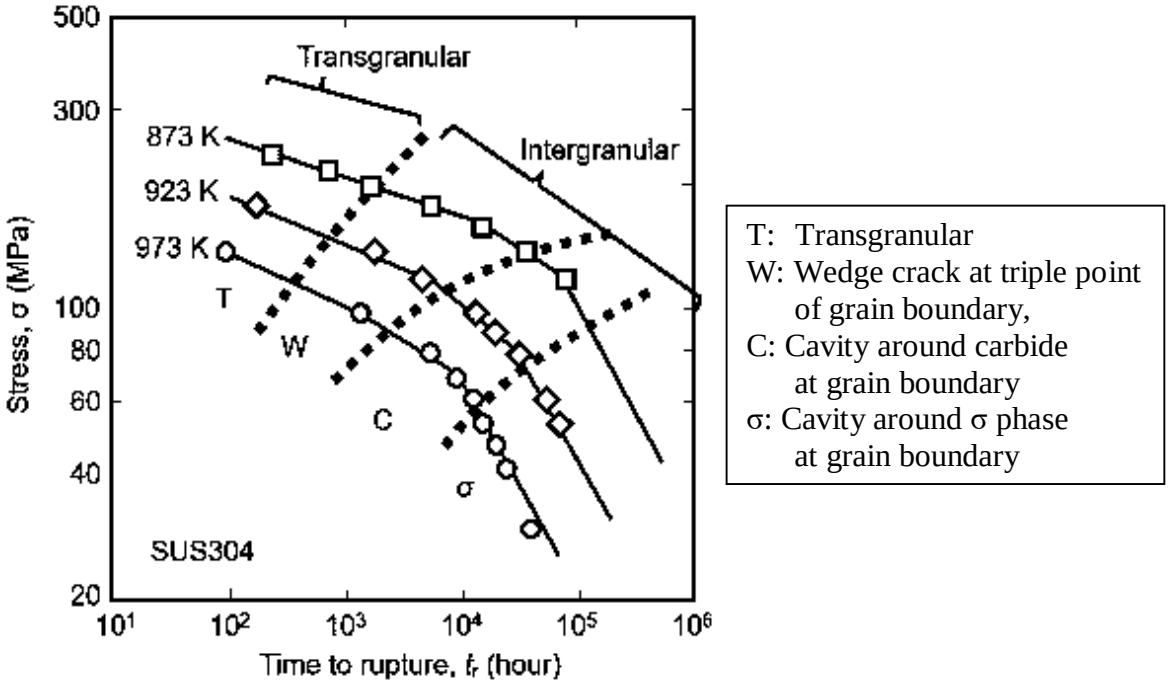

Figure 1.11 Creep fracture mechanism map of SUS304 steel [1.26]. Redrawn by author.

1.3 High temperature hydrogen attack (HTHA)

Regarding the degradation of carbon-strengthened materials, e.g. steels, in high-temperature hydrogen, one of the most prominent failure mechanisms is high-temperature hydrogen attack (HTHA) [1.30-1.33]. The mechanistic ingredients of HTHA have already been well established [1.30-1.33]. Also, an empirical design method against HTHA has been implemented [1.34, 1.35]. The Nelson curves predict HTHA based on process temperature, hydrogen partial pressure and material of construction, although it does not account for material microstructure and applied stress.

However, a fatal accident was caused by HTHA in 2010 [1.36]. A heat exchanger in the Catalytic Reformer/Naphtha Hydrotreater unit ruptured because of HTHA. The investigation of the incident showed that the heat exchanger ruptured was estimated to have operated at a temperature below the applicable Nelson curve. It was concluded that the Nelson curve for this carbon steel is inaccurate and cannot be relied in terms of prevention of HTHA. This incident suggested an industry-wide problem with the Nelson curve for carbon steels. After this accident, studies of HTHA were reactivated [1.37, 1.38].

1.4 Past studies on creep in hydrogen

Regarding the study on creep in hydrogen, I can find some papers [1.39-1.47].

Yokogawa et al. carried out experiments of ASTM A387 Grade 22 welded boiler and pressure vessel steel, JIS SUS304 austenitic stainless steel and JIS SUY electromagnetic iron at 773 K and 823 K in the short creep life region and published the results in the 1980s-90s [1.39-1.42]. Regarding SUS304 austenitic stainless steel shown in Fig. 1.13 [1.42], they showed a reduction in the creep life in hydrogen and an increase in the creep elongation at failure. They concluded that the mechanism of this degradation was hydrogen-related carbide formation based on the observation of the carbide. The shape of the grain boundary carbides was plate-shaped in hydrogen and spheroidal-shaped in argon. They inferred that hydrogen reduced the interfacial energy of the carbide and hydrogen affected the dynamic precipitation of carbides at grain boundaries. Then the plate-shaped carbides might result in the reduced creep life.

The SUY also showed reduced creep life by hydrogen as shown in Fig. 1.14 [1.40]. In this creep test, the creep elongation was decreased in hydrogen. They reported that SUY contained a small amount of carbon, and that carbon produced methane bubbles on the grain boundaries. As a result, the creep life of the SUY was reduced in hydrogen. This inference was the same as the mechanism of HTHA.

Was et al. carried out creep tests of Ni-16Cr-9Fe alloy and other Ni-Cr-Fe alloys in a high-pressure and high-temperature water environment at 633K [1.43-1.45] for nuclear reactors. They reported that hydrogen enhanced power-law creep was observed and it resulted in the reduced creep life (Fig. 1.15) [1.43]. They showed that hydrogen increased

the percentage of intergranular cracking. In addition, they discussed the mechanism of the reduced creep life based on hydrogen-enhanced localized plasticity (HELP) [1.43-1.45].

Schuster et al. investigated the creep properties of 75Ni-25Fe, 50Ni-50Fe, and 25Ni-75Fe alloys and Ni and Fe pure metals in helium and hydrogen [1.46]. The gas pressure was held at 28 kPa above atmospheric pressure and temperatures were 898 K, 1073 K and 1198 K. They showed reductions in creep life and ductility in hydrogen as shown in Fig. 1.16 [1.46]. According to their experiments, hydrogen caused an earlier transition into tertiary creep compared to the behavior in helium, while the primary and secondary creep rates were not affected by the test atmosphere. They considered mechanisms for how hydrogen affected the creep life from the viewpoints of hydrogen attack, hydrogen-increased diffusivity of Fe and Ni atoms, hydrides, interactions between interstitial hydrogen and dislocations and hydrogen-lowered surface energy. However, they concluded that none were entirely consistent with their experimental results.

McCoy and Douglas carried out creep testing of type 304 stainless steel in various environments including hydrogen at 1089 K and 1200 K [1.47]. They revealed that the creep life of the type 304 stainless steel in hydrogen was reduced compared to that in air at 1200 K (Fig. 1.17), while it was equivalent to that in argon at 1089 K. Based on the results that hydrogen was deleterious at higher temperature, they postulated that removal of carbon by hydrogen reduced the creep life.

Table 1.1 summarizes the testing conditions, results and mechanisms argued in these papers. According to this table, it is similar that the creep life is reduced by hydrogen. However, an opposite trend is found in the effect of hydrogen on creep elongation. The mechanisms argued were different between papers. The current mechanistic insight on the

creep in hydrogen is undeveloped. The study of creep in hydrogen is required for emerging high-temperature hydrogen technologies.

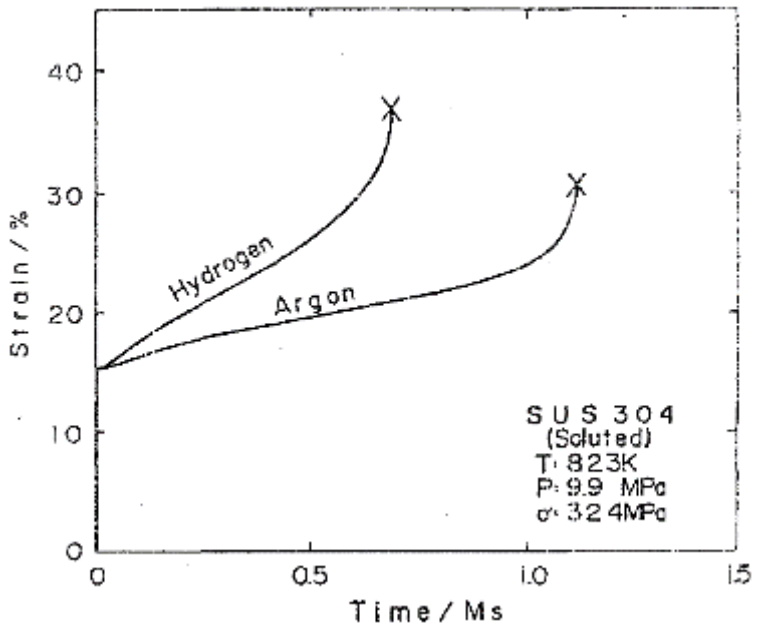

Figure 1.13 Creep curves of SUS304 in hydrogen obtained by Yokogawa, et al. [1.42].

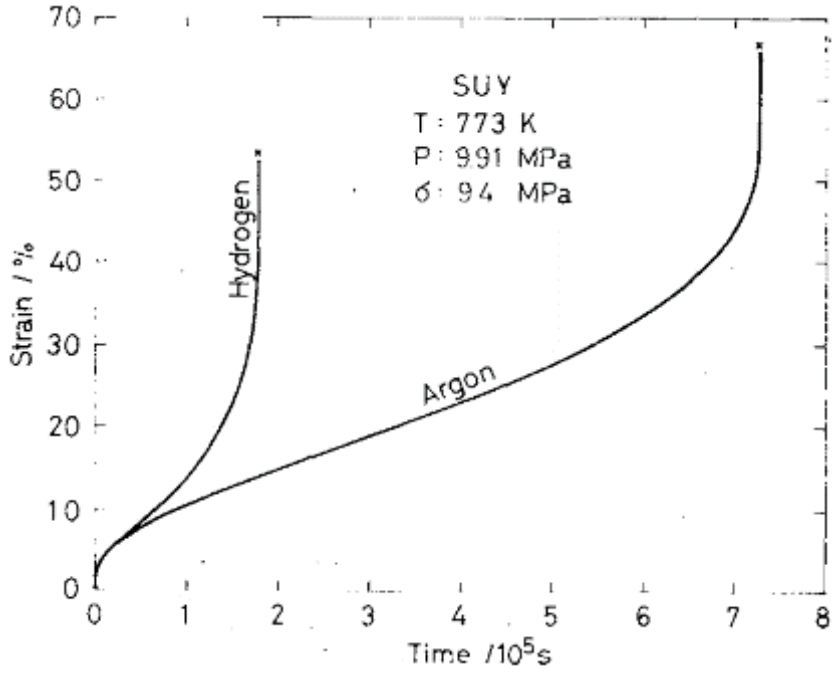

Figure 1.14 Creep curves of SUY in hydrogen obtained by Yokogawa, et al. [1.40].

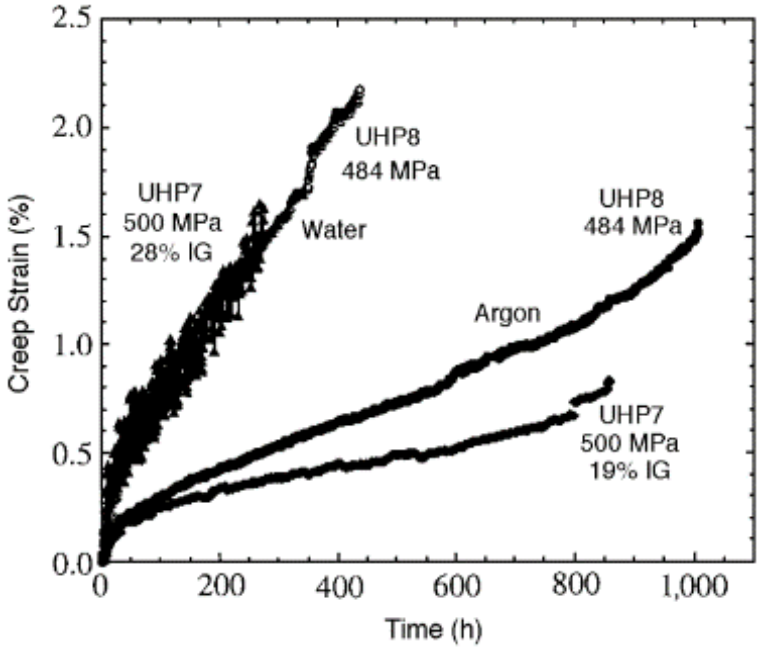

Figure 1.15 Creep curves of Ni-Cr-Fe alloy in water obtained by Was, et al. [1.43].

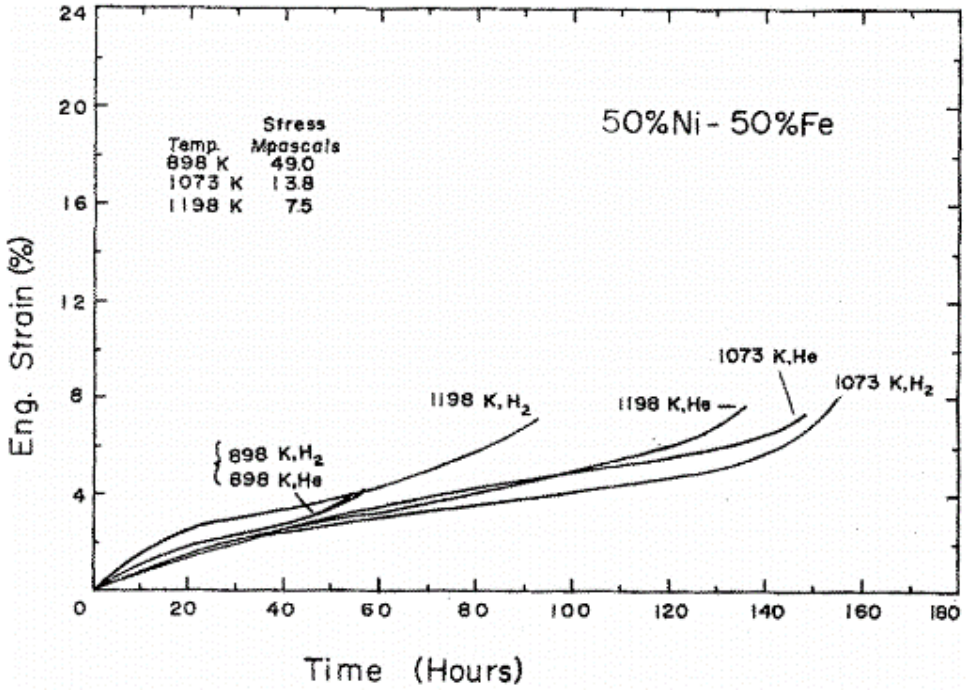

Figure 1.16 Creep curves of 50%Ni-50%Fe in hydrogen obtained by Schuster, et al. [1.46].

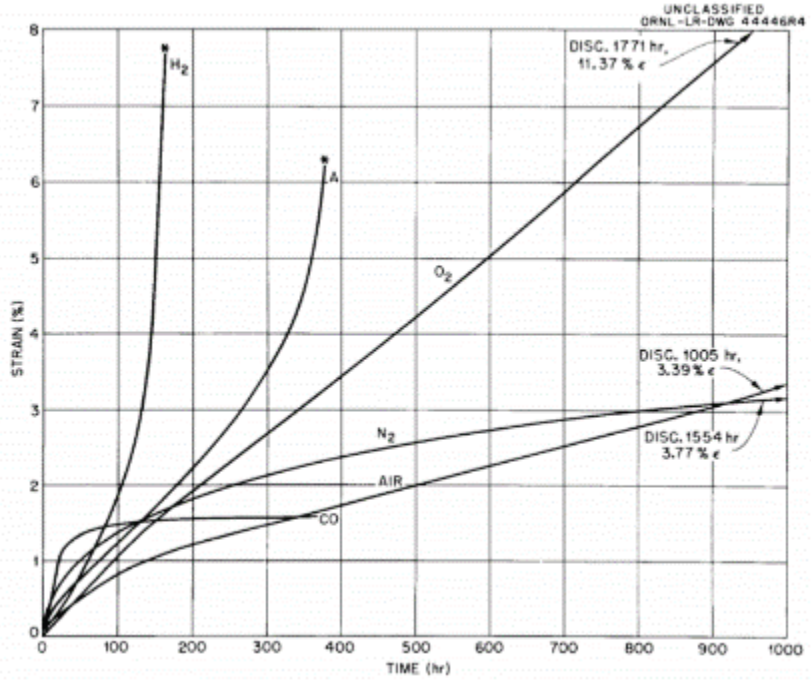

Figure 1.17 Creep curves of 304 stainless steels in hydrogen obtained by McCoy and Douglas. [1.47].

Table 1.1 Past studies on creep in hydrogen.

Authors	**Target devices**	**Material**	**Temperature, *T* Gas pressure, *p***	**Hydrogen effect on creep properties**	**Mechanism considered**
Yokogawa et al. [1.42]	Hydrogen-energy conversion devices Aerospace	SUS304	T = 823 K p = 9.9 MPa	Reduction in the creep life Acceleration of the creep rate Increase in the creep elongation	Effect of hydrogen on the carbide formation
Yokogawa et al. [1.40]	Petro-chemical	SUY	T = 773 K p = 9.91 MPa	Reduction in the creep life Acceleration of the creep rate Decreased creep elongation	Decarburization
Was et al.[1.43]	Nuclear reactor	Ni-16Cr-9Fe	T = 633 K (in 19.9 MPa water)	Reduction in the creep life Acceleration of the creep rate Increase in the IG cracking	Hydrogen-enhanced localized plasticity (HELP)
Schuster et al. [1.46]	Broad hydrogen applications	x%Ni-y%Fe x = 0, 25, 50, 75, 100 %	T = 898, 1073 and 1198 K p = 28 kPa	Reduction in the creep life Early transition to the tertiary creep No change in the creep elongation	Not revealed (Excluded mechanisms are described in Chapter 1.4)
McCoy and Douglas [1.47]	Fuel element capsules in Experimental Gas-Cooled Reactor	304 stainless steel	T = 1089 and 1200 K p = 8.27 MPa	(T = 1089 K): No effect of hydrogen (T = 1089 K): Decrease in the creep life	Decarburization

1.5 Objective of this study

As described in the previous subsection, the study on the creep in hydrogen has not achieved a sufficient level of understanding of the phenomenon and mechanisms. As shown in Table 1.1, multiple possible mechanisms for hydrogen-affected creep were argued. However, there is no definitive conclusion on the mechanism. The creep data in high-temperature hydrogen is also very limited.

Based on these situations, the objective of this study is to derive mechanistic insight into the degradation of metals in high-temperature hydrogen in order to enable the safety of evolving hydrogen technologies that operate at elevated temperature. Particularly, this study tried to concretely establish how hydrogen affects creep mechanisms for SUS304 stainless steel.

1.5 References for Chapter 1

1. International Energy Agency (IEA), “Market Report Series: Energy Efficiency 2018 *Analysis and Outlooks to 2040*”, 2018
2. International Energy Agency (IEA), “System Integration of Renewables – An update on Best Practice”, 2018
3. Kyushu Electric Power Company, “Past output control results” (2020), https://www.kyuden.co.jp/td_power_usages/out_ctrl_history.html
4. Agency for Natural Resource and Energy, Ministry of Economy, Trade and Industry, Japan, “Fukushima Hydrogen Energy Research Field (FH2R)”, 2018, https://www.enecho.meti.go.jp/about/special/johoteikyo/fukushimasuiso.html
5. Ministry of Economy, Trade and Industry, Japan, "Basic Hydrogen Strategy", 2017
6. Ministry of Economy, Trade and Industry, Japan, "Strategy for Developing Hydrogen and Fuel-Cell Technologies", 2019
7. Ministry of Economy, Trade and Industry, Japan, "Fifth Basic Energy Plan", 2018
8. Ministry of Economy, Trade and Industry, Japan, "Strategic Roadmap for Hydrogen and Fuel Cells", 2019
9. “French National Hydrogen Strategy”, France, 2018
10. “Korea Hydrogen Economy Roadmap”, Korea, 2019
11. R. Peters, R. Deja, M. Engelbracht, M Frank, V.N. Nguyen, L. Blum, D. Stolten, “Efficiency analysis of a hydrogen-fueled solid oxide fuel cell system with anode off-gas recirculation”, *Journal of Power Sources*, Vol. 328, 2016, pp. 105-113
12. H. Ghezel-Ayagh, Brian P. Borglum, “Review of Progress in Solid Oxide Fuel Cell at Fuel Cell Energy” *ECS Transactions*, Vol. 80, 2017, pp. 47-56
13. V. Hacker, S. Matsushima, “Fuel Cells and Hydrogen”, 1st ed. 2018, pp.1-13
14. F.A. Leckie, D.R. Hayhurst, “Creep rupture of structures”, *Proceedings of the royal society* A, 1974

15. I.A. Shibli, S.R. Holdsworth, G. Merckling, “Creep and Fracture in High Temperature Components: Design and Life Assessment Issues”, (London, Europian Creep Collaborative Committee, 2005), pp. 3-58
16. “In-flight engine failure involving Sikorsky S-76C helicopter, VH-EXU” Australian Transport Safety Bureau, AO-2013-124, 2016
17. A.J. McEvily, “Metal Failures – Mechanisms, Analysis, Prevention”, 2nd ed. (John Wiley & Sons, Inc., 2013)
18. The Society of Materials Science, Japan “Strength and Fracture of Materials”, 4th ed. 2011, pp. 144-169
19. The Society of Materials Science, Japan “High Temperature Strength of Materials”, 3rd ed. 2016, pp. 63-120
20. S. Kikuchi, M Adachi, “Basic of deformation at high temperature”, *Zairyo,* Vol. 30-328, 1981, pp. 94-144
21. H.J. Frost, M.F. Ashby, “Deformation-mechanism maps: the plasticity and creep of metals and ceramics”, (Oxford: Pergamon Press, 1982), pp. 60-70
22. F.K.G. Odgvist, “Mathematical theory of creep and creep rupture”, (ed. G. Temple, I.M. James, Oxford, Clarendon press., 1966), pp. 5-7
23. M.F. Ashby, R.A. Verrall, “Diffusion-accommodated flow and superplasticity”, *Acta Metallurgica,* Vol. 21, 1973, pp. 149-163
24. M.D. Paoli, M. Bennett, “Microscopic Rheological Deformation of the Lithosphere”, chapter 2.4, 1979
25. O.D. Sherby, J. Weertman, “Diffusion-controlled dislocation creep: A defence”, *Acta Metallurgica,* Vol. 27, 1979, pp. 387-400
26. H. Nakakuki, K. Maruyama, H. Oikawa, K. Yagi, “Collective Evaluation of Temperature Life in Austenitic Stainless Steels”, *Tetsu-to-Hagane,* Vol. 81, 1995, pp. 64-68
27. NIMS Creep Data Sheets No. 1. Tokyo, Tsukuba, National Institute for Materials Science, 2007

28. F. Abe, “Creep-resistant steels”, ed. F. Abe, T-U Kern, R. Viswanathan, (Boca Raton: CRC Press, 2008), pp. 1-14
29. NIMS, Press Release, “New World’s Record for Longest Creep Test Data is Expected!”, https://www.nims.go.jp/eng/news/press/2011/02/p201102240.html, 2011
30. A.A. Sagüés, B.O. Hall, H. Wiedersich, “On the Mechanisms of Hydrogen Attack”, *Scripta Metallurgica*, Vol. 12, Issue 3, 1978, pp. 319-326
31. P.G. Shewmon, “Hydrogen Attack of Pressure-Vessel Steels”, *Materials Science and Technology*, Vol. 1, 1985, pp. 2-11
32. M. McKimpson, P.G. Shewmon, “Initial Hydrogen Attack Kinetics in a Carbon Steel”, *Metallurgical Transactions A*, Vol. 12A, 1981, pp. 825-834
33. L.C. Weiner, “Kinetics and Mechanism of Hydrogen Attack of Steel”, *CORROSION*, Vol. 17, No. 3, 1961, pp. 137-143
34. G.A. Nelson, “Hydrogenation Plant Steels”, in *Hydrogen Damage*, ed. C.D. Beachem, (Metals Park, OH: American Society for Metals, 1977), pp. 377-397
35. API Technical Report 941, The Technical Basis Document for API RP 941, 2008, pp. 127
36. “Investigation Report – Catastrophic Rupture of Heat Exchanger,” U.S. Chemical Safety and Hazard Investigation Board, 2010-08-I-WA, 2014
37. M.L. Martin, M. Dadfarnia, A. Nagao, S. Wang, P. Sofronis, “Enumeration of the hydrogen-enhanced localized plasticity mechanism for hydrogen embrittlement in structural materials”, *Acta Materialia*, Vol. 140, 2017, pp. 300-304
38. M. Dadfarnia, M.L. Martin, D.E. Moore, S.E. Orwig, P. Sofronis, “A model for high temperature hydrogen attack in carbon steels under constrained void growth”, *International Journal of Fracture*, Vol. 219, 2019, pp. 1-17
39. K. Yokogawa, S. Fukuyama, K. Kudo, “Apparatus for creep rupture testing in high-pressure hydrogen at elevated temperatures”, *Review of Scientific Instruments*, Vol. 53, No. 1, 1982, pp. 86-89

40. K. Yokogawa, S. Fukuyama, K. Kudo, “Effect of stress on hydrogen attack of commercial pure iron”, *Japan Inst. Metals*, Vol. 46, No. 10, 1982, pp. 1009-1017
41. K. Yokogawa, S. Fukuyama, K. Kudo, P.G. Shewmon, “Effect of hydrogen attack on tensile and creep properties of low carbon steel”, *International Journal of Pressure Vessels and Piping*, Vol. 37, Issue 5, 1989, pp. 365-385
42. K. Yokogawa, S. Fukuyama, “Hydrogen embrittlement of metallic materials”, *Hydrogen Energy System*, Vol. 22, No. 2, 1997, pp. 18-25
43. T.M. Angeliu, D.J. Paraventi, G. S. Was, “Creep and Intergranular Cracking Behavior of Nickel-Chromium-Iron-Carbon Alloys in 360°C Water”, *CORROSION*, Vol. 51, No. 11, 1995, pp. 837-848
44. D.J. Paraventi, G. S. Was, “Environmentally Enhanced Deformation of Ultra-High-Purity Ni-16Cr-9Fe Alloys”, *Metallurgical and Materials Transactions*, Vol. 31A, 2000, pp. 2383-2388
45. D.J. Paraventi, T.M. Angeliu, G. S. Was, “Effect of Hydrogen on Creep in High-Purity Ni-16Cr-9Fe Alloys at 360°C”, *CORROSION*, Vol. 58, No. 8, 2002, pp. 675-686
46. G.B.A. Schuster, R.A. Yeske, C.J. Altstetter, “The Effect of Hydrogen on the Creep Rupture Properties of Fe-Ni Alloys”, *Metallurgical Transactions*, Vol. 11A, 1980, pp. 1657-1664
47. H.E. McCoy, D.A. Douglas, “Effect of Environment on the Creep Properties of Type 304 Stainless Steel at Elevated Temperatures”, (Oak Ridge: Oak Ridge National Laboratory, 1962)

2 Development of a testing machine and testing method for material strength in high-temperature hydrogen environment

2.1 Introduction

The first challenge of the study on the material strength in high-temperature hydrogen environment was to establish the testing method. For every experiment, safety is firstly important. Particularly, the nature of hydrogen, which is flammable, the wide flammability range from 4 % to 75 % and ease of leakage, requires extra care for ensuring safety. In addition, high temperature hydrogen may cause degradation not only in the specimen but also the materials of the testing machine. In fact, there were many accidents caused by hydrogen embrittlement [2.1], high temperature hydrogen attack (HTHA) [2.2], operation errors [2.3] and ignition of hydrogen gas from another ignition sources [2.4]. Development of the testing machine that enables material testing in high-temperature hydrogen is a very big challenge itself.

Regarding the testing machine to assess material strength in hydrogen gas environment, one of the primary issues is how gas tightness is achieved. Actually, several types of gas sealing methods are used. Figure 2.1 shows a fatigue testing machine with a 99 MPa hydrogen gas chamber [2.5]. The gas tightness between the gas chamber and moving position is achieved by a sliding seal. The gas tightness increases with an increase in the contacting force between the seal material and piston or chamber. On the other hand, the increase in contacting force restricts the speed of relative motion between the seal and mating surface. Due to this trade-off relation of sealing performance and piston speed, this type of seal only allows slow loading frequency such as 1 Hz [2.5, 2.6] when the hydrogen gas pressure is very high. In addition, wear of the seal material is always a concern. Furthermore,

the temperature range at which material testing is carried out is restricted to a narrow range around room temperature since the seal material is a polymer.

Figure 2.2 shows a tension and compression loading testing machine with an atmospheric pressure hydrogen gas chamber [2.7]. The feature of this gas chamber is that a bellows is used as a chamber body. The relative displacement between the chamber and loading shaft that is caused by the motion of the loading shaft is absorbed by the deformation of the bellows. This structure allows the use of a flat copper gasket. There is no concern about leakage due to wear of the seal material, loading frequency and testing temperature. However, this structure also causes some problems. The deformation of the bellows shares the applied load to the specimen and therefore, adjustment of the testing load is required when the load is measured by a load cell installed outside of the chamber. The greatest drawback is that hydrogen pressure is limited to low values because the bellows cannot bear high pressure.

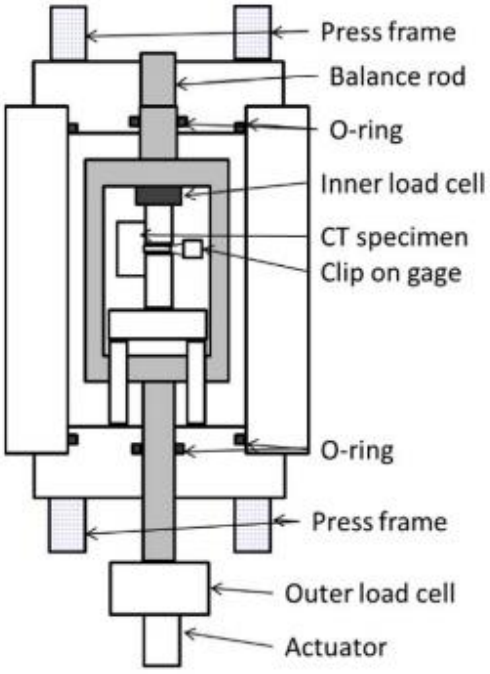

Figure 2.1. Fatigue testing machine with 99 MPa hydrogen gas chamber [2.5].

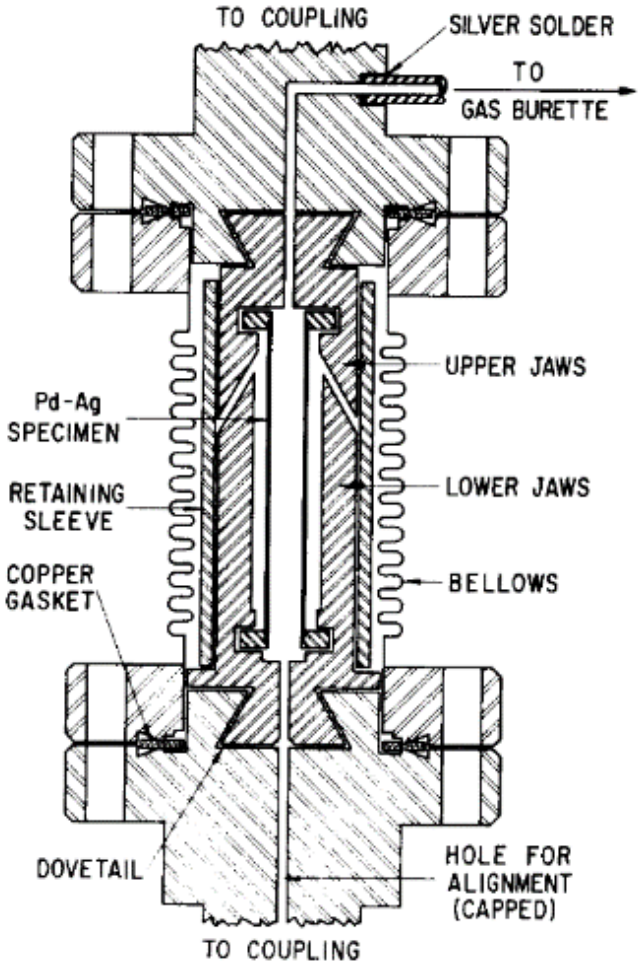

Figure 2.2. Tensile and compression testing machine with atmospheric pressure hydrogen gas chamber [2.7].

2.2 Development of the testing machine

The purpose of this chapter is to present the development of a new testing machine and establish a testing protocol for SSRT and creep testing in high-temperature hydrogen. The testing conditions aiming at the realization are as follows:

Temperature: Room temperature - 873 K

Gas pressure: vacuum - 1 MPa

Loading rate in SSRT: 10^{-5} /s

The target for the testing temperature was 873 K, as the temperature of hydrogen gas supplied to the SOFC. Also, since the SOFC operates with a relatively low gas pressure around atmospheric pressure, the gas pressure was set at 1 MPa. In order to carry out the SSRT in high-temperature hydrogen, the strain rate was set at 10^{-5} /s.

In this study, I tried two types of heating system for the hydrogen gas, which are internal and external heating. The internal heater has some merits such as better heating efficiency and uniform heating. However, it caused some problems. The external heater also has some merit, such as a smaller hydrogen chamber and more simple chamber structure. On the other hand, the heating efficiency is relatively low. As the result of the trial, I decided to use the external heater. Details of the trial are as follows.

2.2.1 Internal heating system

I made every effort to ensure the safety of the creep testing machine. For instance, the testing machine monitors hydrogen gas leakage, testing load, temperatures in the hydrogen gas chamber and heater, displacement of the actuator, gas pressure and so on. Once a problem is detected, the heater and hydrogen gas supply are shutdown. As for the mechanical protection, double explosion-proof cabinets cover the testing machine. Forced ventilation of the explosion-proof cabinets is performed. Remote monitoring is done by a web camera attached in the cabinet.

Figures 2.3 and 2.4 respectively show the photograph and structural drawing of the testing machine I developed in this study. The testing machine consists of a loading flame, actuator, loading shafts, gas chambers, bellows, gas system, temperature controller and heater. Similar to the testing machine shown in the previous figure, a bellows is used for absorbing relative displacement between the loading shaft and chamber. It enables the use of a metal gasket. Then, effective sealing of hydrogen in a temperature range from room temperature to 873 K was achieved. Observation windows are installed to the chamber for the strain measurement by the digital image correlation (DIC) method. Details of DIC are described in Chapter 2.3. The rotation of the motor is converted into a linear motion with a ball screw and a linear slider, and a load is applied to the specimen by linear motion of the loading shaft. The load applied to the specimen was measured by the load cell installed at the end of the loading shaft outside of the gas chamber. The stress of the bellows for the deformation along the loading axis is very small compared with that of the specimen. Since the load that the bellows shares with the specimen is proportional to the displacement of the bellows, the stress of the specimen was calibrated by considering this bellows load.

An important conclusion that I recognized through the development of this testing machine is that the use of an internal heater is very difficult. Originally, the creep testing machine has a heater inside of the gas chamber, as a result of considering heating efficiency and uniform heating. The heater is molded by brass.

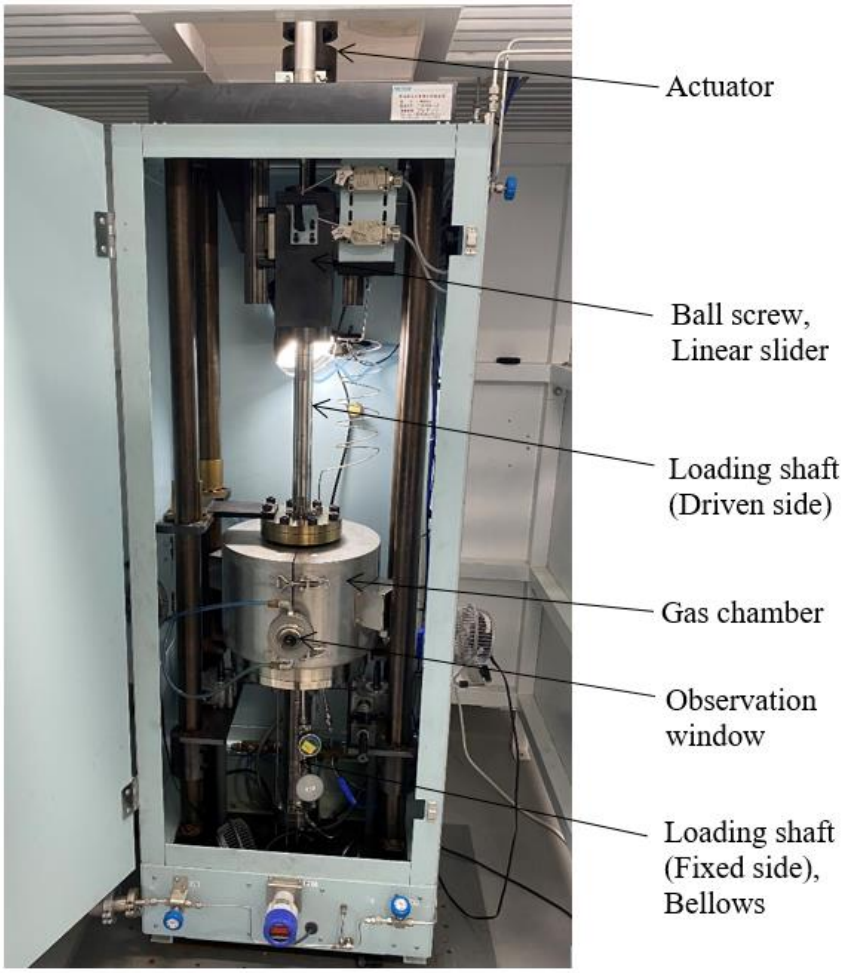

Figure. 2.3 Photograph of the testing machine.

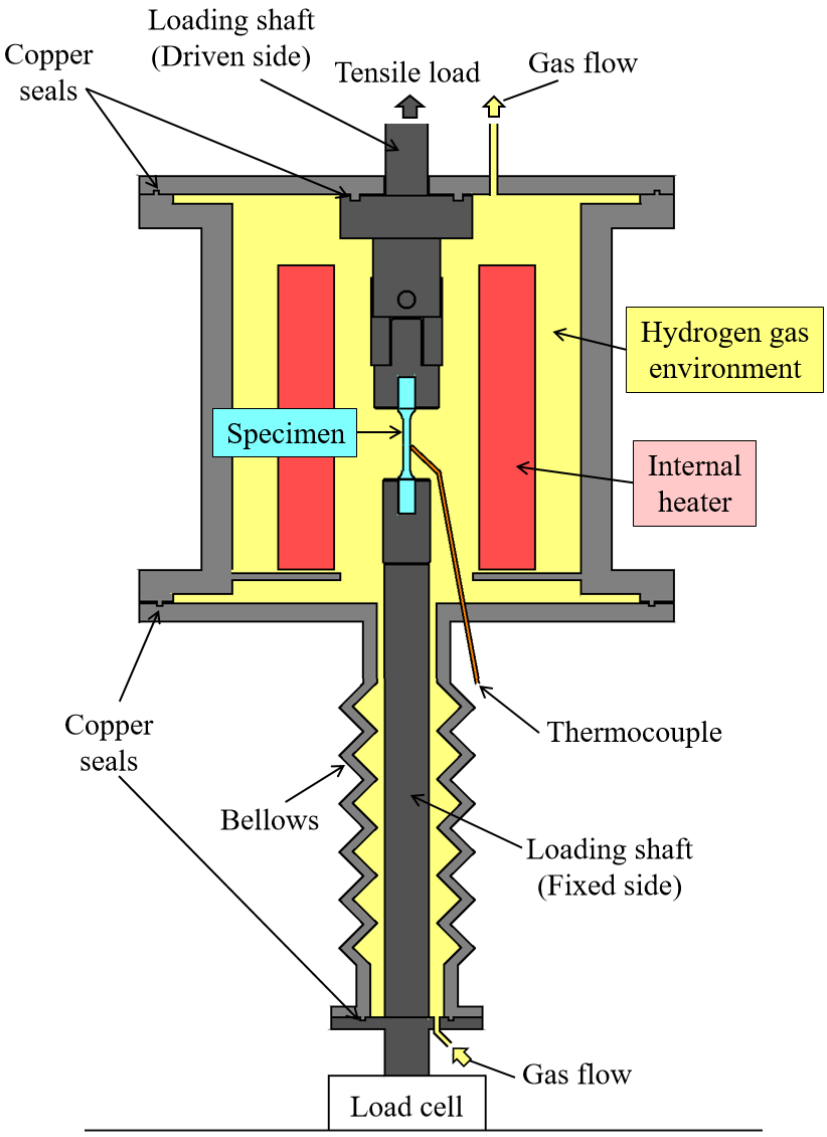

Figure 2.4 Creep testing machine firstly developed.

A tensile test of the SUS304 in Ar at 873 K was carried out as a trial run of the testing machine. I confirmed that the test was finished without any problems in terms of measurement of material strength and safety. Figure 2.5 shows the result of the tensile test in hydrogen. The material was the SUS304 stainless steel. A round bar specimen with a diameter of 4 mm and a gauge length of 30 mm was used. The temperature and hydrogen gas pressure at which the tensile test was carried out were 773 K and 0.12 MPa absolute, respectively. The strain rate was 10^{-3} /s. However, I encountered a serious problem when the tensile test in hydrogen was carried out.

The photograph of the internal heater after the tensile test in 773 K hydrogen gas is shown in Fig. 2.6. I found elusion of zinc from the brass molding of the internal heater. The brass lost its color, instead it showed the color of copper. Figure 2.7 shows the SEM observation and EDS analysis of the specimen surface after the tensile test in 773 K hydrogen gas. The surface was covered by granular-shape deposits. The EDS revealed that the deposits are made of zinc. No copper was detected on the specimen surface. It is considered that zinc caused a reaction with the hot hydrogen and transferred to the specimen. This kind of contaminations of the test environment and specimen were not allowable. In addition, zinc causes liquid metal embrittlement [2.8, 2.9]. Based on this experience, I decided changing the heating method.

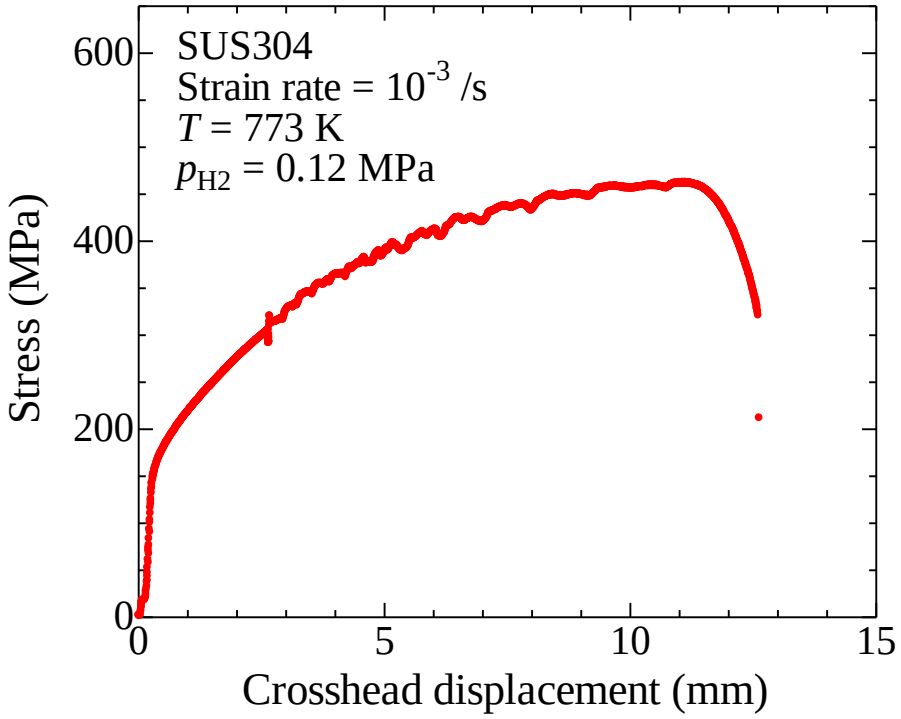

Figure 2.5 Stress-crosshead displacement curve during test run of testing machine with internal heating system.

Figure 2.6 Appearance of the brass cast-in heater installed in hydrogen gas chamber after the tensile test in hydrogen at 773 K.

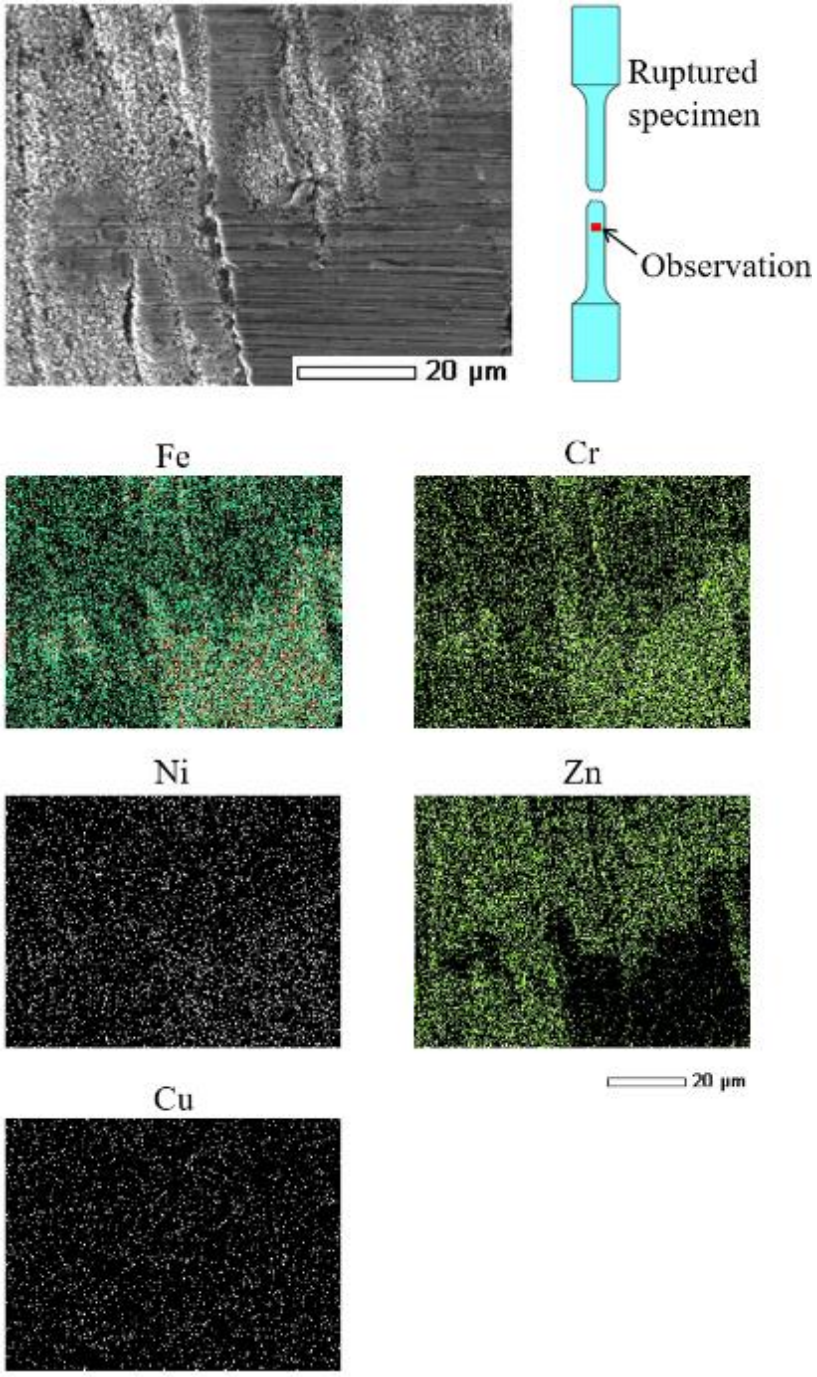

Figure 2.7 SEM image and detection results by EDS on the surface of the specimen after tensile test in 773 K hydrogen with internal heating system.

2.2.2 External heating system

Figure 2.8 shows the testing machine that has an external heater. As shown in the figure, the heater is separated from the testing environment by a stainless steel wall. Contamination of the testing environment was prevented by this structure. The target temperature, which was 873 K, was achieved although the heating efficiency was lower than the internal heating.

An SSRT of the SUS304 stainless steel was carried out in 873 K hydrogen gas at a gas pressure of 0.12 MPa as a trial run of the testing machine with the external heating system. The strain rate was 10^{-5} /s. Figure 2.9 shows the stress-crosshead displacement curve. The specimen surface after the SSRT in 873 K hydrogen gas is shown in Fig. 2.10. I confirmed a clean specimen surface.

Figure 2.11 shows the creep rupture curves obtained by Shinya et. al. [2.10]. The creep data in this thesis are also superposed to their creep rupture curves (Details of the creep test for SUS304 are described in Chapter 3). The data in this thesis are plotted on the extension line that represents Shinya's creep data. Finally, I developed the testing machine that enables creep testing in hydrogen at 873 K.

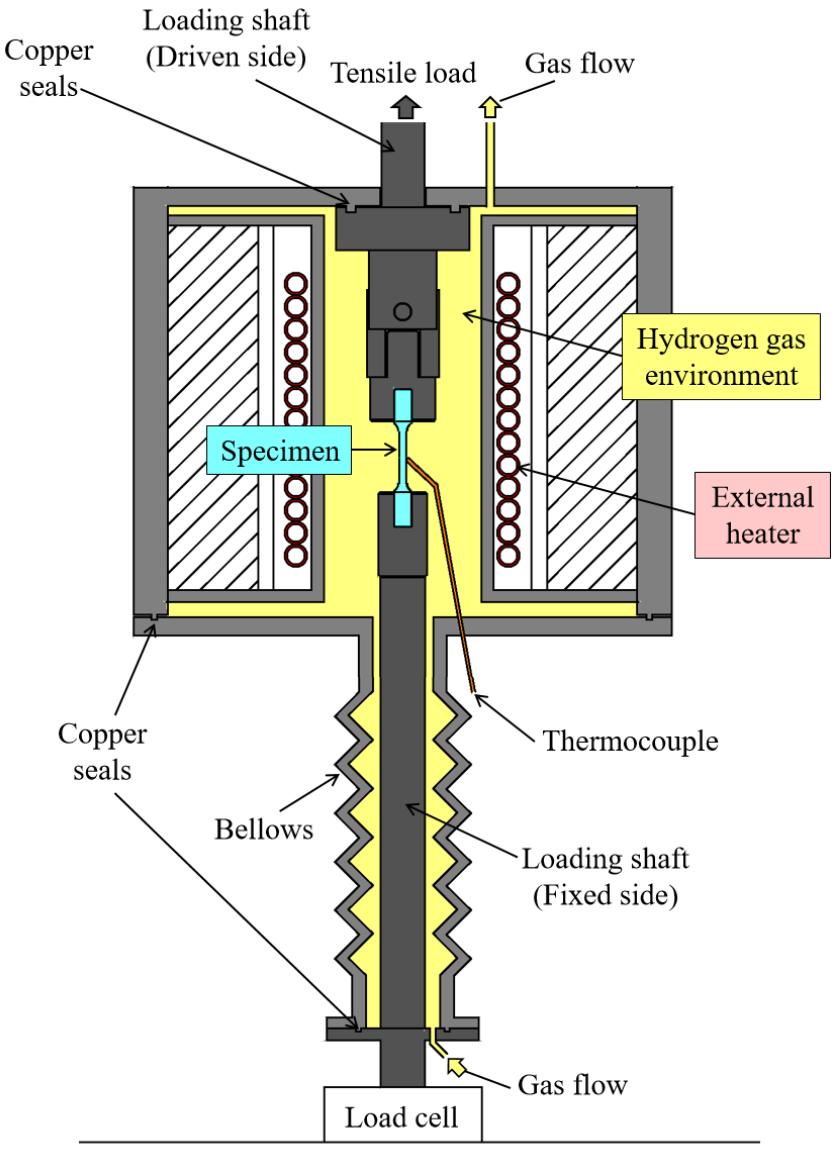

Figure 2.8 Testing machine using an external heating system.

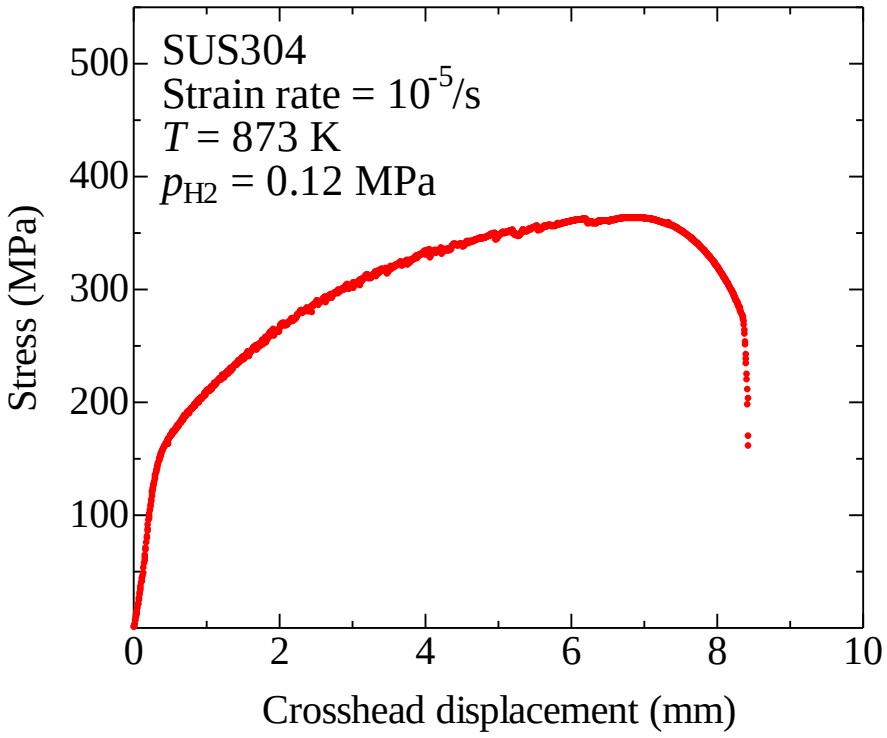

Figure 2.9 Stress-crosshead displacement curve in 873 K hydrogen gas obtained by the testing machine with the external heating system.

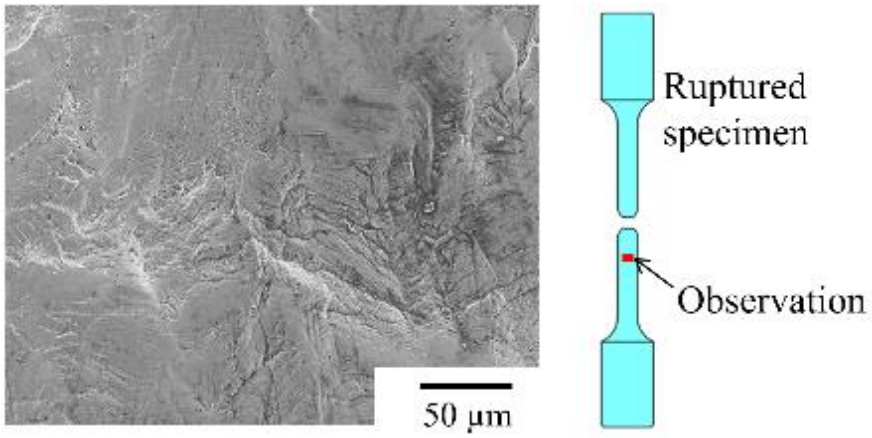

Figure 2.10 Surface of the ruptured specimen after the SSRT in 873 K hydrogen with the external heating system.

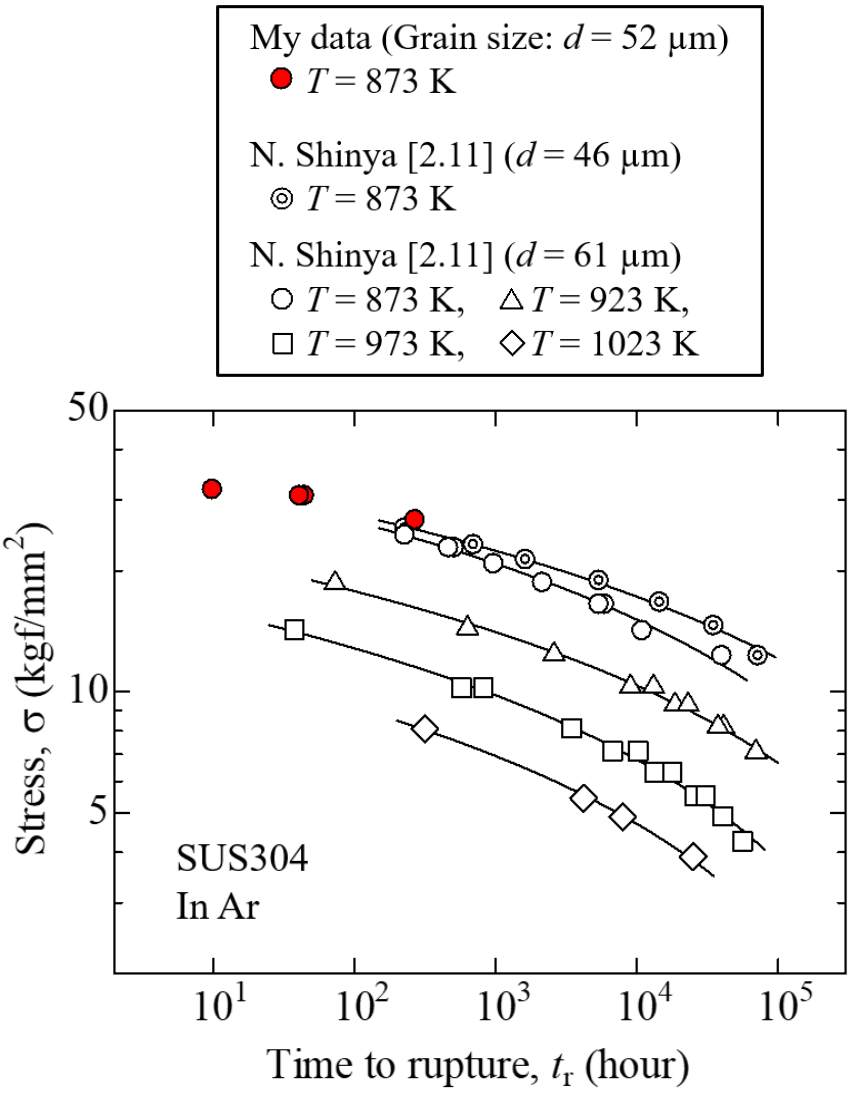

Fig. 2.11 Creep data of the SUS304 superposed on Shinya's creep rupture curves [2.10].

Redrawn by author.

2.3 Application of the Digital Image Correlation (DIC) method for strain measurement in high-temperature hydrogen

Measurement of strain is sometimes necessary and beneficial for the study on creep properties. Ogata et al. measured the strain of the specimen at high temperature with a normal displacement sensor attached outside the furnace using a long contact rod [2.11]. This method is very simple and good for the test in air. However, an extra measure is necessary to separate the testing environment and the external environment without obstructing the moment of the contact rod.

I used a Digital Image Correlation (DIC) method to measure strain during the creep tests in hydrogen instead of the contacting method. Fig. 2.12. shows the setting of strain measurement by the DIC method used in this study. Two reference points on the specimen were photographed with a high resolution digital still camera through the observation window of the hydrogen gas chamber during the testing. The strain was calculated from the distance between the two reference points. The initial distance between the two reference points was 2 mm. One of the features of this system is that a digital still camera with 24 Megapixel resolution was used for the DIC because the accuracy of the strain measurement is directly affected by the pixel size of the photograph.

An SSRT of the SUS304 stainless steel in air at room temperature was carried out in order to ensure the accuracy of the strain measurement by the DIC method. The stress-strain curve is shown in Fig. 2.13. The strain was measured by both the DIC method and strain gauge. The red plots are the data of the DIC method and the black curve is the data of the strain gauge. The strain measured by the DIC method agreed well with the data obtained

using the strain gauge. The mismatch between the strain gauge and DIC was 0.05 % of the strain value at the maximum.

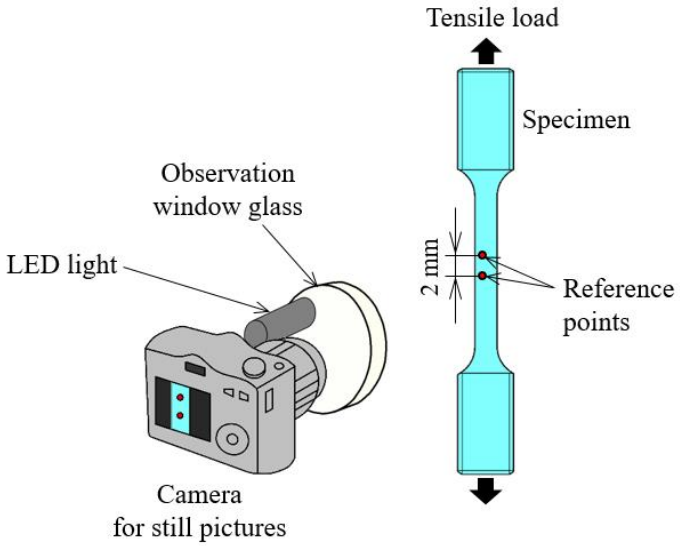

Figure 2.12 Strain measurement by the DIC method in this study.

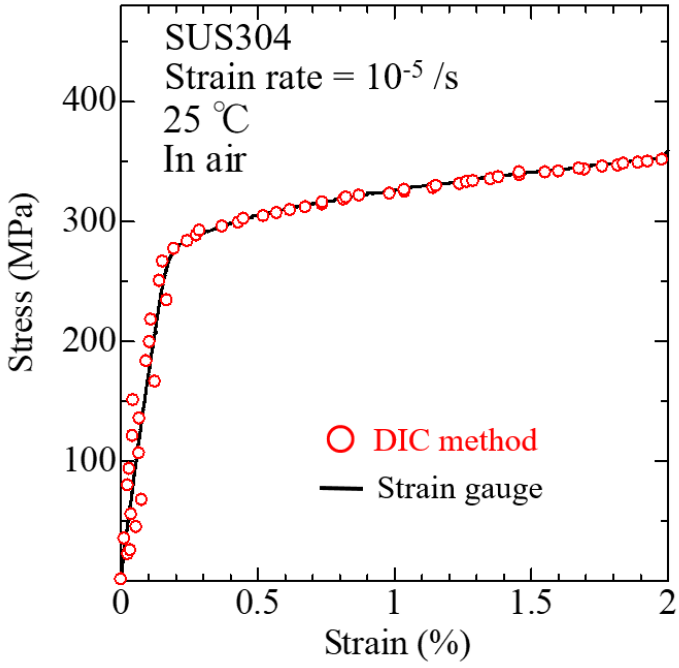

Figure 2.13 Strain measurement by the DIC method in this study.

2.4 Conclusion

Two types of heating system were tested, an internal heating system and an external one. As the result, I adopted the external heating system.

1. The internal heater molded by brass was not suitable for the experiment in high-temperature hydrogen, because zinc was separated from the brass and transferred to the specimen surface.

2. The external heater hydrogen gas chamber enabled the material testing in high-temperature hydrogen safely and without contamination.

3. The digital image correlation (DIC) method was applied to the strain measurement in high-temperature hydrogen. The accuracy of the strain measurement was 0.05 % of the strain value.

2.5 References

1. “Investigation of the Hydrogen Release Incident at the AC Transit Emeryville Facility (Revised)”, A.P. Harris and C.W. San Marchi, Sandia National Laboratories, SAND2012-8642, 2012
2. “Investigation Report – Catastrophic Rupture of Heat Exchanger,” U.S. Chemical Safety and Hazard Investigation Board, 2010-08-I-WA, 2014
3. K. Mikoda, Y. Suwa, “Analysis of the Accident Example of the Domestic Hydrogen Infrastructure in Japan”, *Hydrogen energy system*, Vol. 31, No. 1, 2006, pp. 73-78
4. “The Hindenburg Hydrogen Fire: Fatal Flaws in the Addison Bain Incendiary-Paint Theory”, A.J. Dessler, 2004
5. M. Yoshikawa, T. Matsuo, N. Tsutsumi, H. Matsunaga, S. Matsuoka, “Effects of hydrogen gas pressure and test frequency on fatigue crack growth properties of low carbon steel in 0.1-90 MPa hydrogen gas”, *Transactions of the JSME*, Vol. 80, No. 817, 2014, pp. 1-16
6. H. Matsunaga, M. Yoshikawa, R. Kondo, J. Yamabe, S. Matsunaga, “Slow strain rate tensile and fatigue properties of Cr-Mo and carbon steels in a 115 MPa hydrogen gas atmosphere”, *International journal of Hydrogen Energy*, Vol. 40, 2015, pp. 5739-5748
7. H.A. Wriedt, R.A. Oriani, “Effect of tensile and compressive elastic stress on equilibrium hydrogen solubility in a solid”, *Acta Metallurgica*, Vol. 18, 1970, pp. 753-760
8. M.H Kamdar, “Liquid Metal Embrittlement”, *Treatise on Materials Science & Technology*, Vol. 25, 1983, pp. 361-459
9. C.W. Lee, D.W. Fan, I.R. Sohn, S-J. Lee, B.C. Cooman, “Liquid-metal-induced embrittlement of Zn-coated hot stamping steel”, *Metallurgical and materials transactions A*, Vol. 43A, 2012, pp. 5122-5127

10. N. Shinya, J. Kyono, H. Tanaka, M. Murata, S. Yokoi, “Creep Rupture Properties and Creep Fracture Mechanism Maps for Type 304 Stainless Steel”, *Tetsu-to-Hagane*, Vol. 69, Issue 14, 1983, pp. 1668-1675
11. T. Ogata, K. Ishikawa, T. Yuri, O. Umezawa, “Creep and discontinuous deformation behavior of austenitic steels at cryogenic temperature”, *11th International Conference on Magnet Technology*, 1990, pp. 749-753

3 Effect of hydrogen on the creep of the SUS304

3.1 Introduction

In this chapter, the creep tests of the SUS304 austenitic stainless steel were carried out at 873 K in argon and hydrogen gas. The pressure of hydrogen at which the creep test was carried out was 0.12 MPa. According to the past studies on the creep in hydrogen, reduction in the creep life in hydrogen is reported in some studies [3.1-3.8] as described in Chapter 1. My motivation to study the creep in hydrogen is to contribute to emerging high-temperature energy conversion technologies through the study on materials. On the other hand, past studies have different objectives and different testing conditions, i.e. Was et al. [3.4-3.6] carried out the creep test of Ni-16Cr-9Fe in 19.9 MPa water at 633 K targeting a nuclear reactor, McCoy and Douglas [3.7] carried out the creep tests of type 304 stainless steel in the temperature range from 1089 K to 1200 K under gas pressures ranging from 8.3 MPa to 23 MPa targeting fuel element capsules in the Experimental Gas-Cooled Reactor (EGCR). As for the mechanism by which hydrogen affects the creep properties of austenitic alloys, the literature considered multiple and different mechanisms. However, the arguments for the mechanism are not definitive. In addition, although I consider the preheater of the SOFC system to determine the testing conditions for this study, the alloy type and temperature range related to SOFCs, e.g. SUS304 stainless steel at temperatures up to 1073 K, is not definitive. For these reasons, the objective of this study is to concretely establish how hydrogen affects creep mechanisms for the SUS304 stainless steel at the preheating temperatures relevant to SOFC operation.

3.2 Experimental procedure

The material used was JIS SUS304 austenitic stainless steel. An optical image of the microstructure in Fig. 3.1 shows austenite grains with average size 52 μm, annealing twins, and clusters of inclusions. The inclusions along the rolling direction, which is the vertical direction in the figure, were manganese sulfides and the inclusions at grain boundaries were chromium carbides.

The chemical composition of the SUS304 is shown in Table 3.1. The material was solution treated by heating at 1353 K followed by water cooling. The mechanical properties at 298 K in air are shown in Table 3.2. A tensile test was also carried out at 873 K in argon. The strain rate was the same for both tests, which was 10^{-3} /s.

The creep test of JIS SUS304L in hydrogen was additionally carried out in order to examine the mechanism, more specifically to clarify the roles of decarburization and carbide formation. The chemical composition and mechanical properties of the SUS304L at room temperature are also shown in Tables 3.1 and 3.3.

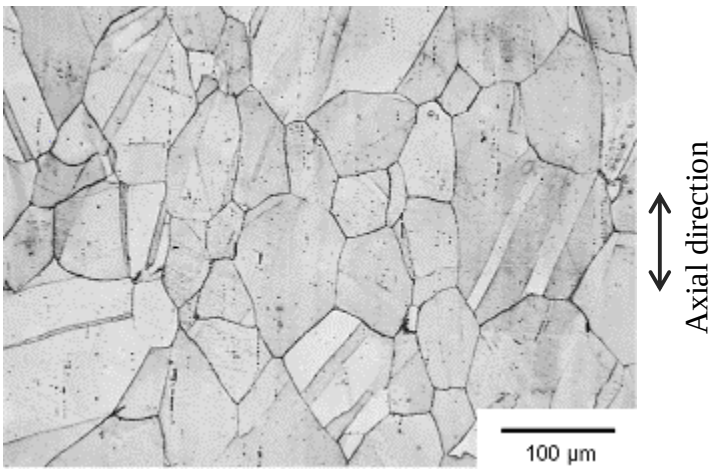

Figure 3.1. Microstructure of the SUS304.

Table 3.1. Chemical composition of test materials (mass%).

	C	Si	Mn	P	S	Ni	Cr
SUS304	0.05	0.24	1.7	0.04	0.028	8.04	18.67
SUS304L	0.013	0.04	1.04	0.03	0.020	9.44	18.04

Table 3.2. Mechanical properties of the SUS304 in argon.

Temperature of tensile test (K)	0.2% proof strength (MPa)	Ultimate tensile strength (MPa)	Elongation (%)	Reduction of area (%)
298	336	671	61	78
873	173	393	34	69

Table 3.3. Mechanical properties of the SUS304L in argon.

Temperature of tensile test (K)	0.2% proof strength (MPa)	Ultimate tensile strength (MPa)	Elongation (%)	Reduction of area (%)
298	295	613	52	74

Figure 3.2 shows the shape and dimensions of the creep specimen. A round bar specimen with a diameter of 4 mm and a gauge length of 30 mm was used. The creep testing was carried out in accordance with the JIS Z2271 standard [3.9]. The creep test was interrupted at 1000 hours if no failure occurred. The absolute gas pressure at which the creep tests were carried out was 0.12 MPa. The temperature of hydrogen and argon gas was 873 K, in accordance with the temperature of hydrogen gas supplied to SOFCs.

Figure 3.3 shows the steps for the preparation of the test environment. After vacuuming and nitrogen gas purging of the gas chamber were repeated four times, a vacuum of the chamber was kept more than 10 hours. Thereafter, following baking of the chamber at 873 K under vacuum for 2 hours, the hydrogen and argon environments were established. Prior to the start of the creep test in hydrogen, the specimen was soaked for three hours in the testing environment in order to achieve uniform hydrogen distribution across its diameter.

The hydrogen concentration, C_{H}, was calculated from the following equation [3.10]:

$$C_{\mathrm{H}} = K\sqrt{f} = K_0 \exp\left(-\frac{\Delta H}{RT}\right)\sqrt{f} \qquad (3.1)$$

where K is the hydrogen solubility, which is calculated by $K_0 = 135$ $(\frac{\mathrm{mol\ H_2}}{\mathrm{m^3\ \sqrt{MPa}}})$, $K_0 = 5.6$ $(\frac{\mathrm{kJ}}{\mathrm{mol}})$ [3.10], R is the gas constant and f is the fugacity. The saturated hydrogen concentration in my experiment (temperature, T = 873 K, fugacity, f = 0.12 MPa) was estimated at 5.3 mass ppm.

For the creep test in argon, the same soaking was applied to provide consistent thermal history to the specimen. An open gas system in which flow was continuously

maintained through the chamber during testing [3.11] was used to prevent impurity contamination of the environment. The gas flow rate was 40 mL/min.

SSRT tests were also performed on the SUS304 in accordance with ASTM G129 [3.12] at temperatures ranging from 298 K to 873 K in order to gain insight about hydrogen embrittlement mechanisms that may also have to be considered for interpreting the creep test results. The notion is that any embrittlement mechanism that may be observed during short term SSRT at elevated temperature may also operate during the long term creep tests. The specimen was soaked for three hours in the testing environment before the SSRT. The strain rate was 10^{-5} /s.

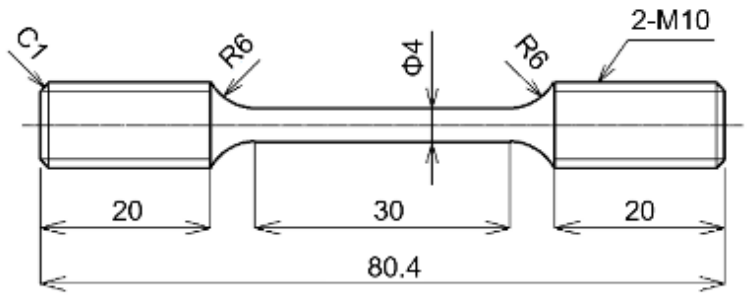

Figure 3.2. Shape and size of the creep specimen (Dimensions are in mm).

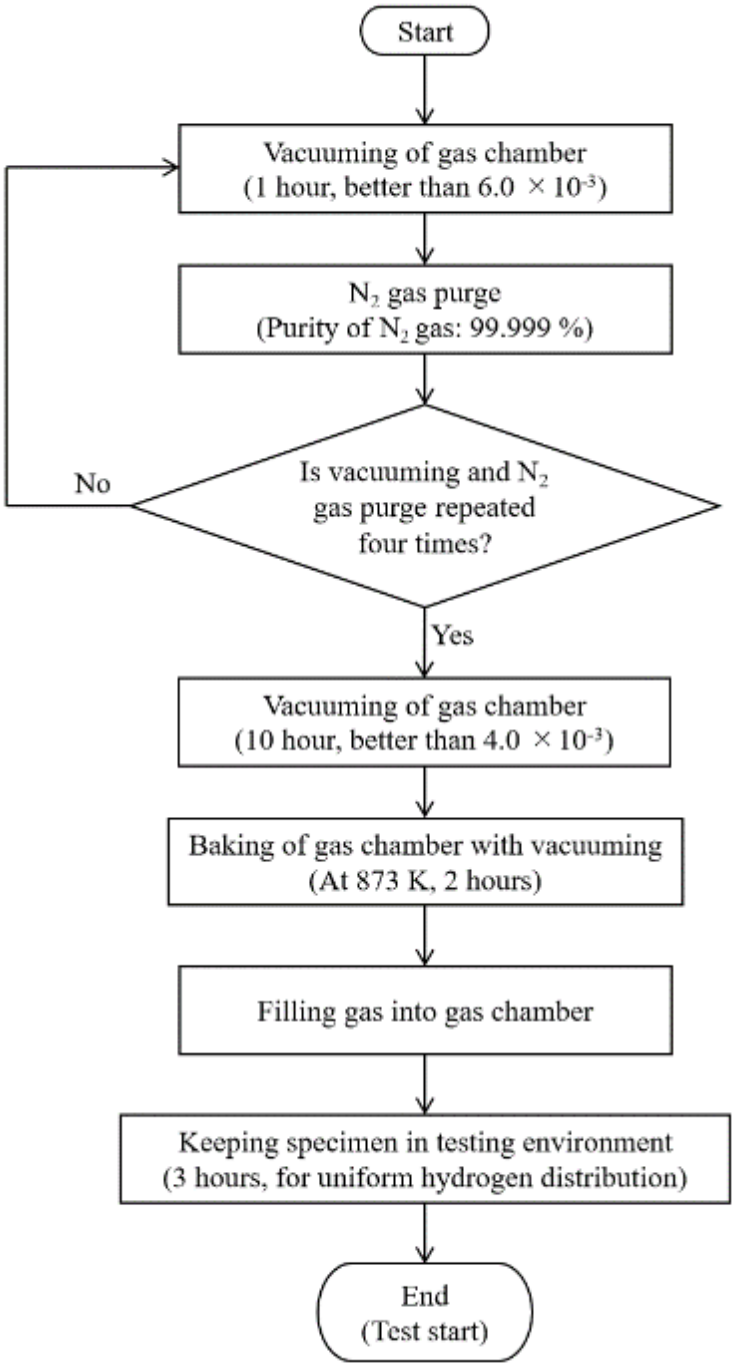

Figure 3.3. Preparation of the testing environment before the creep test.

3.3 Test results

Figure 3.4 shows the creep curves of the SUS304. The test results of the time to rupture, elongation and reduction of area are summarized in Table 3.4. The creep rate in the steady state (secondary) creep region in hydrogen was significantly increased compared to that in argon. As a result, the creep life in hydrogen was drastically reduced. Interestingly, the crosshead displacement at fracture in the creep test in hydrogen was greater than that in argon for the same creep stress.

Figure 3.5 shows the creep rupture data of the SUS304. The comparison of the creep lives between the two environments is shown in Table 3.5. The relative creep life, which is the time to rupture in hydrogen over time to rupture in argon, is shown in Table 3.5 and Fig. 3.6. The creep life in hydrogen was decreased over the entire stress range applied during the creep testing. Although creep data in argon at $\sigma = 200$ MPa were not taken because the time for the test predicted was too long, the apparent trend was that the ratio of creep life in hydrogen to that in argon decreased with decreasing applied stress. In other words, the effect of hydrogen on the creep life became more pronounced as the applied stress decreased. The results suggest the need for additional experiments particularly in the long creep life region for the design of high-temperature hydrogen equipment and components.

In Fig 3.5, the slope of the creep rupture curve changed at the applied stress of 310 MPa. The reason for the change in the slope was the difference of the mechanism creep deformation between 320 MPa applied stress and 310 MPa and lower. The detail of the creep deformation mechanism is described in Chapter 3.4.4.

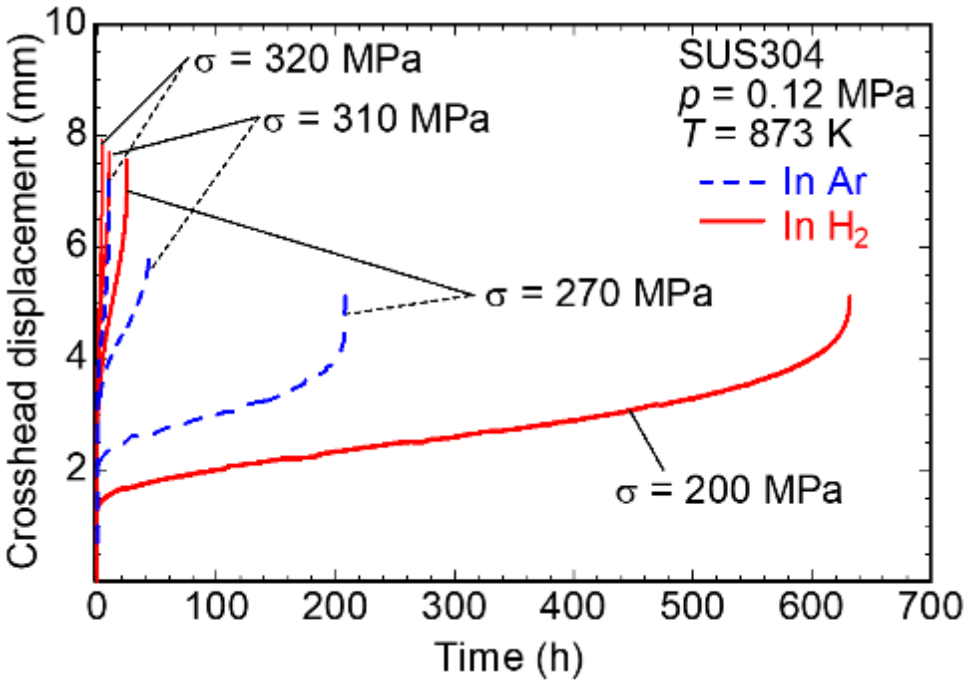

Figure 3.4 Effect of hydrogen on the creep curves of the SUS304 steel.

Table 3.4 Creep elongation and reduction of area of the SUS304.

	Stress (MPa)	Time to rupture (hour)	Elongation (%)	Reduction of area (%)	Minimum strain rate (/h)
In Ar	320	9.9	21.8	53.6	7.52×10^{-3}
	310	44.1	19.3	50.4	1.27×10^{-3}
	310	43.0	18.4	47.0	1.29×10^{-3}
	270	270.0	15.3	17.8	1.89×10^{-4}
In H_2	320	3.5	26.7	68.3	2.69×10^{-2}
	310	8.7	22.9	61.9	1.04×10^{-2}
	270	24.9	22.3	57.3	4.11×10^{-3}
	200	632.2	15.1	37.4	1.91×10^{-4}

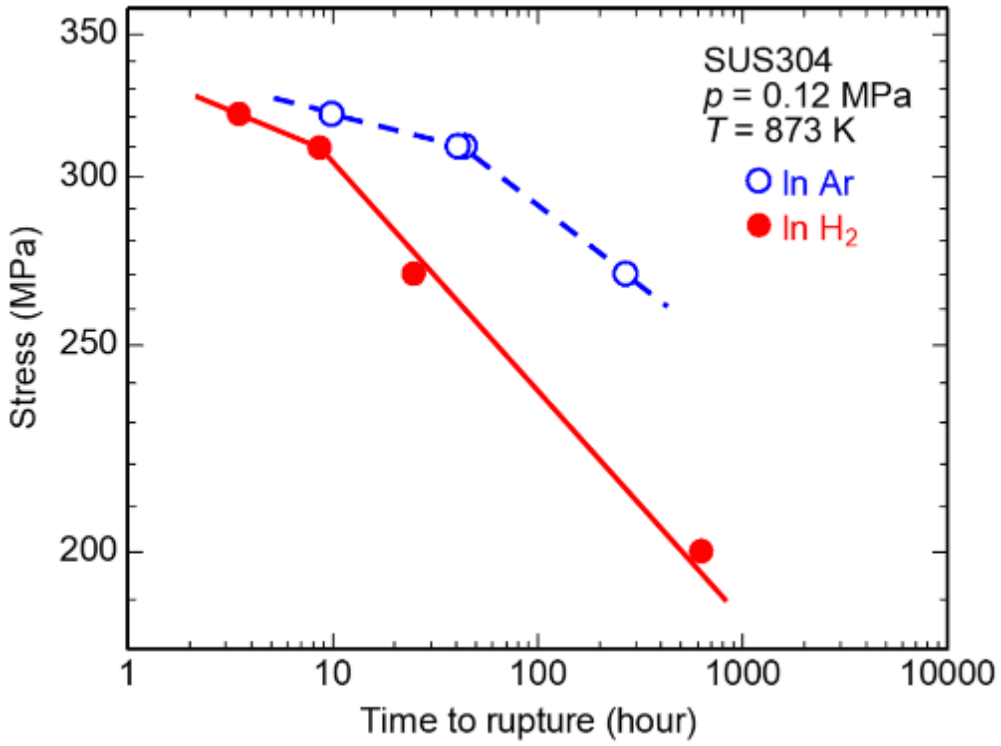

Figure 3.5 Effect of hydrogen on creep rupture of the SUS304 steel.

Table 3.5 Comparison of the creep life of the SUS304 in hydrogen and argon.

Stress (MPa)	Time to rupture, t_r (hour)		Relative creep life, $\frac{t_{r,H2}}{t_{r,Ar}}$
	In H_2, $t_{r,H2}$	In Ar, $t_{r,Ar}$	
320	3.5	9.9	0.35
310	8.7	43	0.20
270	25	208	0.12
200	632	-	-

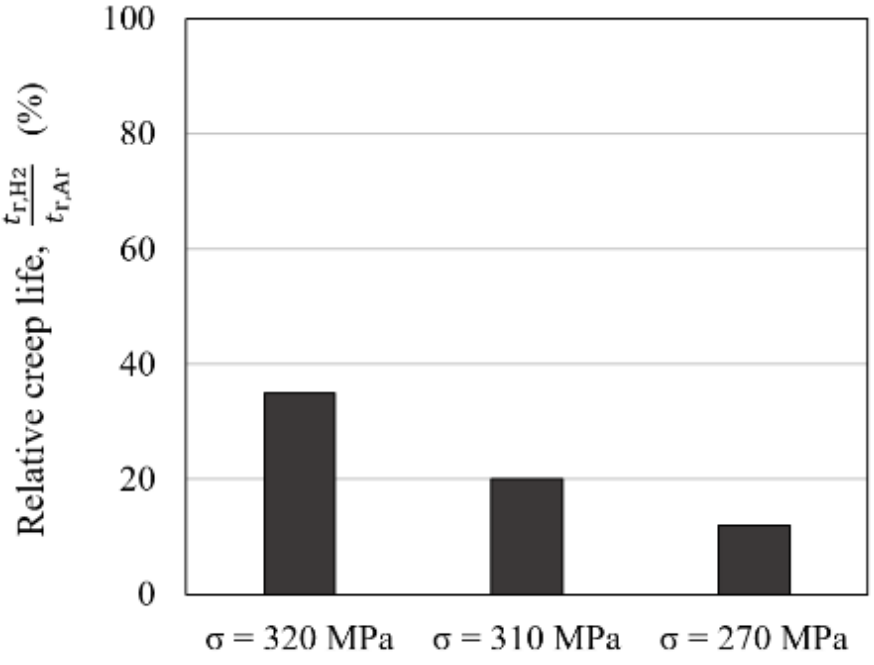

Figure 3.6 Relative creep life in hydrogen and in argon.

The results on creep response in the presence of hydrogen are similar to Yokogawa's experimental results [3.3]. The results that Yokogawa et al. obtained are shown in Fig. 3.7 [3.3]. The material was SUS304 with both the solution and sensitization heat treatment. The temperature was 823 K and the hydrogen gas pressure was 9.9 MPa. Similar to my results, the effect of hydrogen on the creep life was pronounced with increase in the creep life to a certain extent in both materials.

On the other hand, there were clear differences in the testing parameters between Yokogawa's experiment and my experiment. The hydrogen gas pressure was 9.9 MPa in Yokogawa's experiments and 0.12 MPa in my experiment. A significant reduction in the creep life was induced even when the hydrogen gas pressure was only near atmospheric. The saturated hydrogen concentration estimated following Equation (3.1) [3.10] was 46.3 mass ppm for Yokogawa's experiment and 5.3 mass ppm for my experiment.

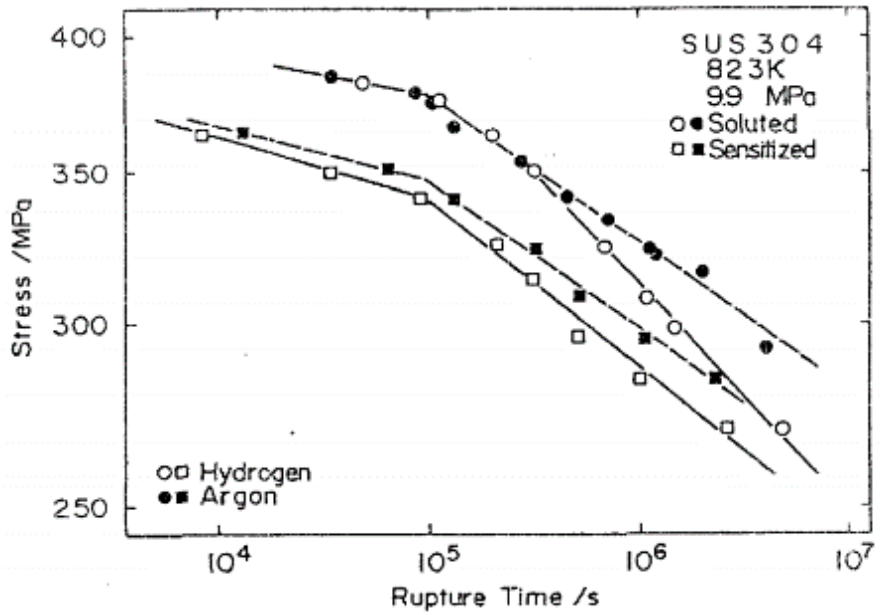

Fig. 3.7 Creep rupture curves of the SUS304 with solution and sensitization treatment in 9.9 MPa hydrogen and argon at 823 K [3.3].

Figures 3.8 and 3.9 show respectively the elongation in uniaxial tension after the creep test and the reduction of area as a function of the applied stress. Figures 3.10 and 3.11 show respectively the elongation and the reduction of area as a function of the creep life. Here, elongation was the extension of the specimen gauge length and the reduction of area was the percent contraction of the specimen cross-sectional area at the point of rupture. The elongation and the reduction of area were larger in hydrogen than in argon for both comparisons based on the applied stress and the creep life. Generally, creep elongation and the reduction of area increase with a decrease in creep life [3.13]. Even though this trend is considered, an obvious trend is that hydrogen increased creep elongation and the reduction of area.

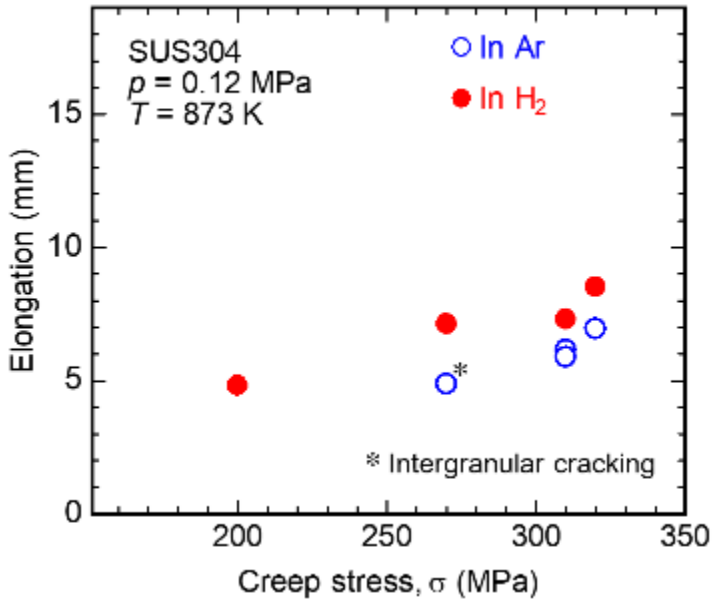

Figure 3.8 Relationship between creep elongation and creep stress.

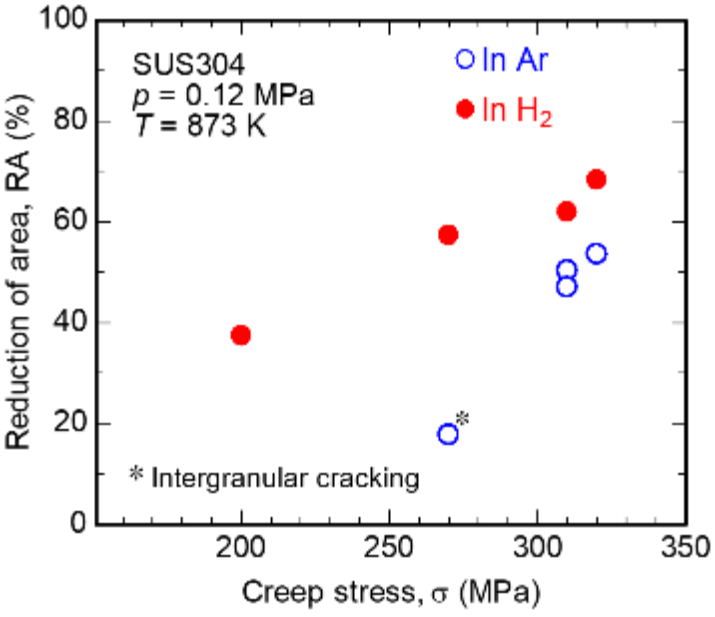

Figure 3.9 Relationship between reduction of area and creep stress.

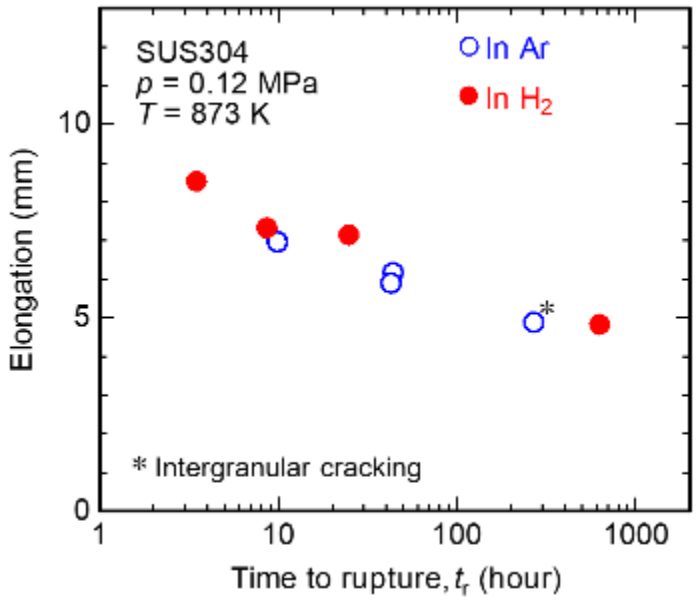

Figure 3.10 Relationship between creep elongation and creep life.

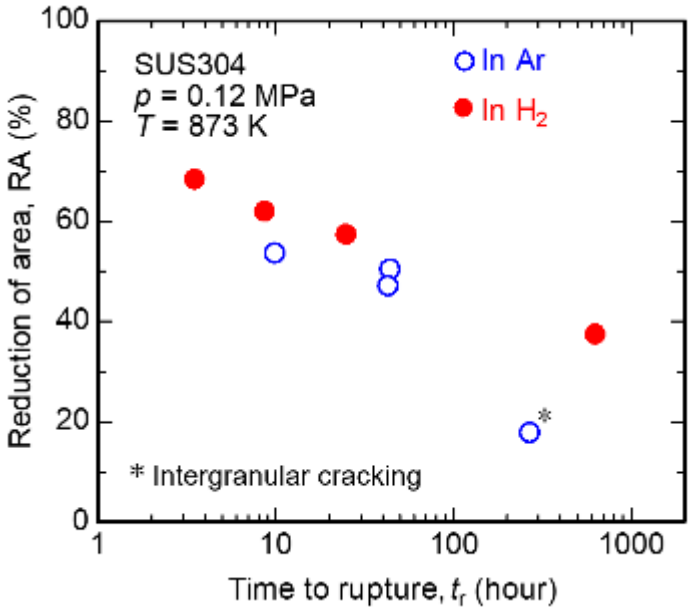

Figure 3.11 Relationship between reduction of area and creep life.

Examination of the fracture surfaces indicates that the transition of the fracture mode to intergranular cracking is delayed in hydrogen compared to argon. Figures 3.12 and 3.13 show the profiles of the fractured specimens and fracture surfaces. When the applied stress was 320 MPa, fracture surfaces in both argon and hydrogen displayed dimples resulting from microvoid coalesence.

When the applied stress was 310 MPa, the fracture surface in argon consisted of dimples and facets that resemble the signature of intergranular cracking. Figure 3.14 (a) shows a longitudinal section of the specimen ruptured at 310 MPa applied stress in argon. Cracks and voids were found along the grain boundaries. Based on this observation, I presumed that the facets on the fracture surface were created by intergranular cracking. On the other hand, the fracture surface produced in hydrogen at this stress level was totally covered by dimples.

When the applied stress was 270 MPa, the fracture surface in argon displayed predominantly facets characteristic of intergranular cracking. This kind of change in the morphology of the fracture surface depending on the stress level or creep life was typically observed in this material [3.13-3.16]. As shown in Fig. 3.12, the change in fracture mode from microvoid coalescence to intergranular cracking was reflected in the reduction of area trends. In Fig. 3.9, the reduction of area in argon decreased with decrease in the stress as shown by * in the figure. That is because the percentage of the intergranular cracking increased with decrease in the stress as shown in Fig. 3.12.

Figure 3.14 (b) shows a longitudinal section of the specimen ruptured at 270 MPa applied stress in hydrogen. Cracks were found along the grain boundaries. The fracture surface in hydrogen at 270 MPa applied stress showed both dimples and intergranular cracking.

Similarly, when the applied stress was 200 MPa, the fracture surface in hydrogen consisted of dimples and intergranular cracking. An important conclusion that I can draw from the fracture surface observations is that intergranular cracking was less prevalent in hydrogen compared to argon.

Detail observations of dimple and intergranular cracking were shown in Figs. 3.15, 3.16 and 3.17. There was no significant difference between argon and hydrogen in terms of the size and shape of dimples at any stress in the creep test. Regarding intergranular cracking, Yokogawa et al. [3.2] and Was et al [3.4] reported that hydrogen enhanced void formation at the grain boundary. In this study, as shown in Fig. 3.17, no clear evidence that microvoid formation occurred in hydrogen was found through the observation of the intergranular cracking surfaces.

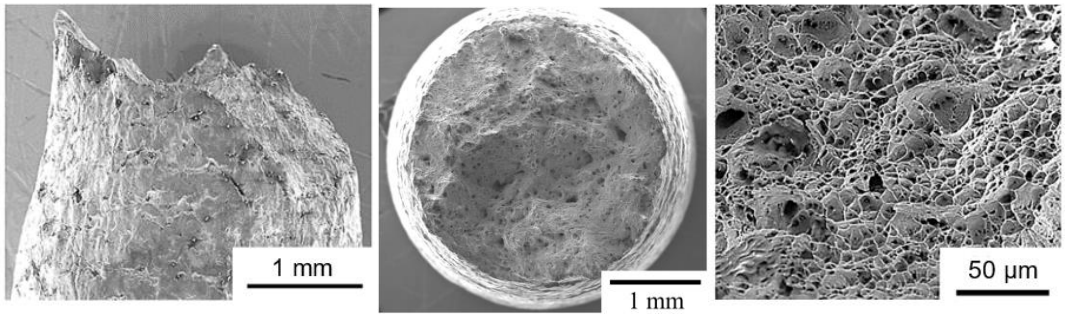

(a) σ = 320 MPa, t_r = 9.9 h

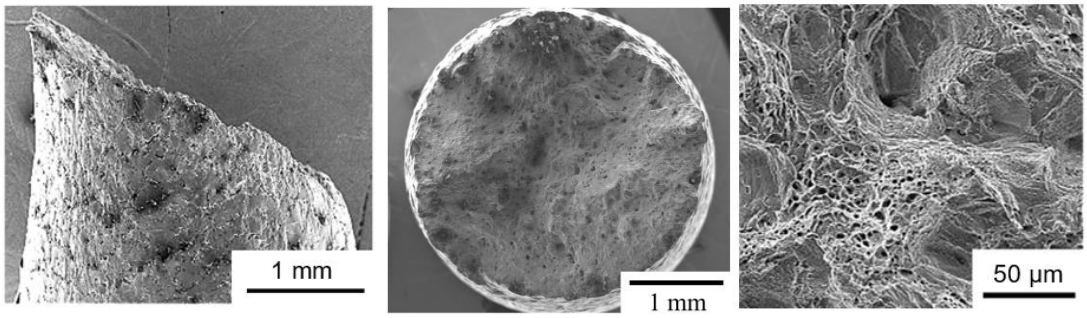

(b) σ = 310 MPa, t_r = 43 h

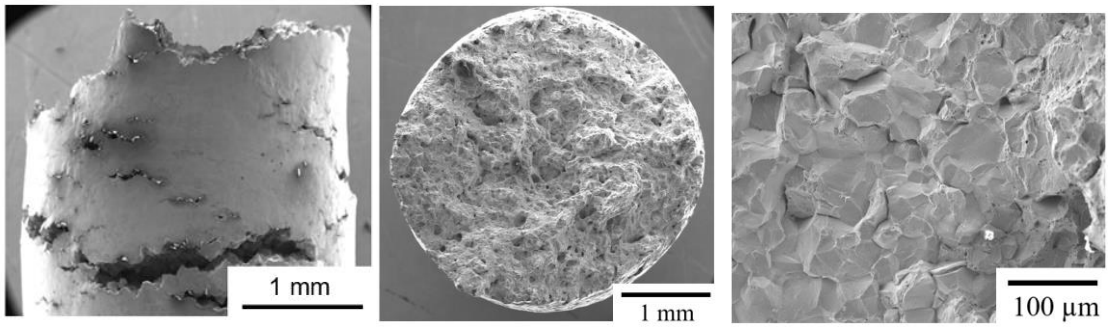

(c) σ = 270 MPa, t_r = 208 h

Figure 3.12 Fracture profiles and fracture surfaces in argon.

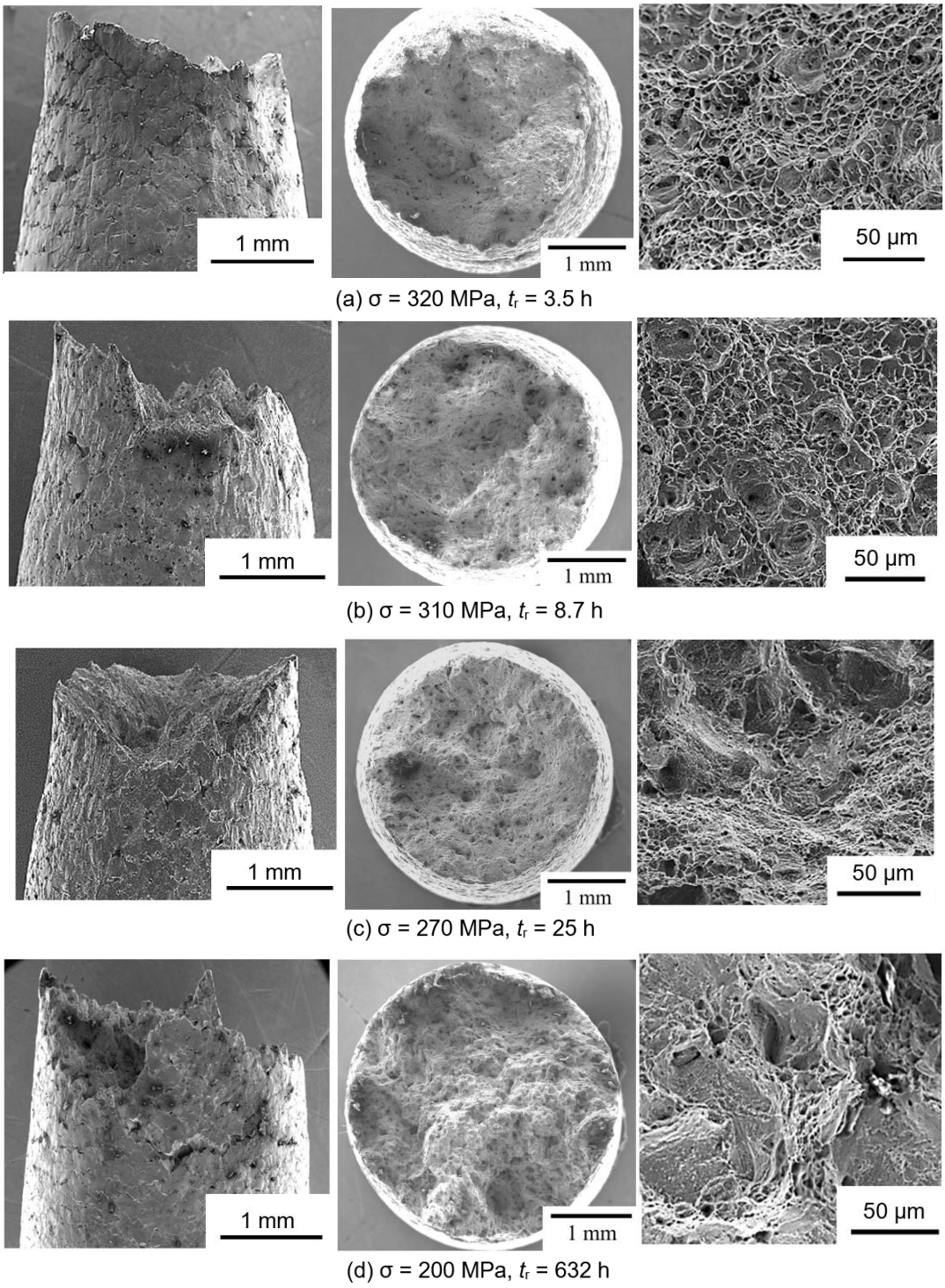

Figure 3.13 Fracture profiles and fracture surfaces in hydrogen.

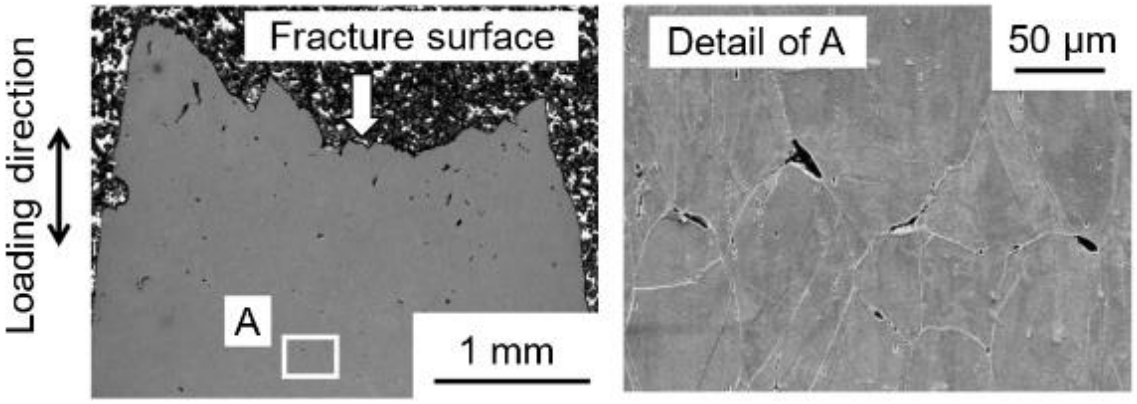

(a) In argon, σ = 310 MPa, t_r = 43 h

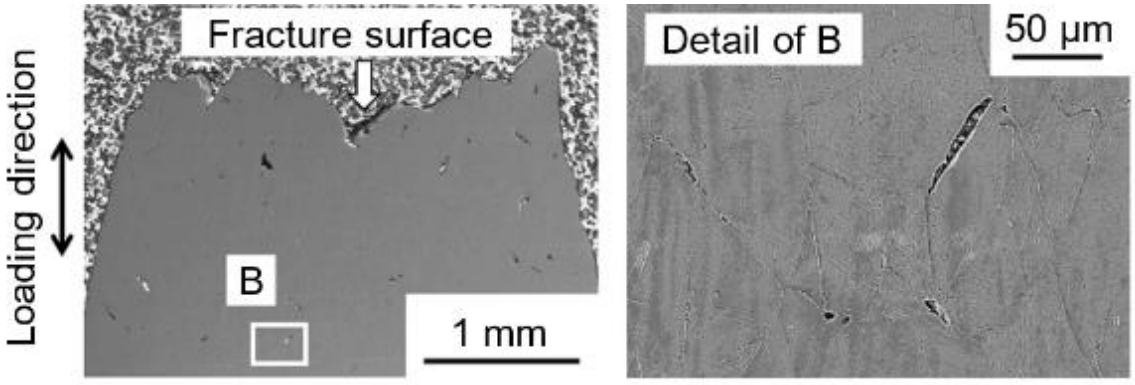

(b) In hydrogen, σ = 270 MPa, t_r = 25 h

Figure 3.14 Longitudinal section of the ruptured specimens.

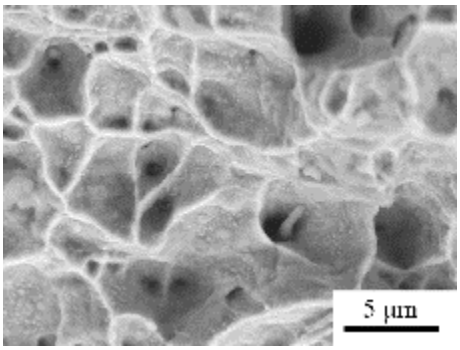

(a) σ = 320 MPa, t_r = 9.9 h

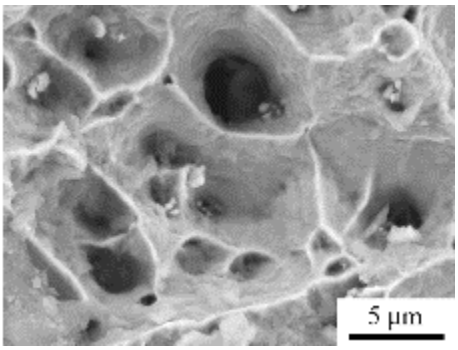

(b) σ = 310 MPa, t_r = 43 h

Figure 3.15 Detail observation of dimples and grain boundary fracture in argon.

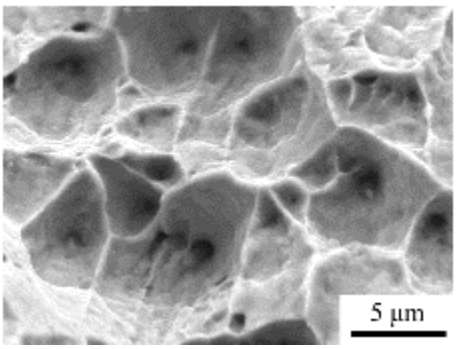

(a) σ = 320 MPa, t_r = 3.5 h

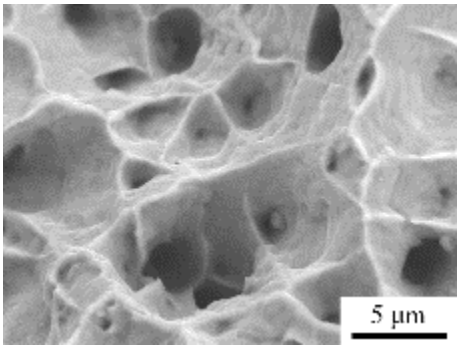

(b) σ = 310 MPa, t_r = 8.7 h

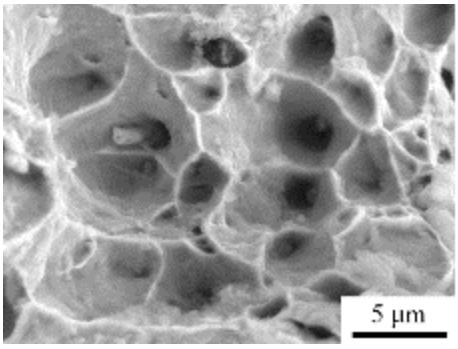

(c) σ = 270 MPa, t_r = 25 h

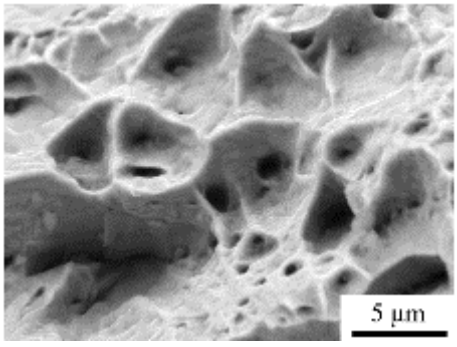

(d) σ = 200 MPa, t_r = 632 h

Figure 3.16 Detail observation of dimples and grain boundary fracture in hydrogen.

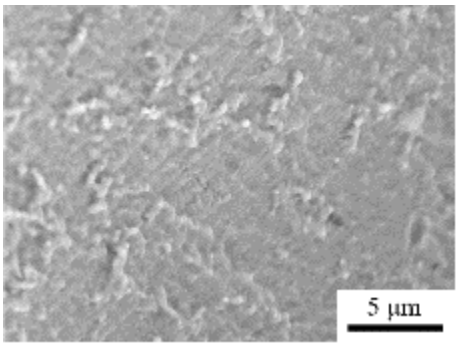

(a) In argon, σ = 310 MPa, t_r = 43 h

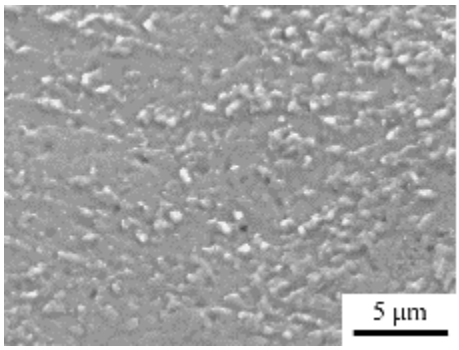

(b) In argon, σ = 270 MPa, t_r = 208 h

Figure 3.17 Detail observation of the grain boundary fracture surface in argon.

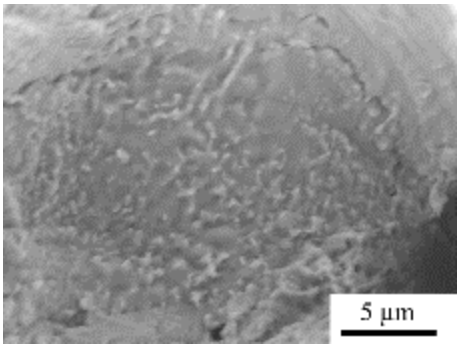

(a) σ = 270 MPa, t_r = 25 h

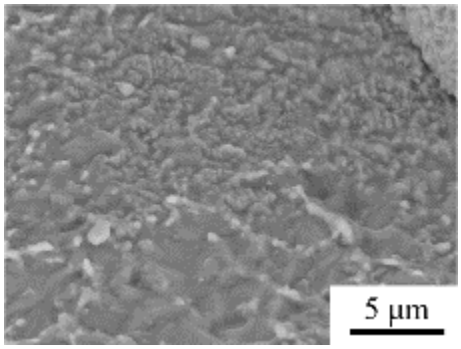

(b) σ = 200 MPa, t_r = 632 h

Figure 3.18 Detail observation of the grain boundary fracture surface in hydrogen.

3.4 Discussion of mechanism of reduced creep life by hydrogen

Regarding the results that demonstrated hydrogen-accelerated creep rupture, I considered four candidate mechanisms, which are 1. Decarburization, 2. Carbide formation, 3. Hydrogen-enhanced localized plasticity (HELP) and 4. Promoted dislocation climb due to enhanced lattice diffusion by hydrogen. In the following section, these mechanisms are evaluated, and it is concluded that only one is plausible.

3.4.1 Decarburization

The first candidate mechanism was decarburization by hydrogen. It is well understood that HTHA is caused by lowering the matrix strength due to decarburization and crack formation by the creation of methane bubbles [3.17-3.20]. The lowered matrix strength contributes to voids and crack formation. One possibility is that these HTHA mechanisms were responsible for the reduced creep life of SUS304 in hydrogen. As stated in Section 1.4, McCoy and Douglas postulated HTHA as the cause of the reduced creep life of the type 304 stainless steel based on their result that the creep life of the type 304 stainless steel in hydrogen was reduced compared to that in air at 1200 K, while it was equivalent to that in argon at 1089 K [3.4].

This possible mechanism was explored by measuring the total carbon content in the material before and after creep testing using an infrared absorption method after combustion. Figure 3. 19 shows the machine for the measurement of the carbon content (EMIA-Expert). When the sample is burned, the carbon in the sample becomes carbon dioxide and carbon monoxide. By detecting the generated carbon dioxide and carbon monoxide by using an infrared detector, the carbon content was measured. As shown in Fig. 3.20, the samples for

this measurement were taken from the fractured specimen. Five samples were extracted from each specimen. The weight of each sample was 1.0 g.

The measured values of the total carbon content are shown in Table 3.6. There was no significant change in the total carbon content before and after the creep tests. Also, there was no change in the carbon content for the specimen in argon compared to the one in hydrogen. In conclusion, the possibility that decarburization promoted creep in hydrogen is unlikely.

The carbon content was determined based on the amount of CO_2 generated during sample burning. It means that the result is not concerned about where the carbon came from. Therefore, if the HTHA mechanism worked and the carbon stayed in the material as methane, decarburization could not be detected. Further detailed inspection of carbon content may be needed, but there was no clear evidence that methane bubble formed as shown in Fig. 3.18.

Figure 3.19 Photograph of the machine for the carbon measurement.

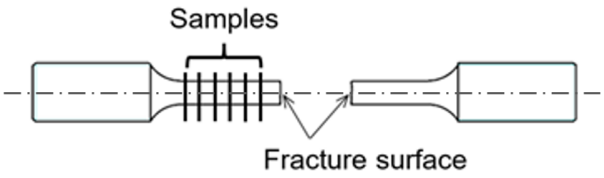

Figure 3.20 Location of extracted samples for the measurement of carbon content.

Table 3.6 Carbon content of the SUS304 before and after creep test (mass %).

	Before creep test	After creep test in hydrogen (σ = 310 MPa, t_r = 8.7 hour)	After creep test in argon (σ = 310 MPa, t_r = 43 hour)
Sample 1	0.053163	0.054227	0.056161
Sample 2	0.054628	0.052664	0.052169
Sample 3	0.055175	0.055661	0.051740
Sample 4	0.054461	0.053509	0.054315
Sample 5	0.055700	0.052383	0.055149
Average	0.0546	0.0539	0.0537
Standard deviation	0.00085	0.0012	0.0017

3.4.2 Carbide formation

The second possible reason for accelerated creep in hydrogen was carbide formation. Yokogawa et al. suggested that hydrogen-related carbide formation could affect the creep properties of the SUS304 at 823 K [3.3]. They described that hydrogen decreased the interfacial energy of the carbide and changed the morphology of grain boundary carbides from spheroidal-shaped in argon to plate-shaped in hydrogen. The plate-shaped carbide at the grain boundary mitigated the grain boundary sliding and led to the reduced creep life.

This prospect was examined by performing an additional creep test on SUS304L, which is a low carbon variant of SUS304. As shown in Table 2.1, the carbon content of the SUS304L was lower than that in the SUS304. I could argue that the reduction of creep life in hydrogen would be less pronounced in low-carbon material if the cause of accelerated creep rupture in hydrogen was the carbide.

The creep curves of the SUS304L are shown in Fig. 3.21 along with those for SUS304. Clearly, the SUS304L experienced a larger reduction of creep life than SUS304 both in hydrogen and argon. As a result, it can be argued that the potential effect of carbide formation on reduced creep life in hydrogen was minor.

The result of the SUS304L also backs up the consideration on the effect of decarburization, because the reduction in the creep life of the SUS304L occurred similar to that of the SUS304. This result also suggests that the effect of decarburization was not dominant.

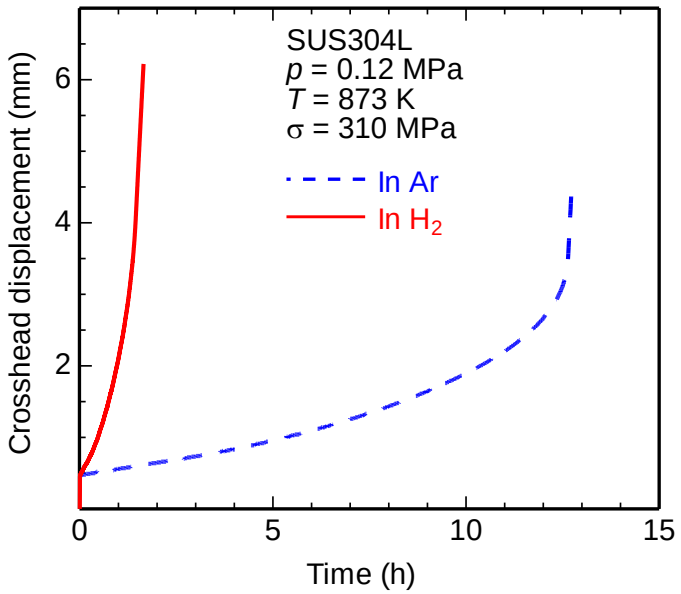

Figure 3. 21 Effect of hydrogen on the creep curves of the SUS304L steel.

3.4.3 Hydrogen-enhanced localized plasticity (HELP)

The third possible mechanism for hydrogen-accelerated creep rupture was hydrogen-enhanced localized plasticity (HELP), as invoked by Was et al. in interpreting their creep tests of the Ni-Cr-Fe alloys in primary water at 633 K [3.3-3.6].

Was et al. showed that accelerated creep rate due to hydrogen was caused in primary water as shown in Fig. 3.22 [3.6]. They discussed this accelerated creep rate by hydrogen based on the equation (3. 2) by Barrerr and Nix [3.21] for the creep deformation, which is dominated by the climb-controlled motion of dislocations.

$$\dot{\varepsilon} = \frac{2\pi\beta D_1 b^3}{a_0^3}\left[\frac{\sigma - \sigma_i}{G}\right]^2 \sinh\left(\frac{b^2\lambda(\sigma - \sigma_i)}{2kT}\right) \qquad (3.2)$$

where D_1 is the lattice self-diffusion coefficient, β is the number of lattice sites per unit cell, b is the Burgers vector, a_0 is the lattice parameter, G is shear modulus, k is Boltzmann's constant and λ is the spacing between jogs. Was et al. fixed all values in the equation (3. 2) except for the strain rate, $\dot{\varepsilon}$, applied stress, σ, and internal stress, σ_i. Then, they calculated the internal stress in both argon and hydrogen from their results in Fig. 3.22. As a result, they found that hydrogen reduced the internal stress that indicated hydrogen-reduced activation area of dislocations. Based on this investigation, they concluded that hydrogen contributed to a mechanism involving enhanced dislocation glide due to the HELP mechanism.

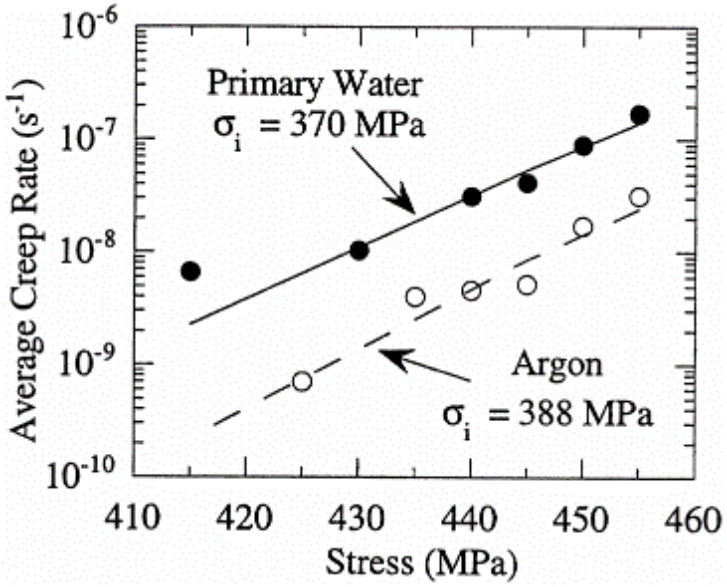

Fig. 3.22 Measured creep rates (symbols) and calculated creep rates from the Barrett and Nix model (lines) by Was et al. [3.6].

For consideration of the HELP mechanism in this study, the SSRT tests of the SUS304 were carried out in argon and hydrogen gas at temperatures of 298, 373, 573 and 873 K.

Figure 3.23 shows the results of the SSRT tests. At 298 K, the material showed typical hydrogen embrittlement, which caused the reduction in the elongation of the specimen in hydrogen compared to that in argon. On the other hand, at 373 K and higher temperatures, there was no ductility loss in hydrogen. This suggests that no hydrogen embrittlement occurred in this experiment at 373 K and higher temperatures.

The result that no hydrogen embrittlement occurred at high temperature is consistent with past studies demonstrating that the SUS304 suffers from hydrogen embrittlement at ambient and sub-ambient temperatures [3.22, 3.23], while no hydrogen embrittlement occurs

at high temperature [3.23, 3.24]. As has been reported, most importantly, the absence of hydrogen embrittlement at high temperatures is related to diminished hydrogen-dislocation interactions at high temperatures [3.25, 3.26]. In addition, suppression of the strain-induced martensitic transformation is another cause of no hydrogen embrittlement at high temperature of the SUS304 [3.22, 3.23].

The SSRT results demonstrated that hydrogen embrittlement was manifested through ductility loss at 298 K, and the predominant mechanistic interpretation in the literature for reduced ductility in hydrogen-exposed austenitic stainless steel involves HELP [3.25, 3.27]. On the other hand, the ductility was not reduced during the SSRT in hydrogen at 373K and higher temperatures, indicating that HELP is not active at these temperatures.

The reason HELP becomes inactive as temperature increases is that there is no interaction between hydrogen and dislocations at high temperature. At low temperature where hydrogen has interaction with the dislocation, hydrogen enhances dislocation mobility and it results in localized plasticity. However, at high temperature, since the binding energy between hydrogen and the dislocation is reduced, hydrogen trapping in the dislocation stress field diminishes at elevated temperature [3.25, 3.26].

I therefore conclude that HELP (more specifically, hydrogen-enhanced dislocation glide) cannot operate during this creep testing at 873 K. In addition, intergranular fracture was promoted in the creep tests by Was et al. [3.5]. This trend is opposite to my experiment that intergranular fracture is delayed in hydrogen compared to argon. This difference of the effect of hydrogen on the fracture morphology also implies that the mechanism activated in my experiment is different from the experiment by Was et al. It is noteworthy that the experimental conditions were significantly different between Was et al. (633 K in 19.9 MPa water) and this study (873 K in 0.12 MPa hydrogen gas). Also, Was et al. fixed the value of

diffusion coefficient in their consideration. However, I argue that hydrogen affects the diffusion as shown in the next section.

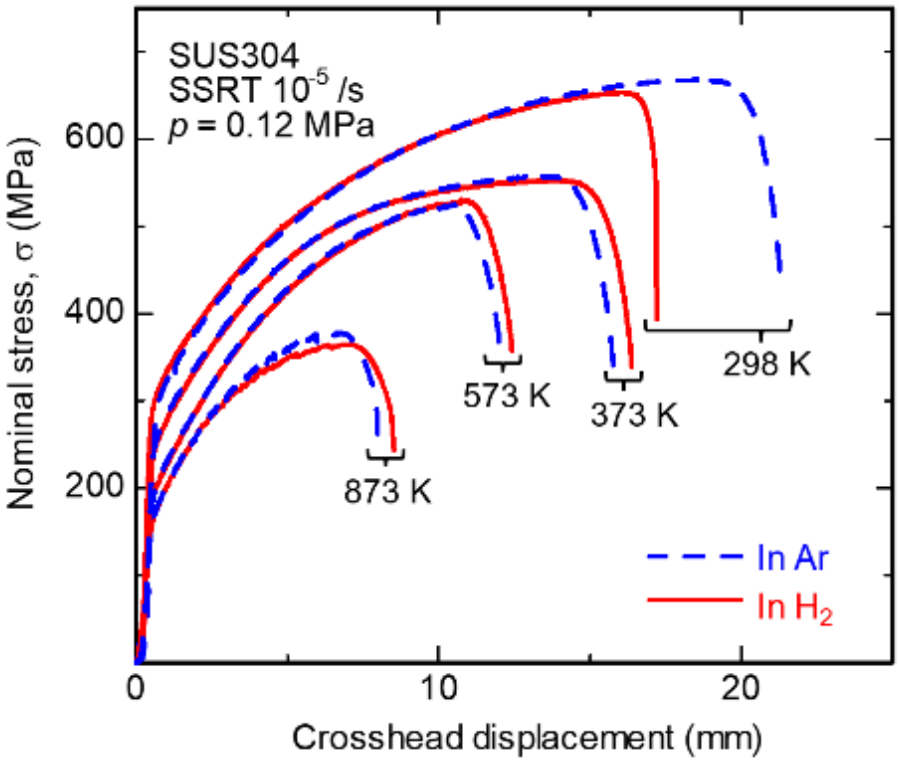

Figure 3.23 Effect of temperature on the SSRT stress-strain curves for the SUS304 steel in argon and hydrogen.

3.4.4 Promoted dislocation climb due to enhanced lattice diffusion by hydrogen

The fourth possible mechanism I considered for hydrogen-accelerated creep rupture was the effect of hydrogen on enhancing vacancy density, thereby accentuating dislocation climb.

There were some studies discussing the effect of hydrogen on vacancy density and resulted self-diffusion promotion by Fukai et al. [3.28-3.37]. Fig. 3.24 shows the result of their TDS analysis of Ni after exposure to 3 GPa hydrogen at 950 ℃ for 2 hours [3.33, 3.36]. There were clear peaks at 107 ℃ (P_0), 358 ℃ (P_1) and 519 ℃ (P_2). On the other hand, the peaks at 358 ℃ (P_1) and 519 ℃ (P_2) were not observed in the specimen with the shorter exposure time. It suggested that the peaks at 358 ℃ (P_1) and 519 ℃ (P_2) reflected the increase in the vacancy density due to hydrogen, while the peak at 107 ℃ (P_0) reflected the solute hydrogen in the lattice. Based on this TDS analysis, they concluded that hydrogen increased vacancy density.

Since the TDS measurements by Fukai et al. were carried out after the specimen was cooled down to the room temperature, some uncertainty could be considered. Assuming that the increase in vacancy was only due to thermal activation, if hydrogen stabilized these vacancies, the increase in the vacancy density measured at room temperature is incorrect. Fukai et al. also investigated the increased vacancy due to hydrogen based on the measurement of the lattice parameter at high temperature [3.28, 3.36], because the lattice parameter is affected by the vacancy density. They measured the lattice parameter of Ni during heat treatment in 5 GPa hydrogen gas as shown in Fig. 3.25. An important point in their measurement was that the lattice parameter decreased with increase in the time after which the temperature was kept at 800 ℃. A similar trend that the lattice parameter decreased

with time at a constant temperature was observed in Pd [3.29], γ-iron and α-iron [3.35]. The reason why hydrogen increases vacancy density is that hydrogen trapped in the vacancies reduces the vacancy formation energy [3.32, 3.36].

It is considered that the increased vacancy density can promote self-diffusion, because self-diffusion is dominated by the migration of vacancies as shown in Section 1.4 (Fig. 1.8). After discovering the increase in atomic vacancy concentration due to hydrogen, Fukai et al. also conducted research on the promoted diffusion by hydrogen [3.31, 3.37]. Fig. 3. 26 shows their experimental result of inter-diffusion of the Cu-Ni diffusion couples at several elevated temperatures in 5 GPa hydrogen for 30 min. The result shows that inter-diffusion of Cu into Ni was significantly promoted in hydrogen. They also found promoted self-diffusion due to hydrogen in a Nb single crystal [3.37].

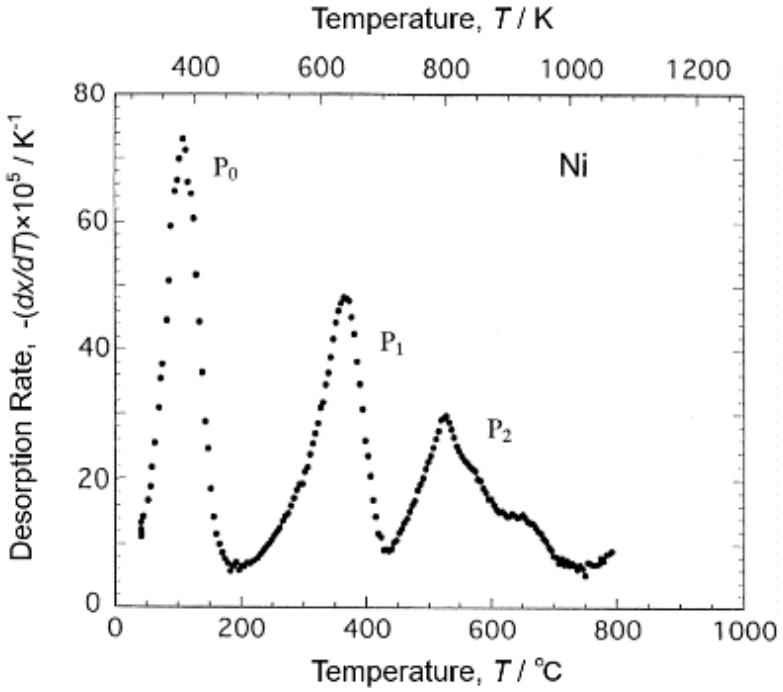

Figure 3.24 Thermal desorption spectra of Ni exposed to 3 GPa hydrogen gas at 950 ℃ for 2 hours [3.33, 3.36].

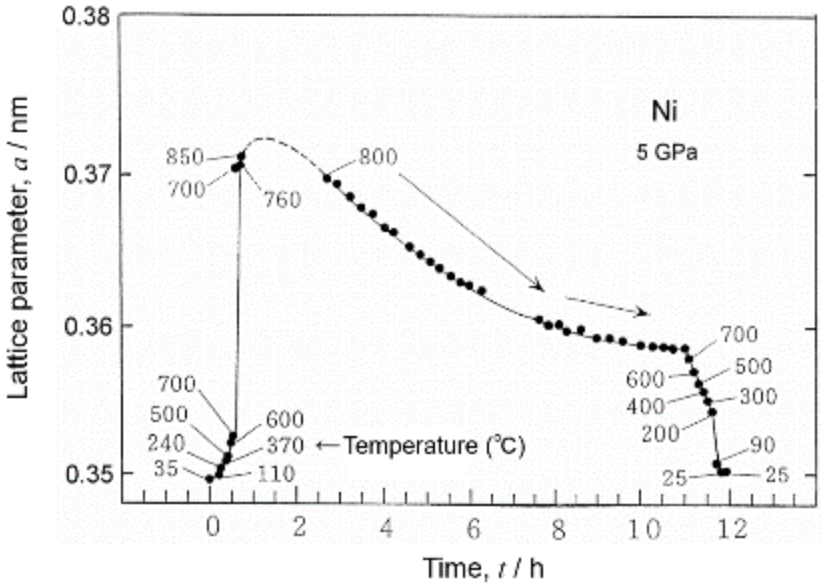

Figure 3.25 Change in the lattice parameter of Ni after exposure to high temperature and high pressure hydrogen gas [3.28, 3.36].

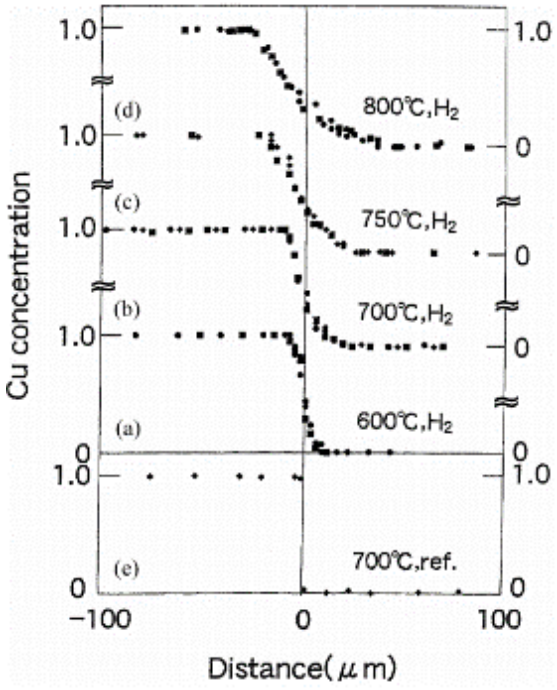

Figure 3.26 Concentration profiles of Cu after diffusion annealing of Cu-Ni diffusion couples for 30 min at several temperatures in 5 GPa hydrogen and 700 ℃ under a mechanical pressure of 5 GPa for reference [3.31, 3.37].

The notion is that the promoted self-diffusion due to the increased vacancy density which was derived from these past studies can affect the creep deformation, because creep deformation is dominated by self-diffusion, as described in Section 1.4.

This vacancy-related mechanism is justified from analyzing several results, including the minimum (steady state) creep strain rates and the fractography. Fig. 3.27 shows the measured steady state strain rates $\dot{\varepsilon}$ plotted as a function of applied stress σ in hydrogen and argon at 873 K. Clearly, the strain rates in hydrogen are larger than in argon over the entire applied stress range in the creep testing. These creep data are superposed on Figure 3.28 which is a redrawing of Frost and Ashby's deformation mechanism map for 304 stainless steel [3.38].

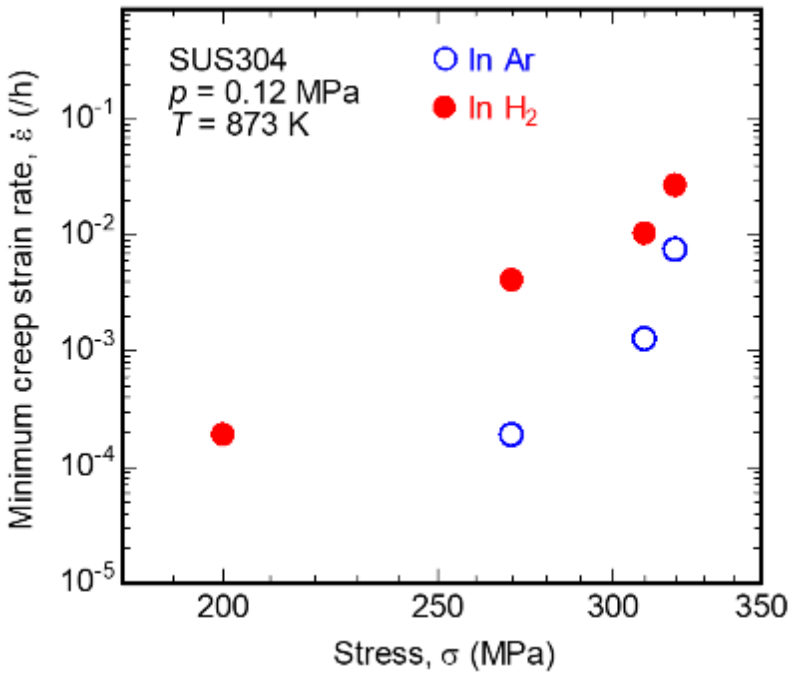

Figure 3.27 Minimum creep strain rate vs. applied stress of the SUS304 steel at 873 K.

On placing the data on Fig. 3.28, I calculated the effective stress and strain rates, respectively, through $\sigma_s = \sigma/\sqrt{3}$ and $\dot{\gamma} = \sqrt{3}\dot{\varepsilon}$, where σ is the applied tensile creep stress and $\dot{\varepsilon}$ is the corresponding steady state creep strain rate. At 873K, the shear modulus μ was calculated as 59.2 GPa [3.38]. Definitely the data for the applied creep stress 320 MPa fall very close to the line separating the power-law and plasticity regimes. I argue that this is the reason that the data for 320 MPa fall off the straight lines that can be used to linearly interpolate the creep data in hydrogen and especially in argon, as indicated by the isotherms of the figure.

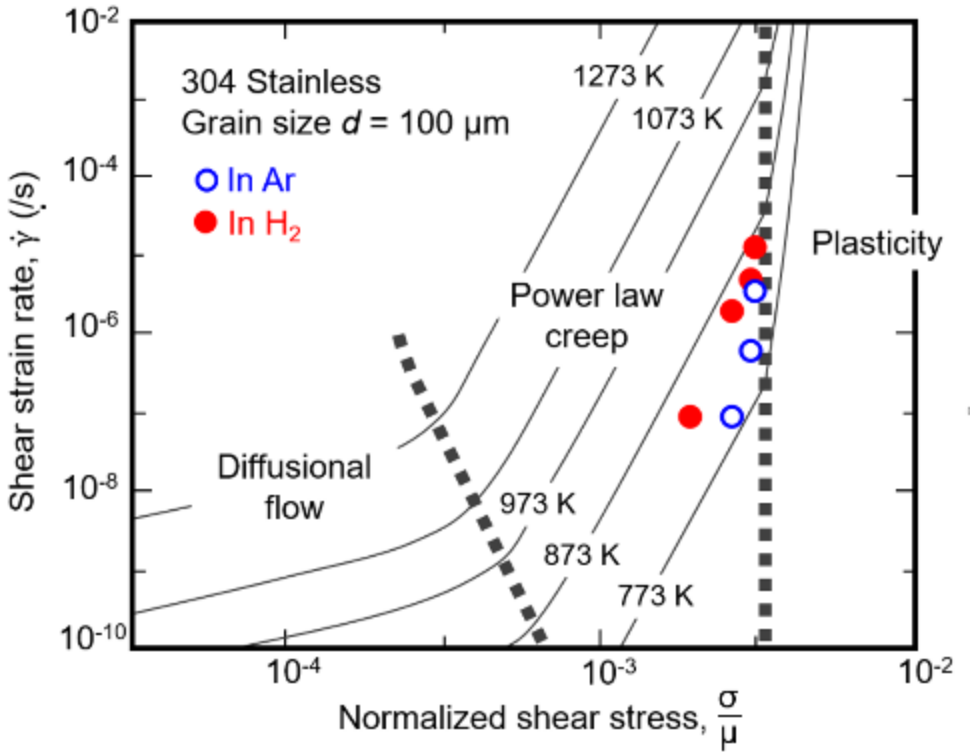

Figure 3.28 Creep data in hydrogen (solid circles) and Ar (open circles) superposed on Frost and Ashby's creep deformation mechanism map for 304 stainless steel [3.38].

To explore this assertion of power-law creep controlled response in hydrogen and argon for all applied stresses except for 320MPa, the data are recast in Fig. 3.29 to conform to the normalized variables in the following analytical creep model expression relating steady state strain rate to applied stress [3.38]:

$$\frac{\dot{\varepsilon}}{\dot{\varepsilon}_0} = A\left(\frac{\sigma}{\mu}\right)^n, \qquad (3.3)$$

where the stress, σ, is normalized by the shear modulus, μ, and strain rate, $\dot{\varepsilon}$, is normalized by the reference strain rate, $\dot{\varepsilon}_0$, and the multiplying factor, A , equals $1.5\text{x}10^{12}$ for 304 stainless steel [3.38]. The reference strain rate, $\dot{\varepsilon}_0$, embodies material properties and temperature effects in the parent creep model as follows:

$$\dot{\varepsilon_0} = \frac{D_v \mu b}{kT} = \frac{D_{v0} \mu b}{kT} \exp\left(-\frac{Q_v}{RT}\right), \qquad (3.4)$$

where D_v is the lattice diffusion coefficient, D_{v0} is the pre-exponential factor, b is the Burgers vector, Q_v is the activation energy for lattice diffusion, k and R are Boltzmann's constant and the gas constant, respectively, and T is the absolute temperature. The applied stress and measured strain rate data points from Fig. 3.27 were converted to normalized quantities in Fig. 3.29 by assigning the following values to parameters in Eqs. 3.3 and 3.4 that are relevant to 304 stainless steel and the test temperature of 873 K [3.38]: μ = 59.2 GPa, b = 0.258 nm, $D_{v0} = 3.7\text{x}10^{-5}$ m^2/s, and Q_v = 280 kJ/mol. These values were applied to normalize the applied stress and measured strain rates in both argon and hydrogen, with the exception of Q_v. For normalizing the measured strain rate in hydrogen, Q_v was modified to 263 kJ/mol, which allowed for collapsing the data in hydrogen and argon so that they can collectively be described by Eq. 3.4.

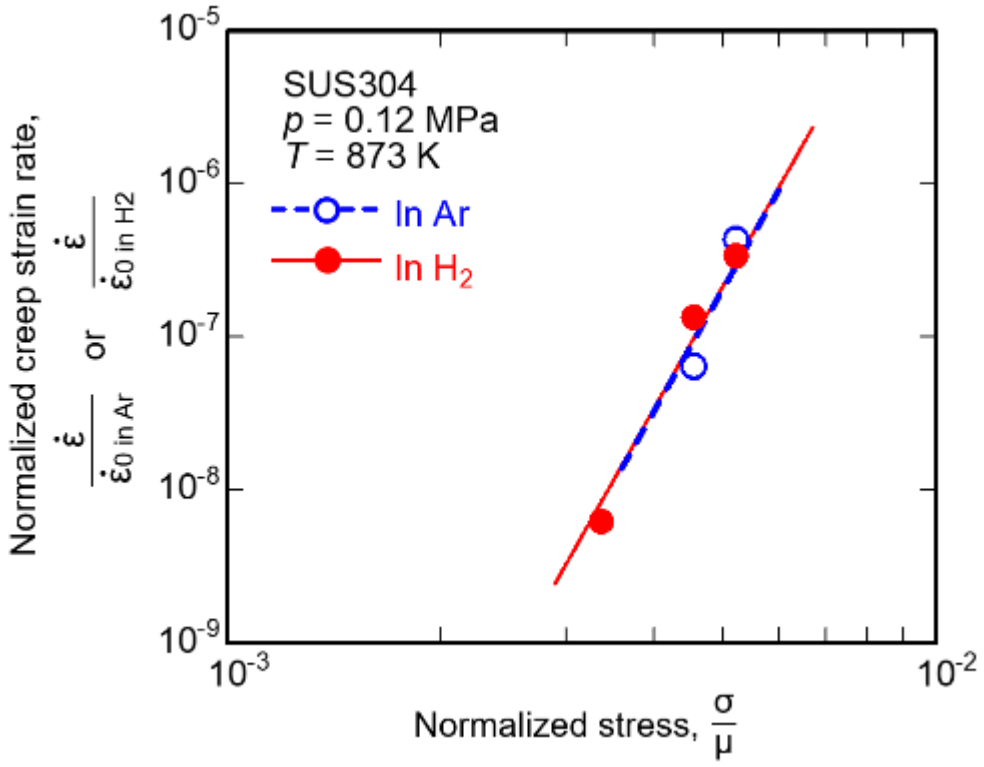

Figure 3.29 Normalized minimum creep strain rate vs. normalized applied stress for the SUS304 steel at 873 K. The lines represent the power law creep Eq. 3.4 with creep exponent n = 8.2 The normalizing reference strain rate $\dot{\varepsilon}_0$ is equal to 0.826/s and 8.596/s in argon and hydrogen, respectively. The parameter μ = 59.2 GPa is the shear modulus and $A = 1.5 \times 10^{12}$ [3.38].

As shown by the coincident lines in Fig. 3.29, Eq. 3.4 well describes the ensemble of normalized data in hydrogen and argon when the creep exponent, n, equals 8.2. The implication of the analysis illustrated in Fig. 3.29 is that the same creep mechanism operates in argon and hydrogen, and the central role of hydrogen may be to accelerate the creep mechanism through increased vacancy density. From fundamental lattice diffusion theory [3.39], the activation energy for vacancy-mediated diffusion, Q_v, is the sum of the activation

energy for migration, Q_m, and the vacancy formation energy, Q_f. The lower value of Q_v reflected in the normalized strain rate data for hydrogen in Fig. 3.29 can then be interpreted as a reduction in the vacancy formation energy, which is consistent with the theory that hydrogen lowers the formation energy of crystal defects (defactant concept [3.40]). Furthermore, the value of the creep exponent (n = 8.2) infers a particular role for hydrogen-enhanced vacancies in the creep mechanism. Specifically, this value of n is consistent with dislocation creep [3.38], in which the creep process may be controlled by dislocation climb. Since dislocation climb is activated by vacancy-mediated lattice diffusion, it follows that hydrogen-enhanced vacancy density can lead to more pronounced dislocation climb.

While the analysis in Fig. 3.29 provides quantitative support for the role of hydrogen-enhanced vacancies in accelerating creep fractography, results also qualitatively affirm a central role of vacancies and their effect on dislocation climb. The observation from fracture surfaces that intergranular cracking was less prevalent in hydrogen compared to argon can be attributed to enhanced vacancy-mediated dislocation climb. Figure 3.14 shows that interior cracks were predominantly observed at triple junctions of grain boundaries. This intergranular cracking results from strain incompatibilities at features such as grain boundary triple points and grain boundary particles. In hydrogen, these strain incompatibilities can be more easily compensated if dislocation climb is stimulated by elevated vacancy concentration, resulting in the delay of intergranular cracking.

Hydrogen-enhanced vacancy formation and its effect on lattice diffusion and dislocation climb can rationalize the steady state creep relationships and the fractography, but some caution must be applied. The vacancy formation energy can be attenuated through hydrogen-vacancy interactions (i.e. trapping), however this interaction diminishes as temperature increases. For example, Tanguy et al. [3.41] developed a model to predict

vacancy concentrations in nickel by considering hydrogen-vacancy interactions and the effect of temperature. Assuming this model applies to 304 stainless steel, the vacancy concentration is increased by only 10% relative to the thermal equilibrium value for the hydrogen concentration (5.3 mass ppm) and temperature (873 K) relevant to the current study. In contrast, McLellan and Xu [3.42] modeled enhanced vacancy formation in FCC iron and illustrated that the vacancy concentration was 100-fold higher than the thermal equilibrium value for the hydrogen concentration and temperature pertinent to the current study. Critically, these inconsistently predicted vacancy concentrations appear to hinge on different hydrogen-vacancy binding energies considered in the two theoretical studies, and the actual binding energy values for 304 stainless steel are not certain. Interestingly, however, the hydrogen-enhanced vacancy concentration inferred by the analysis in Fig. 3.29 is bounded by the theoretical predictions. Specifically, the normalizing strain rates, $\dot{\varepsilon}_0$, applied to the data points in Fig. 3.29 are 8.596 /s and 0.826 /s for hydrogen and argon, respectively. According to Eq. 3.4, the normalizing strain rate is directly proportional to the lattice diffusion coefficient, D_v, so that the ratio of $\dot{\varepsilon}_0$ values in hydrogen and argon is equivalent to the respective ratio of D_v values. Since D_v is in turn proportional to the vacancy concentration [3.39], the ratio of $\dot{\varepsilon}_0$ values is also equivalent to the ratio of vacancy concentrations. This ratio of $\dot{\varepsilon}_0$ in hydrogen to the value in argon is 10, suggesting that hydrogen may increase the vacancy concentration by a similar magnitude relative to the thermal equilibrium value. The implied increase in vacancy concentration by a factor of 10 is between the theoretical predictions from Tanguy et al. (factor of 1.1) and McLellan and Xu (factor of 100).

In summary, enhanced dislocation climb mediated by increased vacancy density is a plausible mechanism for the hydrogen-accelerated creep rupture of 304 stainless steel, but it is not considered definitive. Future efforts will be directed at confirming this mechanism.

3.5 Conclusion

Creep testing of the JIS SUS304 steel were conducted in 0.12 MPa hydrogen and argon gaseous atmospheres at 873 K to investigate the mechanical response of components for advanced high-temperature hydrogen technologies. The results can be summarized as follows:

1. Hydrogen considerably increased the steady state creep strain rate, drastically reduced the creep life, and decreased the percentage of intergranular fracture at lower applied stresses.

2. The creep elongation and reduction in area were higher in hydrogen compared to argon.

3. No decarburization occurred during testing in hydrogen.

4. Creep testing of the lower-carbon SUS304L steel in hydrogen resulted in reduction of the creep life similar to that for SUS304. This result suggests that the potential effect of the interaction of hydrogen with carbides in bringing about creep failure is minor.

5. In the SSRT tests, no hydrogen embrittlement occurred at 373 K and higher temperatures. These results indicate that the hydrogen-enhanced localized plasticity (HELP) mechanism does not operate above 373 K, so that it is not a viable mechanism for hydrogen-accelerated creep rupture at 873 K.

6. From the analysis of the steady state creep data, it can be inferred that hydrogen does not alter the fundamental deformation mechanism of SUS304 steel at 873K, which is dislocation-driven creep described phenomenologically by a power law relationship. The analysis supports the colorable argument that hydrogen reduces the activation energy for

vacancy formation, thereby enhancing the vacancy density and associated lattice diffusion coefficient, which in turn accelerates dislocation climb. As a consequence, hydrogen accelerates the creep response and shortens the creep life. Definitely this argument of hydrogen-enhanced, vacancy-driven dislocation climb needs further investigation.

3.6 References

1. K. Yokogawa, S. Fukuyama, K. Kudo, "Apparatus for creep rupture testing in high-pressure hydrogen at elevated temperatures", *Review of Scientific Instruments*, Vol. 53, No. 1, 1982, pp. 86-89
2. K. Yokogawa, S. Fukuyama, K. Kudo, P.G. Shewmon, "Effect of hydrogen attack on tensile and creep properties of low carbon steel", *International Journal of Pressure Vessels and Piping*, Vol. 37, Issue 5, 1989, pp. 365-385
3. K. Yokogawa, S. Fukuyama, "Hydrogen embrittlement of metallic materials", *Hydrogen Energy System*, Vol. 22, No. 2, 1997, pp. 18-25
4. T.M. Angeliu, D.J. Paraventi, G. S. Was, "Creep and Intergranular Cracking Behavior of Nickel-Chromium-Iron-Carbon Alloys in 360°C Water", *CORROSION*, Vol. 51, No. 11, 1995, pp. 837-848
5. D.J. Paraventi, G. S. Was, "Environmentally Enhanced Deformation of Ultra-High-Purity Ni-16Cr-9Fe Alloys", *Metallurgical and Materials Transactions*, Vol. 31A, 2000, pp. 2383-2388
6. D.J. Paraventi, T.M. Angeliu, G. S. Was, "Effect of Hydrogen on Creep in High-Purity Ni-16Cr-9Fe Alloys at 360°C", *CORROSION*, Vol. 58, No. 8, 2002, pp. 675-686
7. H.E. McCoy, D.A. Douglas, *Effect of Environment on the Creep Properties of Type 304 Stainless Steel at Elevated Temperatures*, (Oak Ridge: Oak Ridge National Laboratory, 1962)
8. G.B.A. Schuster, R.A. Yeske, C.J. Altstetter, "The Effect of Hydrogen on the Creep Rupture Properties of Fe-Ni Alloys", *Metallurgical Transactions*, Vol. 11A, 1980, pp. 1657-1664H.
9. JIS Z2271, "Metallic materials - Uniaxial creep testing in tension - Method of test" (Japan Industrial Standards Committee, 2010)
10. C. San Marchi, B.P. Somerday, S.L. Robinson, "Permeability, solubility and diffusivity of hydrogen isotopes in stainless steels at high gas pressures", *International Journal of Hydrogen Energy*, Vol. 32, 2007, pp. 100-116

11. R. Komoda, M. Kubota, A. Staykov, P. Ginet, F. Barbier, J Furtado, “Inhibitory effect of oxygen on hydrogen-induced fracture of A333 pipe steel”, *Fatigue & Fracture of Engineering Materials & Structures*, Vol. 42, 6, 2019, pp. 1387-1401
12. ASTM G128, “Standard Practice for Slow Strain Rate Testing to Evaluate the Susceptibility of Metallic Materials to Environmentally Assisted Cracking” (West Conshohocken, PA: ASTM International, 2013)
13. N. Shinya, J. Kyono, H. Tanaka, M. Murata, S. Yokoi, “Creep Rupture Properties and Creep Fracture Mechanism Maps for Type 304 Stainless Steel”, *Tetsu-to-Hagane*, Vol. 69, Issue 14, 1983, pp. 1668-1675
14. H. Nakakuki, K. Maruyama, H. Oikawa, K. Yagi, “Collective Evaluation of Temperature Life in Austenitic Stainless Steels”, *Tetsu-to-Hagane*, Vol. 81, 1995, pp. 64-68
15. M.F. Ashby, C. Gnadhi, D.M.R. Taplin, “FRACTURE-MECHANISM MAPS AND THEIR CONSTRUCTION FOR F.C.C. METALS AND ALLOYS”, *Acta Metallurgica*, Vol. 27, 1979, pp. 699-729
16. R.J. Fields, T. Weerasooriya, M.F. Ashby, “Fracture-Mechanisms in Pure Iron, Two Austenitic Steels, and One Ferritic Steel”, *Mettalugical Transactions*, Vol. 11A, 1980, pp. 333-347
17. P.G. Shewmon, “Hydrogen attack of pressure-vessel steels”, *Materials Science and Technology*, Vol. 1, 1985, pp. 2-11
18. M. McKimpson, P.G. Shewmon, “Initial Hydrogen Attack Kinetics in a Carbon Steel”, *Metallurgical Transactions A*, Vol. 12A, 1981, pp. 825-34.
19. L.C. Weiner, “Kinetics and Mechanism of Hydrogen Attack of Steel”, *Corrosion*, Vol. 17, No. 3, 1961, pp. 137-143
20. G.A. Nelson, “Hydrogenation Plant Steels,” in *Hydrogen Damage*, ed. C.D. Beachem, (Metals Park, OH: American Society for Metals, 1977), pp. 377-397.
21. C.R. Barrett and W.D. Nix, “A Model for Steady State Creep Based on the Motion of Jogged Screw Dislocations”, *Acta Metall. Mater.*, Vol. 13, 1965, pp. 1247-1258

22. R.B. Benson Jr., R.K. Dann, L. W. Roberts Jr., "Hydrogen Embrittlement of Stainless Steel", *Transactions of the Metallurgical Society of AIME*, Vol. 242, 1968, pp. 242-251
23. G.R. Caskey "Hydrogen Effects in Stainless Steels" in *Hydrogen Degradation of Ferrous Alloys*, eds. R.A. Oriani, J.P. Hirth, M. Smialowski, (Park Ridge, NJ: Noyes Publications, 1985), pp. 822-862
24. K. Koide, T. Minami, T. Anraku, A. Iwase, H. Inoue, "Susceptibility of SUS304 Steel to Hydrogen Embrittlement in High-pressure Hydrogen Gas at 250℃", *Zairyo-to-Kankyo*, Vol. 63, 2014, pp. 523-527
25. H.K. Birnbaum, P. Sofronis, "Hydrogen-enhanced localized plasticity-a mechanism for hydrogen-related fracture", *Materials Science and Engineering A*, Vol. 176, 1994, pp. 191-202
26. R.A. Oriani, "The diffusion and trapping of hydrogen in steel", *Acta Metallurgica*, Vol. 18, 1970, pp. 147-157
27. C. San March, B.P. Somerday, X. Tang, G.H. Schiroky, "Effects of alloy composition and strain hardening on tensile fracture of hydrogen-precharged type 316 stainless steels", *International Journal of Hydrogen Energy*, Vol. 33, Issue 2, 2008, pp. 889-904
28. Y. Fukai, N. Okuma, "Evidence of Copious Vacancy Formation in Ni and Pd under a High Hydrogen Pressure", *Japanese Journal of Applied Physics*, Vol. 32, 1993, pp. L1256-L1259
29. Y. Fukai, N. Okuma, "Formation of Superabundant Vacancies in Pd Hydride under High Hydrogen Pressures", *PHYSICAL REVIEW LETTERS*, Vol. 73, 1994, pp. 1640-1643
30. H. Osono, T. Kino, Y. Kurokawa, Y. Fukai, "Agglomeration of hydrogen-induced vacancies in nickel", *Journal of Alloys and Compounds*, Vol. 231, 1995, pp. 41-45

31. E. Hayashi, Y. Kurokawa, Y. Fukai, "Hydrogen-Induced Enhancement of Interdiffusion in Cu-Ni Diffusion Couples", *PHYSICAL REVIEW LETTERS*, Vol. 80, 1998, pp. 5588-5590
32. M. Iwamoto, Y. Fukai, "Superabundant Vacancy Formation in Iron under High Hydrogen Pressures: Thermal Desorption Spectroscopy", *Material Transactions, JIM*, Vol. 40, 1999, pp. 606-610
33. Y. Fukai, M. Mizutani, S. Yokota, M. Kanazawa, Y. Miura, T. Watanabe, "Superabundant vacancy-hydrogen clusters in electrodeposited Ni and Cu", *Journal of Alloys and Compounds*, Vol. 356-357, 2003, pp. 270-273
34. Y. Fukai, "Formation of superabundant vacancies in M-H alloys and some of its consequences: a review", *Journal of Alloys and Compounds*, Vol. 356-357, 2003, pp. 263-269
35. T. Hiroi, Y. Fukai, K. Mori, "The phase diagram and superabundant vacancy formation in Fe-H alloys revisited", *Journal of Alloys and Compounds*, Vol. 404-406, 2005, pp. 252-255
36. Y. Fukai, *Materia Japan*, Vol. 50, No. 11, 2011, p.465-472
37. Y. Fukai, *Materia Japan*, Vol. 50, No. 12, 2011, p.521-528
38. H.J. Frost, M.F. Ashby, *Deformation-mechanism maps: the plasticity and creep of metals and ceramics*, (Oxford: Pergamon Press, 1982), pp. 60-70
39. R. Abbaschian, R.E. Reed-Hill, *Physical Metallurgy Principles*, 3rd ed. (Boston: PWS Publishing Company, 1994), pp. 348-388
40. R. Kirchheim, "On the solute-defect interaction in the framework of a defactant concept", *International Journal of Materials Research*, Vol. 100, No. 4, 2009, pp. 483-487
41. D. Tanguy, Y. Wang, D. Connetable, "Stability of vacancy-hydrogen clusters in nickel from first-principles calculations", *Acta Materialia*, Vol. 78, 2014, pp. 135-143
42. R.B. McLellan, Z.R. Xu, "HYDROGEN-INDUCED VACANCIES IN THE IRON LATTICE", *Scripta Materialia*, Vol. 36, 1997, pp. 1201-1205

4.1 Perspective of future research on creep in hydrogen

4.1.1 Introduction

In the previous section, creep tests of the SUS304 were carried out in 873 K hydrogen gas in order to assess the effect of hydrogen on creep of the simplest commercial austenitic stainless steel. The results clearly showed that the creep life of the SUS304 was drastically reduced by hydrogen and that trend became significant with a decrease in applied stress. Here, I consider what is necessary for the further research on creep in hydrogen based on the creep test of the SUS304 that I carried out. The objective of this chapter is to investigate the potential of further research on creep in hydrogen.

When considering the design of the systems and components for high-temperature hydrogen, study on many other materials is necessary. For instance, SUS310S is one of the superior austenitic stainless steels in terms of resistance to high temperature oxidation. Therefore, SUS310S is used as material subjected to high temperature such as heat exchangers, gas turbine components, incinerators, recuperators, combustion chambers, etc. [4.1]. In addition, many kinds of bcc steels such as 9%Cr steel, 12Cr Mo steel, etc. are also used for components subjected to high temperature.

Bcc iron has lower creep resistance compared to fcc iron, because the activation energy for creep deformation, which is the same as the activation energy for lattice diffusion, is lower in bcc iron than that in fcc iron [4.2-4.4]. Therefore, complicated microstructure control is applied to increase creep resistance. This implies different effects of hydrogen on the creep properties of bcc steels and mechanisms by which hydrogen affects the creep properties of bcc steels. On the other hand, it can be considered that the study on a simple material is beneficial to argue the degradation mechanism of the creep in hydrogen.

Then, I briefly investigated the creep life of the SUS310S and pure iron in hydrogen.

4.2 Experimental procedure

The materials used for the creep tests in this chapter were JIS SUS310S austenitic stainless steel and JIS SUY-1 soft electromagnetic iron. The chemical composition of the SUS310S and SUY-1 is shown in Table 4.1. The SUS310S was solution treated by heating at 1323 K followed by water cooling. The SUY-1 was used for the experiment as received. The mechanical properties of these materials at 298 K and 873 K in argon are shown in Tables 4.2 and 4.3. Figure 4.1 shows the microstructure of those materials. The average grain size was 26 μm for the SUS310S and 52 μm for the SUY-1.

The creep testing was carried out in the same procedure as for the SUS304 shown in the Chapter 3. The shape of the specimen is shown in Fig. 4.2. It was the same as the specimen used in the previous chapter. The absolute gas pressure at which the creep tests were carried out was 0.12 MPa. The temperature of hydrogen and argon gas was 873 K. Prior to the start of the creep test in both argon and hydrogen gas, the specimen was soaked for three hours in the testing environment in order to achieve uniform hydrogen distribution across its diameter.

Table 4.1. Chemical composition of test materials (mass%).

Material	C	Si	Mn	P	S	Ni	Cr
SUS310S	0.02	0.27	1.10	0.029	0.001	19.13	24.08
SUY-1	0.02	TR	0.24	0.005	0.004	0.01	0.02

Table 4.2. Mechanical properties of the SUS310S in argon at 298 K and 873 K.

Temperature of tensile test (K)	0.2% proof strength (MPa)	Ultimate tensile strength (MPa)	Elongation (%)	Reduction of area (%)
298	428	581	48	50
873	179	370	27	76

Table 4.3. Mechanical properties of the SUY-1 in argon.

Temperature of tensile test (K)	0.2% proof strength (MPa)	Ultimate tensile strength (MPa)	Elongation (%)	Reduction of area (%)
298	188	297	43	73
873	121	122	18	99

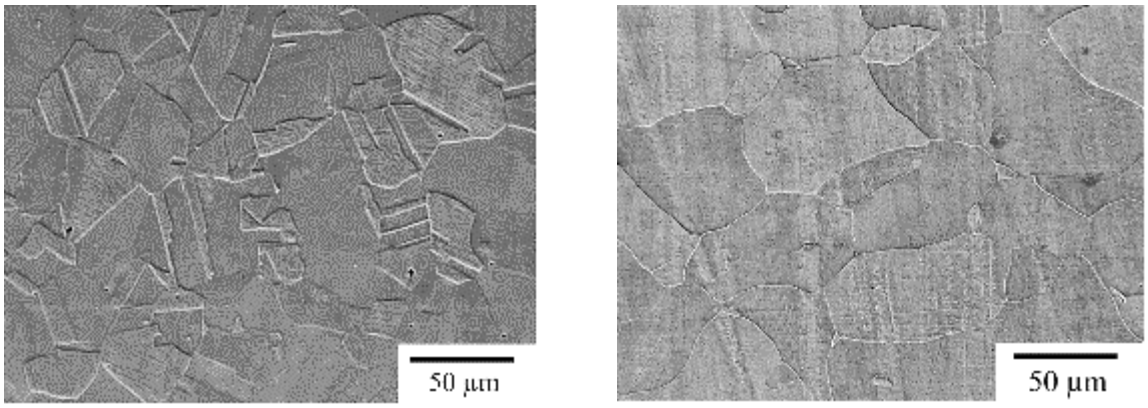

(a) SUS310S (b) SUY-1

Figure 4.1. Microstructure of the tested materials.

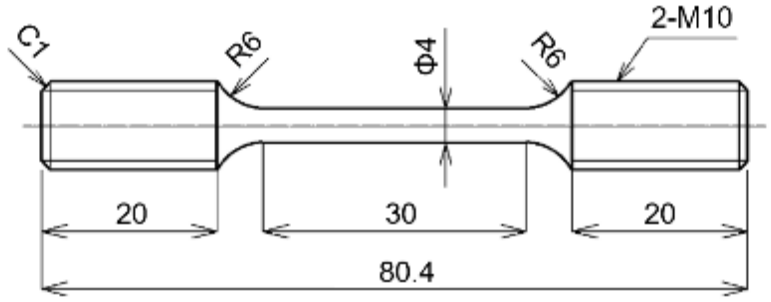

Figure 4.2. Shape and size of the creep specimen (Dimensions are in mm).

4.3 Test results

4.3.1 SUS310S austenitic stainless steel

Figure 4.3 shows the creep curves of the SUS310S. The creep rate in hydrogen was increased compared to that in argon. Consequently, the creep life of the SUS310S in hydrogen was reduced. The relative creep life in hydrogen vs. argon was 0.93 for the SUS310S under the given experimental conditions.

The elongation of the specimen and reduction of area are shown in Table 4.4. Hydrogen increased both the elongation and the reduction of area. These trends for the SUS310S that hydrogen reduces creep life and increased the creep elongation and reduction of area were similar to the SUS304 more or less. According to Table. 3.5, the reduction in the creep life of the SUS304 in hydrogen is more significant compared with that of the SUS310S. However, there should be no misunderstanding about the interpretation of this result. The creep test of the SUS310S was carried out in the very short creep life region (6-7 hour). The effect of hydrogen on the creep life of the SUS304 was more pronounced in the long creep life region as shown in Fig. 3.6. In this context, it is premature to consider that the SUS310S has better resistance against creep in hydrogen compared to the SUS304. The result just shows the fact that the creep properties of the SUS310S is also affected by hydrogen. Further experiments are required to complete the creep rupture curves for the SUS310S in the future.

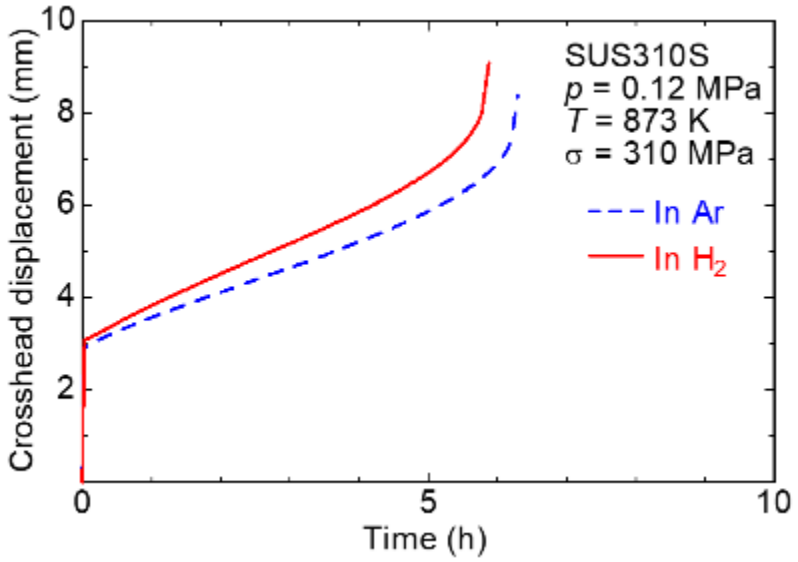

Figure 4.3. Effect of hydrogen on creep rupture of the SUS310S.

Table 4.4. Creep elongation and reduction of area of the SUS310S.

	Applied stress	Elongation	Reduction of area
In argon	310 MPa	26.3 %	69.7 %
In hydrogen	310 MPa	28.5 %	75.9 %

Figure 4.4 shows the fracture surfaces of the SUS310S in argon and hydrogen. The fracture surfaces were mainly covered by dimples, except for the final fracture area both in argon and hydrogen. Figures 4.5 and 4.6 show detail observations of the dimples in argon and hydrogen respectively. The fracture surface consisted of large and deep dimples and small and shallow dimples. There was no significant difference in the size and shape of dimples between argon and hydrogen environment in this study, while the size of dimples is smaller in the SSRT of hydrogen-charged austenitic stainless steels at room temperature [4.5].

According to the fracture profiles of the SUS304 (Fig. 3.12), grain boundary cracks were observed on the entire fracture surface except for the final fracture area when the applied stress was decreased. The effect of hydrogen on the fracture morphology of SUS310S will be revealed in further experiments for longer creep life.

Figure 4.7 shows the profiles of the fractured specimens and specimen surfaces in argon and hydrogen. The effect of hydrogen was observed in the morphology of the surface cracks, although there was no significant difference of the fracture surface. As shown in Fig. 4.7 (a), many cracks were observed with features of grain boundary cracking on the surface of the specimen in argon. On the other hand, the number of the surface cracks was less in the specimen in hydrogen (Fig. 4.7 (c)). Figures 4.7 (b) and (d) show the surface of the specimen at 7 mm distance from the fracture surface. The diameter of the specimen at the observed point was 3.45 mm for the specimen tested in argon and 3.44 mm for the specimen tested in hydrogen. The crack length was longer in argon compared to that in hydrogen, while the true strain was almost the same for both specimens.

Regarding the mechanism that hydrogen reduced the creep life of the SUS310S, the enhanced dislocation climb mediated by increased vacancy density due to hydrogen that I

assumed for the SUS304 is a strong candidate because this material has a similar single austenitic phase microstructure. However, at the moment, there is no definitive conclusion.

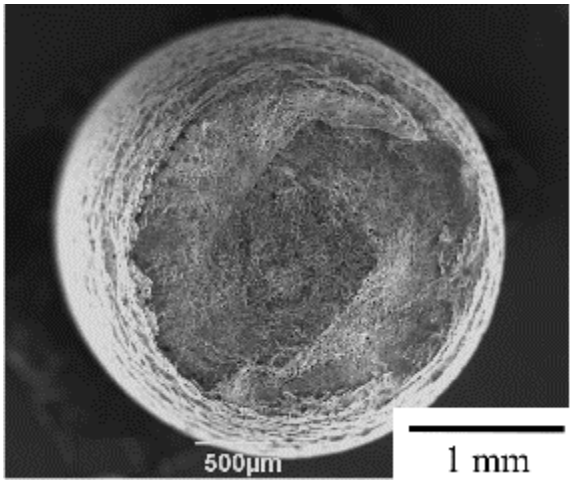

(a) Fracture surface in Ar

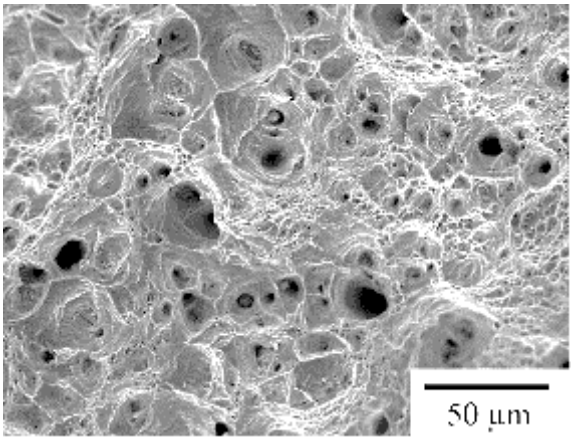

(b) Dimple fracture surface in Ar

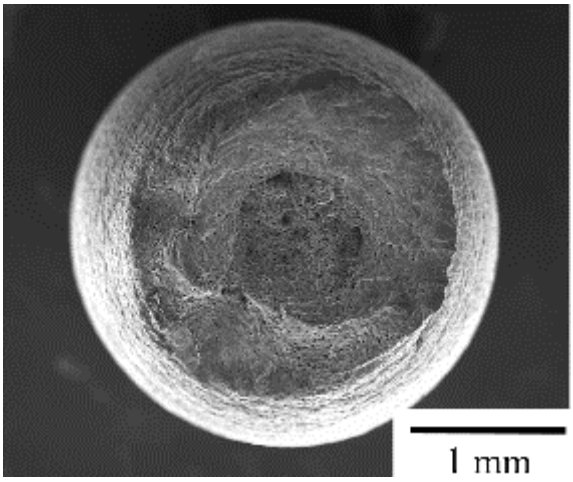

(c) Fracture surface in H_2

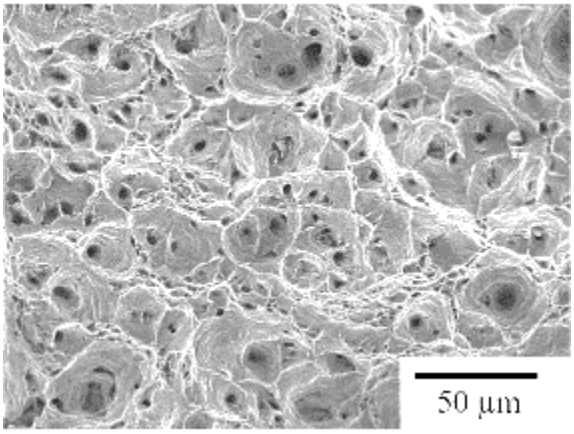

(d) Dimple fracture surface in H_2

Figure 4.4 Creep fracture surfaces of SUS310S at 873 K at the gas pressure of 0.12 MPa with the stress of 310 MPa.

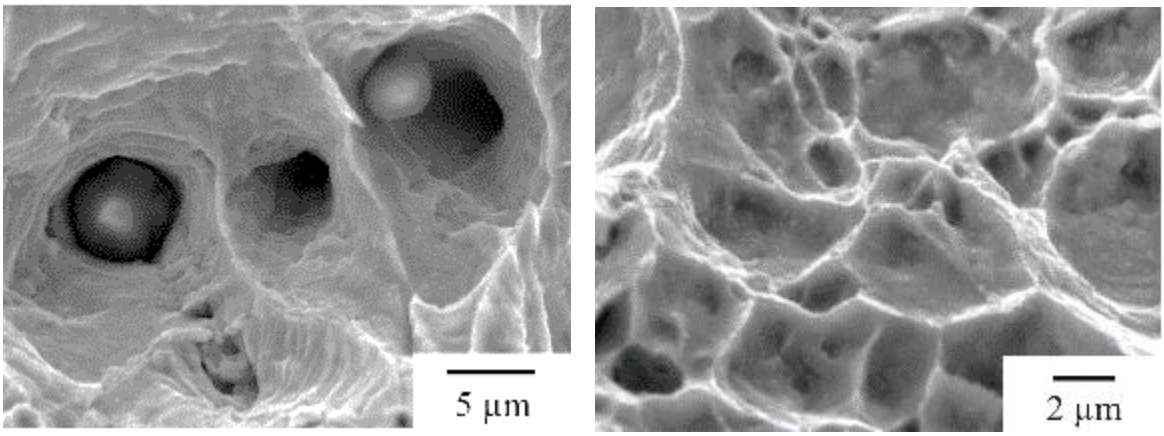

(a) Large and deep dimple (b) Small and shallow dimple

Figure 4.5 Detail observation of dimples on the SUS310S in argon.

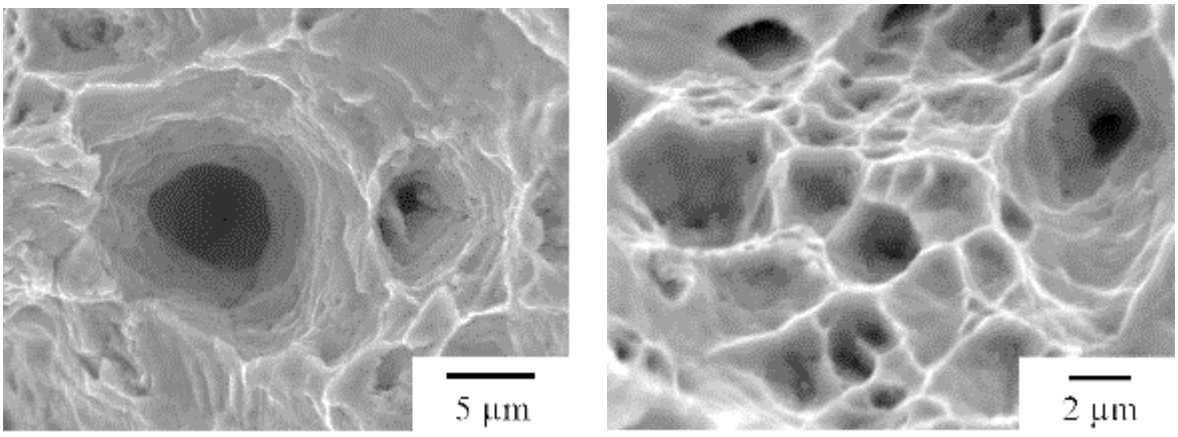

(a) Large and deep dimple (b) Small and shallow dimple

Figure 4.6 Detail observation of dimples on the SUS310S in hydrogen.

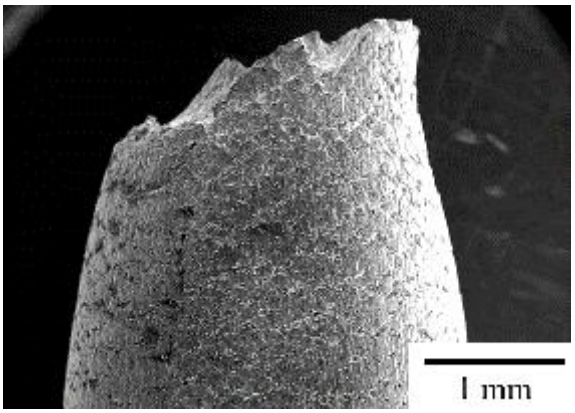

(a) Fracture profile in Ar

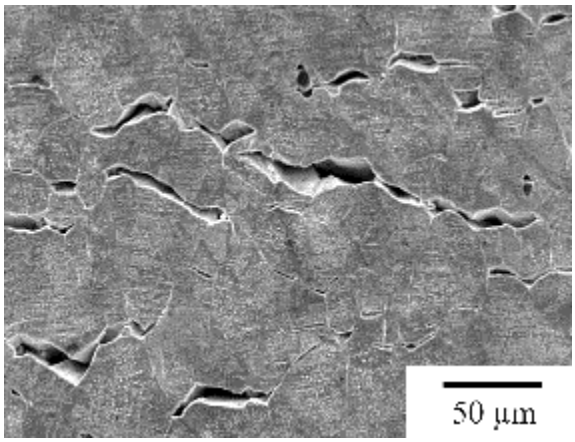

(b) Surface of specimen in Ar
(7 mm from fracture surface)

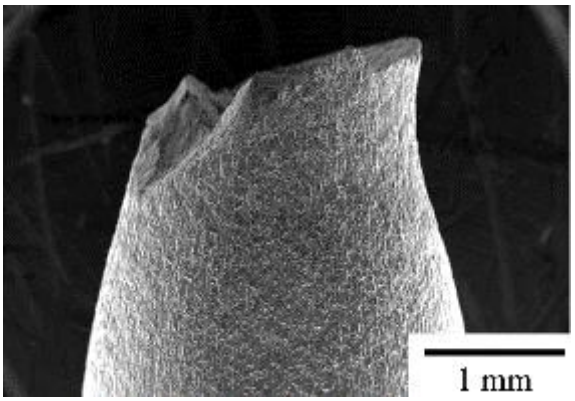

(c) Fracture profile in H_2

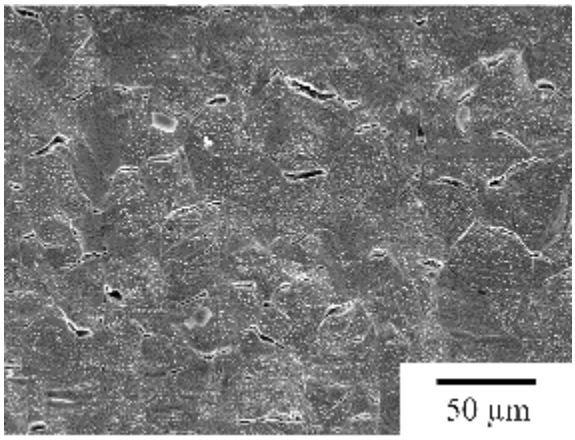

(d) Surface of specimen in H_2
(7 mm from fracture surface)

Figure 4.7 Creep fracture profiles and specimen surfaces of the SUS310S at 873 K at the gas pressure of 0.12 MPa with the stress of 310 MPa.

4.3.2 SUY-1 soft electromagnetic iron

Figure 4.8 shows the creep curves of the SUY-1. The creep rate in the steady-state (secondary) creep region in hydrogen was significantly increased compared to that in argon. As a result, hydrogen significantly reduced the creep life. The relative creep life in hydrogen vs. argon was 0.28 for the SUY-1 at the applied stress of 60 MPa and other given testing conditions. The elongation of the specimen and reduction of area are shown in Table 4.5. Hydrogen slightly increased the elongation and reduction of area.

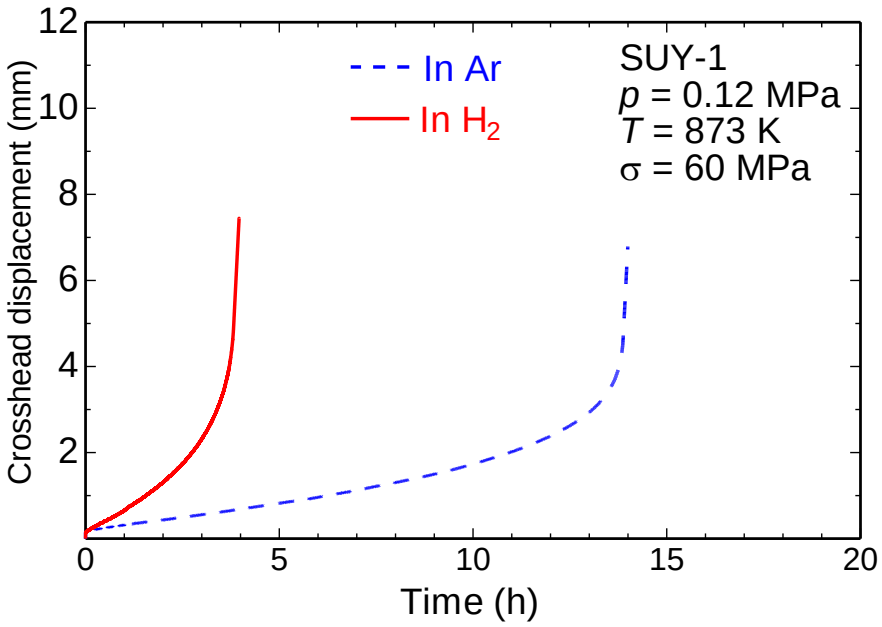

Figure 4.8. Effect of hydrogen on creep rupture of the SUY-1.

Table 4.5. Creep elongation and reduction of area of the SUY-1.

	Applied stress	Elongation	Reduction of area
In Ar	60 MPa	21.5 %	99.2 %
In H_2	60 MPa	23.3 %	99.6 %

Figures 4.9 and 4.10 show the profiles of the fractured specimens and fracture surfaces of the SUY-1 in argon and hydrogen. The specimen displayed chisel-edge fracture in both argon and hydrogen. Also, the specimen had a small fracture surface as shown in Figs. 4.9 (c) and 4.10 (c). For the tensile test of pure iron, chisel-edge fracture is common [4.6]. The fracture surface displayed dimples in both environments.

In a past study on the effect of hydrogen on the creep of bcc iron, Yokogawa et. al. [4.7, 4.8] carried out creep tests of the SUY (0.004 % C) in 773 K hydrogen at the gas pressure of 9.9 MPa. They reported reductions in the creep life in hydrogen and ductility as well. Regarding the creep ductility, the effect of hydrogen was opposite to my experiment, i.e. hydrogen increased the creep elongation and reduction of area in my experiment. Figure 4.11 shows the fracture surfaces in Yokogawa's experiment [4.7]. Their fracture surfaces were dimples in argon and dimples and intergranular cracking in hydrogen. They described hydrogen caused methane bubble formation at the grain boundary. As a result of decarburization and methane bubble formation, the creep ductility in hydrogen was reduced.

Regarding the difference of the results between Yokogawa's experiment and my experiment, nothing can be argued at the moment, because all testing conditions, which are the hydrogen gas pressure, testing temperature and applied stress, were different between their experiment and my experiment. According to the established knowledge about high temperature hydrogen attack (HTHA), decarburization becomes obvious at higher temperature and higher pressure [4.9, 4.10]. The hydrogen gas pressures were 9.9 MPa for Yokogawa's experiment and 0.12 MPa for my experiment. The testing temperatures were 773 K for Yokogawa's experiment and 873 K for my experiment. The longer testing time might also contribute to the HTHA mechanism. Further experiments in the longer life region are required in order to argue these differences.

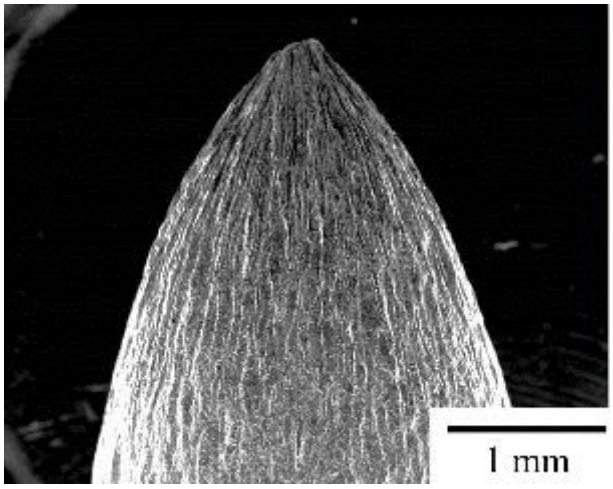

(a) Fracture profile (×30)

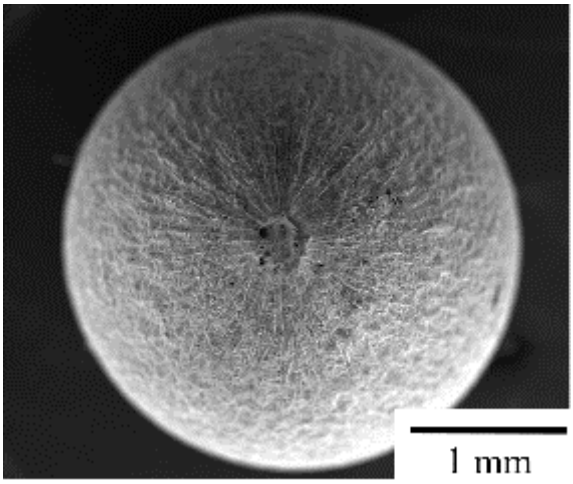

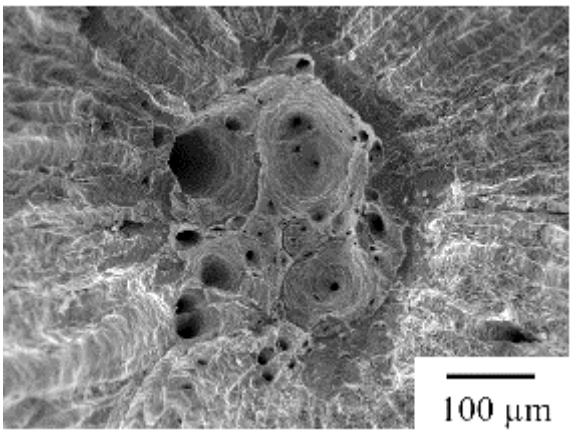

(b) Fracture surface (×30) (c) Fracture surface (×200)

Figure 4.9 Creep fracture profile and fracture surface of the SUY-1 in argon

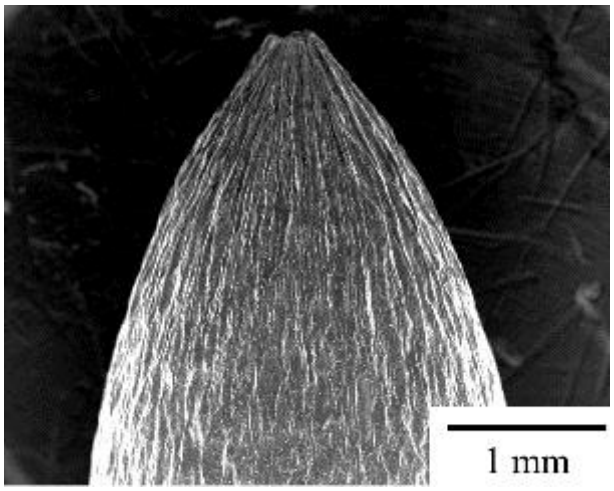

(a) Fracture profile (×30)

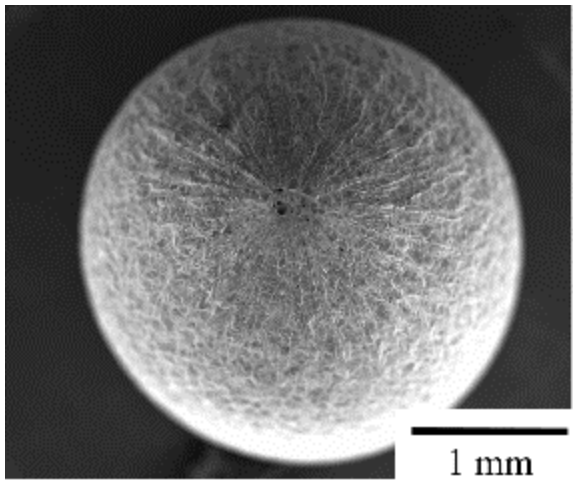

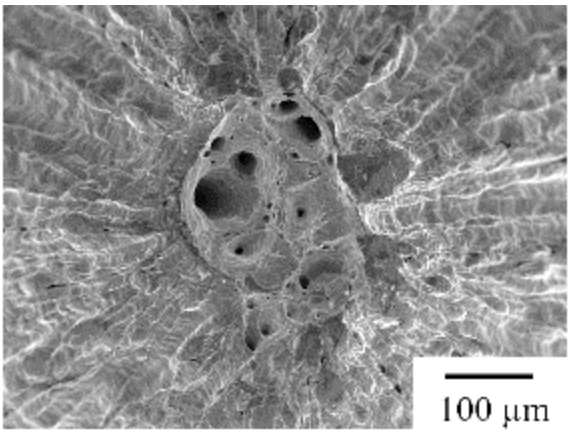

(b) Fracture surface (×30)　　(c) Fracture surface (×200)

Figure 4.10 Creep fracture profile and fracture surface of the SUY-1 in hydrogen

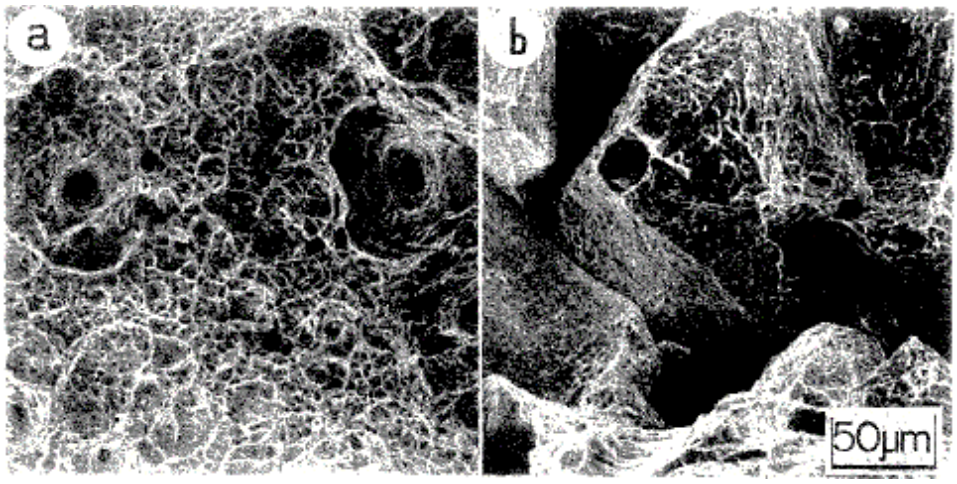

Figure 4.11 Creep fracture surfaces of the SUY in Yokogawa's experiment in 9.91 MPa at 773 K, (a) in argon (creep life was 740 ks), (b) in hydrogen (creep life was 1.5 Ms) [4.7].

Figure 4.12 shows Frost and Ashby's deformation mechanism map for pure iron [4.11]. The conditions in this experiment were plotted on the "plasticity" region. The steady deformation rate of pure metal in the high stress region is dominated by the competition between the evolution of dislocation microstructure (hardening) and its recovery (softening) [4.2, 4.12, 13]. The later process is enabled by climb-induced dislocation pair annihilation. I do not have enough results to discuss the mechanism by which hydrogen reduced the creep life of the SUY-1 at the moment. However, I would suggest the candidate mechanism based on this map. The candidate mechanism is that climb-induced dislocation pair annihilation might be promoted by enhanced vacancy formation by hydrogen. The creep deformation mechanism for pure iron that I consider here is different from that for the SUS304. However, it may be connected to the effect of hydrogen on vacancy formation.

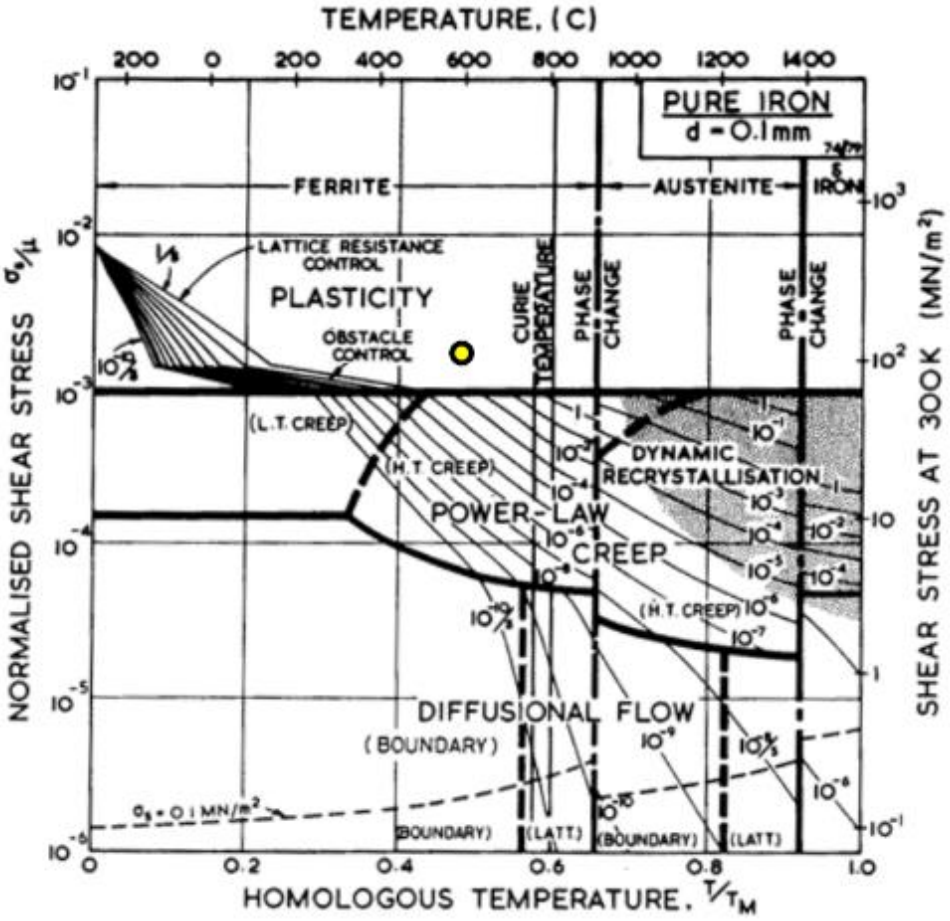

Figure 4.12. Testing condition in this thesis (●) superposed on Frost and Ashby's creep deformation mechanism map for the pure iron [4.11].

4.4 Conclusion

Creep testing of the JIS SUS310S austenitic stainless steel and SUY-1 soft electromagnetic iron were conducted in argon and hydrogen gas at an absolute gas pressure of 0.12 MPa at 873 K to investigate the perspective of future research on creep in hydrogen.

The results obtained in this chapter were very limited. When considering the history of the study on creep, where creep tests have been carried out for a very long period of time, such as over 10 years [4.14, 4.15] and 40 years [4.16], there is no definitive remark here. Nevertheless, I think the results that hydrogen reduced the creep life of SUS310S and SUY-1 would be a strong motivation for further study on creep in hydrogen.

As the result of this study, we obtained significant understanding of the effect of hydrogen on creep properties and argued the mechanism that hydrogen affects the creep life of the SUS304, SUS310S and SUY-1. Regarding further study, as described in this thesis, creep tests in the longer life region are necessary. Also, the study on the effects of various variables such as material, temperature and gas pressure are required. The arguments for the mechanism should be further investigated, although we achieved a certain level of understanding.

4.5 References

1. W.F. Smith, "Structure and Properties of Engineering Alloys", (Ney York: McGraw-Hill, Company, Inc., 1993), pp. 288-332
2. I. Finnie, W.R. Heller, "Creep of Engineering Materials", (New York: Mc Graw-Hill, Company, Inc., 1959), pp. 90-113
3. O.D. Sherby, P.M. Burke, "Mechanical behavior of crystalline solids at elevated temperature", *Progress in Materials Science,* Vol. 13, 1968, pp. 323-390
4. K.E. Amin, A.K. Mukherjee, J.E. Dorn, "A universal law for high-temperature diffusion controlled transient creep", *Journal of the Mechanics and Physics of Solids,* Vol. 18, Issue 6, 1970, pp. 413-426
5. C. San Marchi, B.P> Somerday, X. Tang, G.H. Schiroky, "Effects of alloy composition and strain hardening on tensile fracture of hydrogen-precharged type 316 stainless steels", *International Journal of Hydrogen Energy*, Vol. 33, Issue 2, 2008, pp. 889-904
6. D.R.H. Jones, "Creep failure of overheated boiler, superheater and reformer tubes", *Engineering Failure Analysis,* Vol. 11, 2004, pp. 873-893
7. K. Yokogawa, S. Fukuyama, K. Kudo, "Effect of Stress on Hydrogen Attack of Commercial Pure Iron", *Japan Inst. Metals,* Vol. 10, 1982, pp.1009-1017
8. K. Yokogawa, S. Fukuyama, K. Kudo, P.G. Shewmon, "Effect of Hydrogen Attack on Tensile and Creep Properties of Low Carbon Steel", *International Journal of Pressure Vessels and Piping,* Vol. 37, Issue 5, 1989, pp. 365-385
9. P.G. Shewmon, "Hydrogen attack of pressure-vessel steels", *Materials Science and Technology,* Vol. 1, 1985, pp. 2-11
10. G.A. Nelson, "Hydrogenation Plant Steels," in *Hydrogen Damage,* ed. C.D. Beachem, (Metals Park, OH: American Society for Metals, 1977), pp. 377-397.
11. H.J. Frost, M.F. Ashby, *Deformation-mechanism maps: the plasticity and creep of metals and ceramics,* (Oxford: Pergamon Press, 1982), pp. 60-70
12. J.P. Poirier, "*Plasticité à haute température des solides cristallins*", Paris: EYROLLES. (transferred by A. Oguchi, 1980, Yokendo Press), pp. 106-131

13. S. Kikuchi, M. Adachi, “High-temperature deformation behavior of metals and alloys”, *Zairyo*, Vol. 30, 1981, pp. 94-101
14. NIMS Creep Data Sheets No. 1. Tokyo, Tsukuba, National Institute for Materials Science, 2007
15. F. Abe, “Creep-resistant steels”, ed. F. Abe, T-U Kern, R. Viswanathan, (Boca Raton: CRC Press, 2008), pp. 1-14
16. NIMS, Press Release, “New World’s Record for Longest Creep Test Data is Expected!”, https://www.nims.go.jp/eng/news/press/2011/02/p201102240.html, 2011

5. Conclusion

High-temperature hydrogen environment is a common keyword for the advanced hydrogen-energy conversion devices actively being developed, such as the solid oxide fuel cell (SOFC), solid oxide electrolysis cell (SOEC), regenerative fuel cell (RFC) and hydrogen gas turbines. In spite of the fact that high-temperature hydrogen is a very aggressive environment for structural materials, the study on creep in hydrogen is very limited.

Considering this situation, the objective of this study is to derive mechanistic insight into the degradation of metals in high-temperature hydrogen in order to enable the safety of evolving hydrogen technologies that operate at elevated temperature. Specifically, creep tests of SUS304 were carried out in hydrogen.

General conclusion derived from this thesis is that we clearly demonstrated significant effect of hydrogen on creep properties. Although use of SUS304 is not definitive to SOFC systems, the results of this study provide strong motivation to further study on creep in hydrogen. Reactivation of the study on creep in hydrogen has important meaning in Material Science and Mechanical Engineering when considering safe carbon-neutral society that is provided by advanced hydrogen technologies. The conclusions of each chapter are as follows.

In Chapter 1, the motivation and societal relevance of this study are described based on the tendency of the hydrogen society and a survey of the past studies on creep in hydrogen.

In Chapter 2, the development of the testing machine that enabled creep testing in hydrogen at 873 K was described. Two types of heating systems, which were an internal heating system and an external one, were developed for SSRT and creep testing in high-temperature hydrogen. As the result, we adopted the external heating system.

1. The internal heater molded by brass was not suitable for the experiment in high-temperature hydrogen, because zinc was separated from the brass and transferred to the specimen surface.
2. This problem was fixed by the external heater system. We completed a testing machine for creep in hydrogen.
3. The digital image correlation (DIC) method was applied to measure strain in high-temperature hydrogen. The error of DIC in comparison with the strain gauge was 0.05 %.

In Chapter 3, creep testing of the JIS SUS304 austenitic stainless steel was conducted in 0.12 MPa hydrogen and argon atmospheres at 873 K.

1. Hydrogen considerably increased the steady state creep strain rate, drastically reduced the creep life, and decreased the percentage of intergranular fracture at lower applied stresses.
2. The creep elongation and reduction in area were higher in hydrogen compared to argon.
3. No decarburization occurred during testing in hydrogen.
4. Creep testing of the lower-carbon SUS304L steel in hydrogen resulted in reduction of the creep life similar to that for SUS304. This result suggests that the potential effect of the interaction of hydrogen with carbides in bringing about creep failure is minor.
5. From the analysis of the steady state creep data, it can be inferred that hydrogen does not alter the fundamental deformation mechanism of SUS304 steel at 873K, which is dislocation-driven creep described phenomenologically by a power law relationship. Our analysis supports the colorable argument that hydrogen reduces the activation energy for vacancy formation, thereby enhancing the vacancy density and associated lattice

diffusion coefficient, which in turn accelerates dislocation climb. As a consequence, hydrogen accelerates the creep response and shortens the creep life. Definitely this argument of hydrogen-enhanced, vacancy-driven dislocation climb needs further investigation.

In Chapter 4, creep tests of the JIS SUS310S austenitic stainless steel and SUY-1 soft electromagnetic iron was conducted in argon and hydrogen gas at an absolute gas pressure of 0.12 MPa at 873 K. As a result, hydrogen reduced the creep life of both the SUS310S and SUY-1. Even though the results obtained in chapter 4 were very limited, I think the results that hydrogen reduced the creep life of the SUS310S and SUY-1 would be a strong motivation for further study of creep in hydrogen.

In Chapter 5, the general outline of this thesis is described.

Acknowledgement

This thesis is a summary of the research that I carried out during the doctoral course at the Department of Mechanical Engineering in the Graduate School of Engineering of Kyushu University.

First and foremost, I would like to express my deepest and sincerest gratitude to my supervisor Professor Masanobu Kubota, who led me through a superb journey up to this thesis and provided me with extraordinary guidance, thoughtful encouragement and continuous support throughout my entire research. I am convinced that your faithful education and the experience I gained during this period will be a great force for my future research career.

I would like to sincerely thank Assistant Professor Ryosuke Komoda, who gave me a lot of advice and support, but also taught me about the fun of the research.

I would like to express my deep appreciation to Professor Toshihiro Tsuchiyama, who gave me insightful suggestions and helped as my second supervisor. Thanks to your help from the perspective of materials engineering, I was able to deepen the consideration of this research.

I also would like to sincerely express my deep appreciation to Professor Petros Sofronis, Dr. Brian P. Somerday and Dr. Mohsen Dadfarnia, who gave me a lot of insightful advice and suggestions on this research and gave me thoughtful encouragements.

I am grateful to have received extensive support and help from many people. I would like to express my appreciation to Professor Shigeru Hamada for giving me insightful comments and advice on this thesis. I would like to thank Professors Shinichi Komazaki and Koichi Sato (Kagoshima University) for their thoughtful advice and help, Assistant Professor Hiroyoshi Tanaka (Kyushu University), Associate Professor Arnaud Macadre (Yamaguchi

University), Dr. Vlad Niste (Kyodo Yushi) and Associate Professor Aleksandar Staykov (I2CNER) for their kind support and insightful comments. I also would like to thank my fellow lab mates and research support staff for the discussions and many moments of support.

This study was supported by the Research Fellow of Japan Society for the Promotion of Science (JSPS) for Young Scientists and JSPS KAKENHI Grant Numbers 18J22540 and 16H04237.

This study was supported by the International Institute for Carbon Neutral Energy Research (WPI-I2CNER), sponsored by the World Premier International Research Center Initiative (WPI), MEXT, Japan.

Finally, I would like to thank my family for the grateful support and education. Special thanks go to my parents, Yosuke and Taeko, who always support, understand and encourage me.

Daisuke Takazaki